

TARGETING OF ANTI-CANCER DRUG USING MAGNETIC NANOPARTICLES



by
Berna Gürten

Submitted to Graduate School of Natural and Applied Sciences
in Partial Fulfillment of the Requirements
for the Degree of Master of Science in
Chemical Engineering

Yeditepe University

2016

TARGETING OF ANTI-CANCER DRUGS USING MAGNETIC NANOPARTICLES

APPROVED BY:

Prof. Dr. Seyda Malta
(Thesis Supervisor)



Assoc. Prof. Dr. Ali Demir Sezer



Assist. Prof. Dr. Semin Funda Oğuz



DATE OF APPROVAL: ... / ... / 2016

ACKNOWLEDGEMENTS

I owe thanks to many people who helped in the accomplishment of this project.

First of all, I would like to express my gratitude to my supervisor, Prof. Dr. Seyda Malta for her sincere approach and patient way of teaching and guiding. She helped me and believed in me. It is a pleasure to be able to work with her and most importantly to have someone like her who also established a future for me besides guiding. She was a perfect guide for me to give important decisions throughout my life. No words would be enough to thank for her help and encouragement. She is more than an instructor for me.

I would also like to thank a member of my Tübitak project, Assoc. Prof. Ali Demir Sezer for his support and help. It was an honour and a pleasure to work with him.

Special thanks for my instructors, Prof. Dr. Nurcan Baç, Prof. Dr. Mustafa Özilgen, Prof. Dr. Süheyla Uzman, Assist Prof. Funda Oğuz, Assist Prof. Erde Can and Assist Prof. Güleğül Duman for their encouragement and support.

I would also like to express my deepest appreciation to Assist. Prof. Dr. Cem Levent Altan, who devoted his valuable time to me in every respect. His contributions make me better equipped to overcome the problems. In addition, I would like to thank Elçin Yenigül for her support and help during the experimental studies of TMZ and CDs and Görkem Cemali for her help during the experimental studies and patience, psychological support throughout this study.

Special thanks to all my friends at Chemical Engineering Department, especially Gizem Karakaş for her love, support, patience, sincere help throughout this study. She always believes in me and supports me in every situation. I am so lucky that we were always side by side during this project for three years. Also deepest thanks to all my friends, Ecem Yazar, Sera Erkeçoğlu, İlayda Acaroğlu, Neşe Ayata, Şelale Gülyuva, Ece Akbulut, Melek Şekerci and Barış Emek.

Sincere thanks to my family for their love, patience, understanding and psychological support throughout this study. Special thanks to my father Ahmet Sertaç Gürten and my

mother Leyla Gürten for introducing me with Chemical Engineering and they taught me how to love this occupation. Last but not least, my brother Atakan Gürten for supporting me in every way during the project.



ABSTRACT

TARGETING OF ANTI-CANCER DRUG USING MAGNETIC NANOPARTICLES

Cancer, also called malignancy, is an abnormal growth of cells in the human body which form tissues are called tumors. Specifically, brain tumors are very common and primary brain tumours contain 2% of all adult cancers. Surgery, chemotherapy, radiation therapy and hormone therapy are used in combination for the treatment of cancer however, the anti-cancer drugs which is used in chemotherapy have many toxic effects causing a lot of side effects such as fatigue, hair loss and anemia etc. As a consequence, it is important to find an effective method for the administration of the anti-cancer drugs like drug delivery systems in order to enhance the efficiency and decrease the dose of the drug. The aim of this project is to target an anti-cancer drug temozolomide to the tumor site using magnetic nanoparticles in the presence of an external magnetic field and develop a new drug delivery system. Temozolomide has very low solubility and stability in aqueous medium at neutral conditions thus, an inclusion complex is needed which can be achieved by using various types of cyclodextrins(CDs) having a hydrophobic cavity that can accommodate the drug and increase the solubility. In addition, chitosan is a biocompatible material so, it is used for many biomedical applications. Chitosan can be used in combination with inorganic materials such as magnetic NPs for drug delivery system. It is aimed to encapsulate TMZ in magnetite-CD-chitosan beads and by applying an external magnetic field the total entity is targeted to the tumor site. In this way, minimum dose of drug is administered to the human body and side effects are expected to decrease. Magnetic nanoparticles were synthesized and stabilized by CDs. Heat profiles and weight loss upon heating of CD&TMZ inclusion complexes were shown to differ significantly from those of physical mixtures. The solubility of TMZ was shown to increase in the presence of CD's using UV and HPLC. In the presence of magnetite particles, chitosan-magnetite beads that contain TMZ were prepared. TMZ encapsulation efficiency of different preparation methods were investigated using HPLC and their morphologies were shown using SEM. These beads were then targeted to a specific area where TMZ is shown to accumulate.

ÖZET

KANSER İLACININ MANYETİK NANOPARÇACIKLAR KULLANILARAK HEDEFLENMESİ

Kanser diğer adıyla malignite, hücrelerin anormal çoğalmasıdır, bu çoğalmanın oluşturduğu dokulara tümör denir. Özellikle beyin tümörleri çok yaygındır, birinci derece beyin tümörleri yetişkin kanserlerinin %2'sini oluşturmaktadır. Kanser tedavisi olarak ameliyat, kemoterapi, radyasyon ve hormon terapilerinin kombinasyonları kullanılmaktadır, fakat kemoterapi tedavisi sırasında kansere karşı kullanılan ilaçlar çok sayıda toksik etkiye sahiptir bu etkiler çok sayıda yan etkiye sahiptir örneğin, tükenmişlik, yorgunluk, saç dökülmesi, kansızlık, vb. Sonuç olarak, kanser ilacının yöneltmesi için ilaç taşınım sistemi gibi etkili bir yol oluşturmak verimliliği geliştirmek ve ilaç dozunu azaltmak açısından çok önemlidir. Bu projenin amacı tümörlü olan bölgeye kansere karşı etkili bir ilaç olan Temozolomid'in manyetik nanoparçacıklar tarafından taşınarak dışarıdan manyetik alan uygulanarak hedeflenmesi ve yeni bir ilaç taşınım sistemi oluşturmaktır. Temozolomid sulu çözelti içerisinde ve nötr koşullarda çok düşük stabiliteye ve çözünebilirliğe sahiptir. Böylece ilaca uyum sağlayabilen ve ilacın çözünebilirliğini arttıran farklı çeşit siklodekstrinlerin hidrofobik kavimleri kullanılarak kompleks oluşturması gerekmektedir. Ek olarak, kitozan biyouyumlu bir malzemedir ve bu yüzden, kitozan pek çok biyomedikal uygulamalarda kullanılmaktadır. İlaç taşınım sistemi için, kitozan, inorganik malzemelerle örneğin manyetik nanoparçacıklar ile kombinasyon oluşturabilir. Manyetik kitozan küreciğine Temozolomid sarmalamak ve bu sarmalın dışarıdan uygulanan manyetik alan sayesinde tüm entitinin tümörlü bölgeye hedeflenmesi amaçlanmıştır. Bu şekilde, en az miktar dozda ilaç insan vücuduna alınacaktır ve böylece yan etkilerinin azalması beklenmektedir. Manyetik nanoparçacıklar sentezlenir ve siklodekstrin tarafından stabilize edilir. Siklodekstrin varlığında Temozolomid'in çözünebilirliğinin artması Yüksek Basınç Kromatografisi ve UV Spektroskopisi ile gösterilmiştir. Ek olarak, aralarında oluşan kompleksin ısı profili ve ısı uygulandığında oluşan ağırlık kaybı aralarında oluşan kompleks ve fiziksel karıştırma arasında ciddi fark olduğunu gösterir. Manyetik nanoparçacık-kitozan kürecikleri elde edilir, Taramalı Elektron mikroskopu ile morfolojisi incelenir ve Temozolomid kürecikleri içine sarmalanır ve istenilen bölgeye dışarıdan uygulanan manyetik alan ile hedeflenir.

TABLE OF CONTENTS

ACKNOWLEDGEMENTS.....	iii
ABSTRACT.....	v
ÖZET	vi
TABLE OF CONTENTS.....	vii
LIST OF FIGURES	x
LIST OF TABLES.....	xvii
LIST OF SYMBOLS AND ABBREVIATIONS.....	xix
1. INTRODUCTION	1
2. THEORETICAL BACKGROUND	3
2.1. NANOPARTICLES	3
2.1.1. Therapeutics	3
2.1.2. Diagnostics	3
2.1.3. Imaging	3
2.2. IRON OXIDES	4
2.2.1. Magnetic Behaviour of Iron Oxides	6
2.3. MAGNETITE	10
2.3.1. Magnetite Synthesis Method	10
2.3.1.1. Co-precipitation Method.....	11
2.3.1.2. Thermal Decomposition Method	12
2.3.1.3. Microemulsion Method	13
2.3.1.4. Hydrothermal Synthesis	14
2.5. APPLICATIONS OF MAGNETIC PARTICLES	16
2.5.1. Magnetic Resonance Imaging (MRI)	17
2.5.2. Magnetic Hyperthermia	17
2.5.3. Drug Delivery & Targeting	18
2.5.3.1. Drug Delivery with Nanoparticles.....	19
2.5.3.2. Drug Delivery with Cyclodextrin	23
2.5.3.3. Drug Delivery with Chitosan Nanoparticles.....	25
3. MATERIALS AND METHODS.....	27
3.1. MATERIALS	27
3.1.1. Temozolomide	29
3.1.2. Cyclodextrins	31
3.1.3. Chitosan	37

3.1.3.1. Preparation methods for Chitosan Nanoparticles	40
3.2. METHODS	42
3.2.1. Thermogravimetric Analysis (TGA)	42
3.2.2. Differential Scanning Calorimetry (DSC)	43
3.2.3. Dynamic Light Scattering (DLS)	45
3.2.4. UV-Visible Spectroscopy.....	46
3.2.5. High Pressure Liquid Chromotography (HPLC)	47
3.2.6. Scanning Electron Microscopy (SEM)	48
4. SYNTHESIS OF MAGNETITE NANOPARTICLES AND CHARACTERIZATION	50
4.1. SYNTHESIS OF MAGNETITE NANOPARTICLES	50
4.1.1. Synthesis of Bare Magnetite Nanoparticles	50
4.1.2. Synthesis of Magnetite Nanoparticles with Cyclodextrins	51
4.1.3. Tiron Metal Test to Determine Magnetite Concentration	51
4.2. CHARACTERIZATION OF MAGNETIC NANOPARTICLES	52
4.2.1. Dynamic Light Scattering Measurements	52
4.2.2. Thermogravimetric Analysis Measurements	55
4.2.3. Colloidal Stability of Magnetic Nanoparticles	56
5. PREPARATION METHODS OF INCLUSION COMPLEX BETWEEN CYCLODEXTRINS AND TEMOZOLOMIDE AND CHARACTERIZATIONS	58
5.1. DETERMINATION OF SOLUBILITY OF TEMOZOLOMIDE.....	58
5.2. PREPARATION OF TMZ-CYCLODEXTRIN INCLUSION COMPLEX SOLUTIONS AND PARTICLES.....	58
5.2.1. Preparation Method of TMZ-CD Inclusion Complex Solution	59
5.2.2. Preparation Method of TMZ-CD Inclusion Complex Particles	60
5.2.3. Preparation method of TMZ-CD physical mixtures.....	60
5.3. ULTRAVIOLET-VISIBLE SPECTROSCOPY MEASUREMENTS	61
5.3.1. Calibration Curve of TMZ	61
5.3.2. Solubility Curve of TMZ	61
5.3.3. Enhancement of the Solubility of Temozolomide	62
5.4. HIGH PRESSURE LIQUID CHROMOTOGRAPHY MEASUREMENTS	67
5.5. HEAT PROFILES OF INCLUSION COMPLEXES	71
5.6. THERMOGRAVIMETRIC ANALYSIS OF COMPLEXES	72
5.7. MORPHOLOGY OF THE INCLUSION COMPLEX.....	73
6. TARGETING OF TEMOZOLOMIDE USING MAGNETIC NANOPARTICLES	77

6.1. FORMATION OF CHITOSAN NANOPARTICLES.....	77
6.2. FORMATION OF MAGNETITE-CHITOSAN BEADS.....	78
6.3. FORMATION OF CHITOSAN NPs AND MAGNETITE-CHITOSAN BEADS WITH TMZ.....	78
6.4. ENCAPSULATION OF THE MAGNETITE-CHITOSAN BEADS AND ONLY CHITOSAN NANOPARTICLES.....	80
6.5. TARGETING OF TMZ WITH MAGNETIC PARTICLES	80
6.5.1. Targeting of TMZ with magnetite-CD and magnetite-chitosan beads	80
6.5.2. HPLC Analysis for Targeting Study	81
6.6. DRUG ENCAPSULATION AND TARGETING.....	81
6.6.1. Targeting of magnetite-CD-TMZ particles	81
6.6.2. Encapsulation and Characterization of Chitosan Nanoparticles	84
6.6.2.1. Morphology of the Chitosan Nanoparticles.....	84
6.6.2.2. Size measurement of Chitosan Nanoparticles	88
6.6.2.3. Encapsulation of TMZ in chitosan nanoparticles	90
6.6.3. Magnetite-Chitosan Beads and Characterizations for Targeting Study	90
6.6.3.1. Morphology of the Magnetite-Chitosan Beads.....	90
6.6.3.2. Size Measurements of magnetite-chitosan beads	95
6.6.3.3. Encapsulation of TMZ in bare magnetite-chitosan beads	96
6.6.3.4. Encapsulation of TMZ in b-CD magnetite-chitosan beads	97
6.6.4. Targeting Study of TMZ in magnetite-chitosan beads.....	99
6.6.4.1. Targeting Study of TMZ in magnetite-chitosan beads with thin test section.....	99
6.6.4.2. Targeting Study of TMZ in magnetite-chitosan beads with thick test section.....	101
7. CONCLUSION AND FUTURE WORK	103
REFERENCES	106
APPENDIX A	130

LIST OF FIGURES

Figure 2.1. Biomedical applications of magnetic nanoparticles	4
Figure 2.2. Schematic illustration of the main varieties of magnetic order	7
Figure 2.3. Magnetization M as a function of an applied magnetic field H	9
Figure 2.4. Oversimplified magnetite synthesis reaction	10
Figure 2.5. Schematic representation of Co-precipitation method	11
Figure 2.6. An illustration of magnetite nanoparticles synthesis by thermal decomposition method.....	13
Figure 2.7. An illustration of magnetite nanoparticles synthesis by reverse microemulsion method.....	14
Figure 2.8. General Hyperthermia procedure for cancer therapy	18
Figure 2.9. Types of drug loaded nanoparticles	19
Figure 2.10. MNPs specifically targeted to the tumor tissue with the help of an external magnetic field	23
Figure 3.1. Temozolomide and dacarbazine and their common active metabolite, MTIC	30
Figure 3.2. Physical stability and color comparison of pure TMZ 40°C and 75% Relative Humidity.....	31

Figure 3.3. Different diameters of Cyclodextrins-Structures relations.....	33
Figure 3.4. Hydrophilic outer surface and hydrophobic inner core of cyclodextrins	34
Figure 3.5. Inclusion complex between cyclodextrin and guest molecule	34
Figure 3.6. Kneading method CD/drug inclusion complex	36
Figure 3.7. Lyophilization method CD/drug inclusion complex	36
Figure 3.8. Co-evaporation method CD/drug inclusion complex	37
Figure 3.9. Structure of the chitosan and chitin	38
Figure 3.10. Schematic presentation of chitosan production	39
Figure 3.11. Preparation of chitosan NPs with ionic gelation method	40
Figure 3.12. Preparation of chitosan NPs with emulsion cross-linking method	41
Figure 3.13. Schematic diagram of the method of reverse micellisation	41
Figure 3.14. Schematic diagram of the method of emulsion droplet coalescence	42
Figure 3.15. Thermogravimetric analysis (TGA) instrument	43
Figure 3.16. Differential Scanning Calorimeter	44
Figure 3.17. Accessories used for DSC	44
Figure 3.18. Hydrodynamic diameter for TEM and DLS	45

Figure 3.19. Dynamic Light Scattering	46
Figure 3.20. UV-Visible Spectrophotometer	46
Figure 3.21. Quartz Cuvette	47
Figure 3.22. High Performance Liquid Chromotography	48
Figure 3.23. Scanning Electron Microscopy	48
Figure 4.1. Size distribution of magnetite NPs for first measurement	54
Figure 4.2. Size distribution of magnetite NPs for third measurement.	54
Figure 4.3. Thermogravimetric Analysis for magnetite with and without CD's.....	55
Figure 4.4. Magnetite nanoparticles with and without CD's at t=0, t=40 min and t=5 hrs (Magnetic Nanoparticles 1= Bare, 2=b-CD coated, 3= hyd-b-CD coated, 4= hyd-g-CD coated).....	56
Figure 5.1. Preparation process of TMZ-CD inclusion complex solution.....	59
Figure 5.2. Preparation process of TMZ-CD inclusion complex particles.....	60
Figure 5.3. Calibration curve of TMZ.	61
Figure 5.4. The solubility curve of Temozolomide	62
Figure 5.5. Absorbance of TMZ in the presence of different CD's and only TMZ in 1:1 ratio after the formation of inclusion complex after 24 hours	63

Figure 5.6. Absorbance of TMZ in the presence of different CD's and only TMZ in 1:2 ratio after the formation of inclusion complex after 24 hours	63
Figure 5.7. Absorbance of TMZ in the presence of different CD's and only TMZ in 1:5 ratio after the formation of inclusion complex after 24 hours	64
Figure 5.8. Absorbance of TMZ in the presence of β -CD and only TMZ in all molar ratios after the formation of inclusion complex after 24 hours	65
Figure 5.9. Absorbance of TMZ in the presence of H- β -CD and only TMZ in all molar ratios after the formation of inclusion complex after 24 hours.....	66
Figure 5.10. Absorbance of TMZ in the presence of H- γ -CD and only TMZ in all molar ratios after the formation of inclusion complex after 24 hours.....	66
Figure 5.11. Amount of solubilized TMZ in the presence of CDs and only TMZ in all molar ratios after the formation of inclusion complex after 24 hours	67
Figure 5.12. Typical TMZ scan in HPLC analysis.....	68
Figure 5.13. Calibration curve of TMZ for HPLC analysis	68
Figure 5.14. Amounts of solubilized TMZ in mg/mL after the formation of inclusion complex after one hour	69
Figure 5.15. Amounts of solubilized TMZ in mg/mL after the formation of inclusion complex after 24 hours	70
Figure 5.16. Amounts of solubilized TMZ in mg/mL after the formation of inclusion complex after 48 hours	71
Figure 5.17. DSC curves of TMZ-b-CD inclusion complex and physical mixing	72

Figure 5.18. TGA curves of only TMZ, only β -CD, TMZ- β -CD inclusion complex and physical mixing.....	73
Figure 5.19. SEM images of only TMZ.....	74
Figure 5.20. SEM images of only β -CD	74
Figure 5.21. SEM images of TMZ- β -CD physical mixing.....	75
Figure 5.22. SEM images of TMZ- β -CD inclusion complex.....	76
Figure 5.23. SEM images of TMZ- β -CD inclusion complex (a) and physical mixing (b) comparison.....	76
Figure 6.1. Chitosan formation procedure (first and second method)	78
Figure 6.2. Formation of magnetite-chitosan beads with first method.....	79
Figure 6.3. Formation of magnetite-chitosan beads with second method	79
Figure 6.4. Schematic Diagram of Targeting Study	81
Figure 6.5. Magnet Separation of Magnetic Nanofluid	82
Figure 6.6. Captured magnetite-CD-TMZ nanofluid in the test section using (a) 0.5 %wt CD (b) 0.25 %wt CD after 5 hrs	82
Figure 6.7. Colloidal stability of magnetite nanofluid in water (a) and in 0.1 M HCl (b) after 5 hours.....	83

Figure 6.8. Captured magnetite-CD-TMZ nanofluid in the test section using (a) 0.25% wt CD and (b) 0.125% wt CD after 1 hr	83
Figure 6.9. SEM images of chitosan NPs ($[TPP]_{final} = 0.5\text{wt}\%$; $[chitosan]_{final} = 0.25\text{wt}\%$).....	85
Figure 6.10. SEM images of chitosan NPs ($[TPP]_{final} = 0.75\text{wt}\%$; $[chitosan]_{final} = 0.25\text{wt}\%$).....	85
Figure 6.11. SEM images of chitosan NPs ($[Na_2SO_4.10H_2O]_{final} = 2.5\text{ wt}\%$; $[chitosan]_{final} = 0.10\text{ wt}\%$).....	86
Figure 6.12. SEM images of chitosan NPs ($[Na_2SO_4.10H_2O]_{final} = 2.5\text{ wt}\%$; $[chitosan]_{final} = 0.125\text{ wt}\%$).....	86
Figure 6.13. SEM images of chitosan NPs ($[Na_2SO_4.10H_2O]_{final} = 3.75\text{ wt}\%$; $[chitosan]_{final} = 0.125\text{ wt}\%$).....	87
Figure 6.14. SEM images of chitosan NPs ($[Na_2SO_4.10H_2O]_{final} = 3.75\text{ wt}\%$; $[chitosan]_{final} = 0.25\text{ wt}\%$).....	87
Figure 6.15. SEM images of chitosan NPs ($[Na_2SO_4.10H_2O]_{final} = 3.75\text{ and }1.25\text{ wt}\%$; $[chitosan]_{final} = 0.375\text{-}0.5\text{ wt}\%$)	88
Figure 6.16. Size measurement of chitosan NPs ($[Na_2SO_4.10H_2O]_{final} = 1.25\text{ wt}\%$; $[chitosan]_{final} = 0.125\text{ wt}\%$).....	89
Figure 6.17. SEM images of chitosan NPs ($[Na_2SO_4.10H_2O]_{final} = 1.25\text{ wt}\%$; $[chitosan]_{final} = 0.375\text{ wt}\%$).....	89
Figure 6.18. SEM images of bare magnetite-chitosan beads ($[Na_2SO_4.10H_2O]_{final} = 2.2\text{ wt}\%$; $[chitosan]_{final} = 0.11\text{ wt}\%$; chitosan+bare magnetite solution).....	91

Figure 6.19. SEM images of bare magnetite-chitosan beads ($[\text{Na}_2\text{SO}_4 \cdot 10\text{H}_2\text{O}]_{\text{final}} = 1.1$ wt% ; $[\text{chitosan}]_{\text{final}} = 0.22$ wt% ; salt + bare magnetite solution).....	92
Figure 6.20. SEM images of b-CD magnetite-chitosan beads ($[\text{Na}_2\text{SO}_4 \cdot 10\text{H}_2\text{O}]_{\text{final}} = 1.1$ wt% ; $[\text{chitosan}]_{\text{final}} = 0.22$ wt% ; chitosan + b-CD coated magnetite solution).....	92
Figure 6.21. SEM images of b-CD magnetite-chitosan beads ($[\text{Na}_2\text{SO}_4 \cdot 10\text{H}_2\text{O}]_{\text{final}} = 1.1$ wt% ; $[\text{chitosan}]_{\text{final}} = 0.22$ wt% ; salt + b-CD coated magnetite solution).....	93
Figure 6.22. SEM images of b-CD magnetite-chitosan beads ($[\text{Na}_2\text{SO}_4 \cdot 10\text{H}_2\text{O}]_{\text{final}} = 1.1$ wt% ; $[\text{chitosan}]_{\text{final}} = 0.09$ wt% ; salt + b-CD coated magnetite solution).....	93
Figure 6.23. SEM images of b-CD magnetite-chitosan beads ($[\text{Na}_2\text{SO}_4 \cdot 10\text{H}_2\text{O}]_{\text{final}} = 1.1$ wt% ; $[\text{chitosan}]_{\text{final}} = 0.43$ wt% ; salt + b-CD coated magnetite solution).....	94
Figure 6.24. Size measurement of magnetite-chitosan beads with DLS ($[\text{Na}_2\text{SO}_4 \cdot 10\text{H}_2\text{O}]_{\text{final}} = 1.1$ wt% ; $[\text{chitosan}]_{\text{final}} = 0.11$ wt% ; salt + b-CD coated magnetite solution).....	95
Figure 6.25. Size measurement of magnetite-chitosan beads with DLS ($[\text{Na}_2\text{SO}_4 \cdot 10\text{H}_2\text{O}]_{\text{final}} = 1.1$ wt% ; $[\text{chitosan}]_{\text{final}} = 0.33$ wt% ; salt + b-CD coated magnetite solution).....	96
Figure 6.26. Captured magnetite-chitosan-TMZ nanofluid in the test section (0.5 %wt CD) after 1 hr.....	101

LIST OF TABLES

Table 2.1. Physical and magnetic properties of iron oxides	5
Table 2.2. Properties of different magnetic states.....	8
Table 2.3. Comparison of the synthesis methods of magnetic nanoparticles	15
Table 3.1. Chemicals for the synthesis of magnetite nanoparticles by co-precipitation method.....	27
Table 3.2. Chemicals used for Tiron metal test	28
Table 3.3. Chemicals used for chitosan NPs synthesis	28
Table 3.4. Properties of Temozolomide	29
Table 3.5. Properties of Different Types of Cyclodextrins.....	32
Table 3.6. Properties of Cyclodextrins.....	33
Table 3.7. Properties of Chitosan.....	38
Table 4.1. Amounts of chemicals for bare magnetite nanoparticles.....	51
Table 4.2. Amounts of chemicals for magnetite nanoparticles with cyclodextrin.....	51
Table 4.3. Amounts of chemicals for Tiron Metal Test.....	52
Table 4.4. Size distribution of the magnetite NPs after 1 st and 3 rd measurements.....	53

Table 4.5. % coating of magnetite NPs with different CD's.....	56
Table 4.6. Time to Precipitation for synthesized magnetic NPs.....	57
Table 5.1. Amounts of solubilized TMZ in mg/mL in 0.1 M HCl after the formation of inclusion complex after 24 hours.....	65
Table 5.2. Amounts of solubilized TMZ in mg/mL in 0.1 M HCl after the formation of inclusion complex after one hour and 24 hours.....	69
Table 5.3. Amounts of solubilized TMZ in mg/mL in 0.1 M HCl after the formation of inclusion complex after 48 hours.....	70
Table 6.1. % Encapsulated TMZ in chitosan nanoparticles after and during the formation.....	90
Table 6.2 % Encapsulated TMZ in magnetite-chitosan beads after and during the formation.....	97
Table 6.3. % Encapsulated TMZ in magnetite-chitosan beads comparing salt concentrations.....	98
Table 6.4. % Encapsulated TMZ in magnetite-chitosan beads with only 1.1 wt % final salt concentration.....	98
Table 6.5. Targeting study with thin section (applying 0.3 T magnetic field)	100
Table 6.6. Targeting study with thin section (applying 0.5 T magnetic field)	100
Table 6.7. Targeting study with thick section.....	102

LIST OF SYMBOLS / ABBREVIATIONS

d(h)	Hydrodynamic diameter
D	Translational diffusion coefficient
I	Intensity
k	Boltzmann's constant
T	Absolute temperature
η	Viscosity
λ	Wavelength
Abs	Absorbance
AIC	5-amino-imidazole-4-carboxamide
AOT	Sodium bis(ethyl hexyl) sulfosuccinate
BBB	Blood-brain barrier
CD	Cyclodextrin
CDS	Chemical delivery system
CSF	Cerebrospinal fluid
CTAB	Cetyltrimethylammonium bromide
DLS	Dynamic light scattering
DNA	Deoxyribonucleic acid
DSC	Differential scanning calorimeter
H	Magnetic Field
HPLC	High pressure liquid chromatography
H- β -CD	2-hydroxyl-propyl- β -CD
H- γ -CD	2-hydroxyl-propyl- γ -CD
M	Magnetization

mg	Miligram
MNPs	Magnetic nanoparticles
MRI	Magnetic resonance imaging
MTIC	5-(3-methyl)1-triazen-1-yl-imidazole-4-carboxamide
nm	nanometer
NP	Nanoparticle
PEG	Polyethylene glycol
RES	Reticuloendothelial system
RH	Relative Humidity
RNA	Ribonucleic acid
rpm	Rounds per minute
SEM	Scanning electron microscopy
SPIONs	Superparamagnetic iron oxide nanoparticles
TEM	Transmission electron microscopy
TGA	Thermogravimetric analysis
TMZ	Temozolomide
TPP	Tripoly phosphate
UV-Vis	Ultraviolet visible
w/o	Water-in-oil
wt %	Weight percent

1. INTRODUCTION

Cancers are very common and life-threatening diseases that one of every three American women and one of two men will eventually acquire one of the different types. It is known that men are more prone to suffer cancer than women. Approximately 910 people were diagnosed with some types of cancer every day in UK. All types of cancer can develop at any age, but more than a third of cancers are recognized in people aged 75 and over. [1].

Cancer is a group of diseases characterized by uncontrolled growth and spread of abnormal cells. If the spread is not controlled, it can result in death. Both external factors (infectious organisms, chemicals, tobacco etc.) and internal factors (hormones, immune conditions etc.) cause all types of cancer for human life. For treatment of cancer, surgery, radiation, chemotherapy, biological therapy, hormone therapy and targeted therapy can be used [2].

It is known that there are many toxic effects of drugs, especially anti-cancer drugs. In order to reduce the side effects and minimize the amount of drug administered to the human body, drug delivery systems were developed. These systems enhance the efficiency and decrease the dose of the drug. The aim of this project is to target an anti-cancer drug temozolomide to the tumor site using magnetic nanoparticles in the presence of an external magnetic field and develop a drug delivery system. Temozolomide, an alkylating agent that can be administered orally, has been approved for the treatment of malignant glioma. However, Temozolomide has very low solubility and stability in aqueous medium thus an inclusion complex is needed which can be achieved by using various types of cyclodextrins having a hydrophobic cavity that can envelope the drug and increase the solubility. On the other hand magnetite nanoparticles play an important role in biomedical applications like drug delivery system because of their excellent magnetic properties and biocompatibility. However, these particles need additional surface treatments in order to be stabilized in carrier fluids which is essential for all biomedical applications. It is also expected for cyclodextrins to improve the stability of magnetic nanoparticles in aqueous medium along with increasing the solubility of the drug. In addition, chitosan is a polysaccharide and being a biocompatible material it is used in many biomedical applications. Chitosan can be used in combination with inorganic materials such as magnetic NPs. Therefore, it is expected that magnetite-

chitosan beads with TMZ can be an useful drug delivery system in order to target anti-cancer drug to the desired area applying an external magnetic field. As a consequence it is aimed to encapsulate TMZ in magnetite-CD-chitosan beads and by applying an external magnetic field where the total entity is targeted to the desired site in vitro. In this way, minimum dose of drug is administered to the human body and side effects are expected to decrease.

In this report, general information about nanoparticles, magnetite, its synthetic formation pathways and corresponding applications such as Magnetic Resonance Imaging (MRI), Magnetic Hyperthermia and drug delivery systems with nanoparticles and cyclodextrins are given in the theoretical background section. Then experimental procedures and characterization methods are introduced in Chapter 3. The experimental results on the synthesis of magnetite nanoparticles and characterizations are presented in Chapter 4 while preparation methods of inclusion complex between Temozolomide and cyclodextrins and characterizations are given in Chapter 5. Preparation methods of chitosan nanoparticles, magnetite-chitosan beads are explained in detail and targeting experiments of Temozolomide are given in Chapter 6. Finally conclusion section gives a general summary and potential future work of the study.

2. THEORETICAL BACKGROUND

2.1 NANOPARTICLES

Nanotechnology is the most important science and is the study of manipulating matter on the atomic, molecular, and supramolecular scale. Nanoparticles are very small particles in the size of nanometers which are very common place in nature. They are generally considered to be a number of atoms or molecules bonded together with a structural radius less than 100 nm at least in one dimension. Generally, NPs are used in several biomedical applications as shown Figure 2.1. [3].

2.1.1. Therapeutics

Many types of NPs are used in drug delivery system. Cancer therapy, gene delivery, site-specific targeting are developing therapeutics in order to reduce side effects of the widely-known therapeutics [4]. For example, paclitaxel, doxorubicin which are chemotherapeutic drugs have been loaded onto different types of NPs and these NP systems can be used in cancer therapy [5, 6].

2.1.2. Diagnostics

Nanomaterials are also used for diagnostic. For example, gold (Au) NPs can offer for multiplex diagnostics to possess sensitive, cost effective, efficient and rapid solutions [7-9].

2.1.3. Imaging

Medical imaging for diagnostics, NPs can be used to enhance the efficacy of fluorescent markers. Although many fluorescent markers are common and used in current research, they have various disadvantages, like fluorescence bleaching, the demand of color-matched lasers, etc. Some NPs such as a fluorescence NPs (silica NPs) and magnetic iron oxide NPs

can overcome these problems so, can be used as imaging agents for effective diagnostics and therapeutics [10-13].

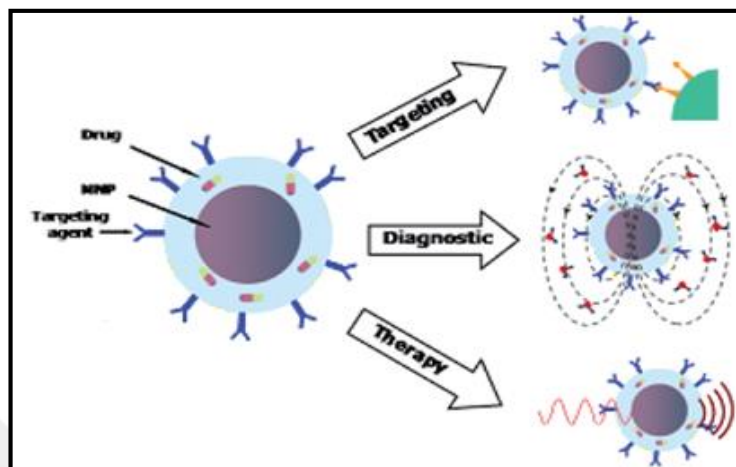


Figure 2.1. Biomedical applications of magnetic nanoparticles [14]

2.2. IRON OXIDES

Sixteen pure phases of iron oxides, i.e., oxides, hydroxides or oxy-hydroxides are known. These are $\text{Fe}(\text{OH})_3$, $\text{Fe}(\text{OH})_2$, $\text{Fe}_5\text{HO}_8 \cdot 4\text{H}_2\text{O}$, Fe_3O_4 , FeO , five polymorphs of FeOOH and four of Fe_2O_3 [15]. Iron oxides have a great significance for many of the processes taking place in ecosystems such as in soils and rocks, lakes and rivers, on the sea floor, in air and in organisms [16]. Moreover, iron oxides in nano-scale are very important because of their extensive applications, such as catalytic materials, wastewater treatment adsorbents, magnetic recording devices, magnetic data storage devices, bioseparation etc.[15]. Iron oxide can exist exist in several forms such as iron oxide (FeO), goethite ($\alpha\text{-FeOOH}$), magnetite (Fe_3O_4), amorphous hydrous ferric oxide (FeOOH), and iron(III) oxide phases such as maghemite ($\gamma\text{-Fe}_2\text{O}_3$), and hematite ($\alpha\text{-Fe}_2\text{O}_3$). Some of their physical and magnetic properties are given in Table 2.1. In addition, iron oxides have several advantages over Fe and Co nanoparticles, e.g., better oxidative stability, compatibility in nonaqueous systems, and nontoxicity [15].

Hematite ($\alpha\text{-Fe}_2\text{O}_3$) is the oldest known of the Fe oxides and is thermodynamically the most stable iron oxides under aerobic surface conditions and therefore, it is the most widespread Fe oxides in soils and rocks.

Table 2.1. Physical and magnetic properties of iron oxides [15]

Property	Hematite	Magnetite	Maghemite
Molecular formula	$\alpha\text{-Fe}_2\text{O}_3$	Fe_3O_4	$\gamma\text{-Fe}_2\text{O}_3$
Density (g/cm^3)	5.26	5.18	4.87
Melting Point, $^\circ\text{C}$	1350	1583-1597	-
Hardness	6.5	5.5	5
Type of magnetism	Weakly ferromagnetic or antiferromagnetic	Ferromagnetic	Ferrimagnetic
Curie Temperature, K	956	850	820-986

It is also known as ferric oxide, specularite or specular iron ore. Color of hematite is blood-red if finely divided, and if coarsely crystalline, black or grey. It is excessively stable at ambient conditions, and frequently is the end product of the transformation of other iron oxides [16, 17].

Magnetite is also known as black iron oxide, magnetic iron ore, or ferrous ferrite. It exhibits the strongest magnetism of any transition metal oxide [16, 17]. If magnetite is under oxidizing conditions ($\text{H}_2\text{O}_2, \text{O}_2$), it is known that magnetite is unstable. In addition, it can be transformed to hematite and maghemite at higher temperatures [18]. Moreover, magnetite have non-toxicity, high biocompatibility and biodegradability so, it is also suitable for nanotechnology and biotechnology areas [19].

Maghemite ($\gamma\text{-Fe}_2\text{O}_3$) occurs in soils or rocks as a product of heating of different iron oxides. It is metastable with respect to hematite, and forms continuous solid solutions with magnetite [16]. Maghemite can be oxidized to the magnetite, in this case the color change is observed from black to red-brown.

When the temperature exceeds 500 °C, ferromagnetic low temperature phase maghemite can be easily transformed into the antiferromagnetic more stable phase hematite. Thus, optimization of the preparation procedure is extremely important in order to prevent formation of undesired product(s). The particle size also plays a critical role. In general, typical particle sizes for the ferro- to superparamagnetic phase transformation are between 10 and 20 nm for oxides [20]. Several researchers have shown that polymers and surfactants can be used in NP synthesis to limit the particle size by affecting the nucleation and growth stages [21-23].

2.2.1. Magnetic Behavior of Iron Oxides

The interaction between Fe ions on adjacent sites is the most significant attribute in order to designate the electron spinings in non-parallel or parallel alignment [24]. Among the different types of iron oxide, magnetite have the highest saturation magnetization (92 emu/g) because of the electron delocalization that can occur between adjoining site of both Fe²⁺ and Fe³⁺ [25].

Relative motion of electric charge of material (spin motion) cause magnetism. Characterization of magnetic phase of materials are determined using magnetism [25]. Magnetism can be classified into five types : diamagnetism, paramagnetism, ferromagnetism, antiferromagnetism and ferrimagnetis as schematically represented in Figure 2.2.

Diamagnetism is a main property of all materials that induced magnetic field in a opposite direction to an externally applied magnetic field, and include small repulsion by a magnetic field. Diamagnetic substance have negative magnetic susceptibility and magnetic susceptibility is independent of the temperature [15].

In the paramagnetic state as seen Figure 2.2, the individual atomic magnetic moments are aligned randomly with respect to each other, and the crystal has a zero net magnetic moment. If an external magnetic field is applied to this crystal, some of these moments will align, and the crystal will have a small net magnetic moment [16]. Superparamagnetism appears when the size of a particle becomes small enough to exhibit single domain and because of thermal agitation the magnetic moment fluctuates in random direction.

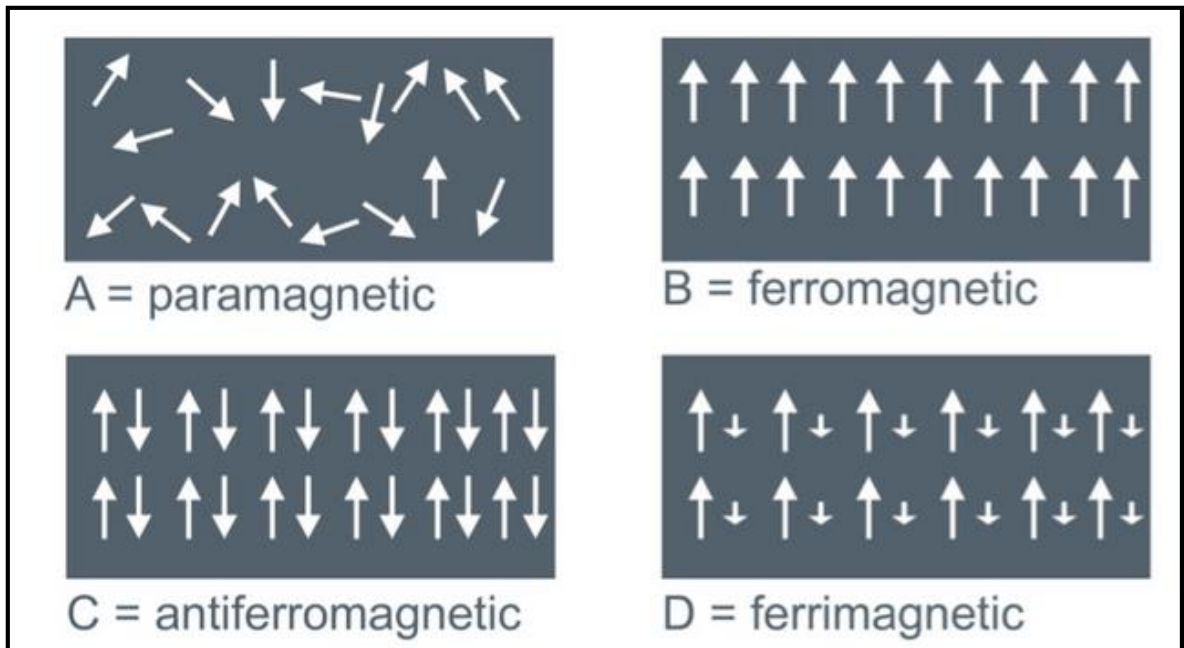


Figure 2.2. Schematic illustration of the main varieties of magnetic order [16]

If the external magnetic field is removed, superparamagnetic nanoparticles do not have net magnetization because of the rapid reversal of the magnetic moment [26]. For instance, the superparamagnetic properties were observed for α - Fe_2O_3 , γ - Fe_2O_3 and Fe_3O_4 with diameters smaller than 20 nm [27], 10 nm [28] and 6 nm [28], respectively.



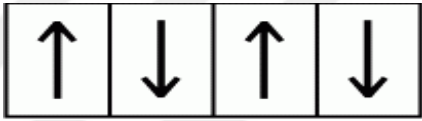
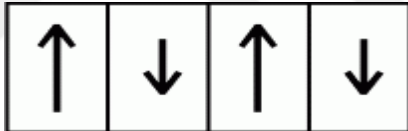

In a ferromagnetic material, the alignment of the electron spins is parallel as shown Figure 2.2. Ferromagnetism substance align equal atomic magnetic moments and produce large net magnetic moment. Therefore, the interaction is attractive towards magnetic pole [29]. With raising temperature, the ordered arrangement of the spins decreases because of the thermal fluctuations of the individual magnetic moments [16].

In an antiferromagnetic substance having magnetic moments of equal magnitude and materials are aligned in an anti-parallel manner is shown Figure 2.2. Such substances produce zero overall magnetic moment. Increasing the temperature usually causes susceptibility to increase because the antiparallel ordering is disrupted [16].

Nevertheless, ferrimagnetic substances consist different strengths of magnetic moments that aligned in an anti-parallel manner like antiferromagnetic materials. However, in this case, the different electron spins have unequal moments, so that a ferrimagnetic substance produce

net magnetic moment in contrast with antiferromagnetic materials is shown Table 2.2 [16, 29].

Table 2.2. Properties of different magnetic states [30]

Type	Arrangement	Lattice	Net
Ferromagnetic	Alignment within the lattice		
Antiferromagnetic	Sublattices, A&B, aligned but antiparallel, equal		None
Ferrimagnetic	Sublattices, A&B, aligned antiparallel, unequal		

Antiferromagnetic, ferromagnetic, and ferrimagnetic materials have a domain structure: single domain refers only the particles in a range from 50 to 500 nm size. The spins within a domain are either parallel or antiparallel, but the different domains have different spin orientations. If high magnetic field applied sufficiently, the domains in a ferro-or antiferromagnetic substance can be eliminated. Therefore, the magnetic field is increased, the spins in the domains become aligned increasingly. If high enough magnetic field is applied, saturation magnetization is reached i.e. the spins of all the domains are parallel [16].

A property which only exists in ferromagnetic substances demonstrates is given Figure 2.3. The magnetization curve displays a hysteresis loop, because all domains do not return to their original orientations when magnetic field (H) is decreased after the saturation magnetization value is attained. This curve refers to the magnetic properties of magnetic

particles are described by the induced magnetization (M) on the applied magnetic field (H) [31, 32].

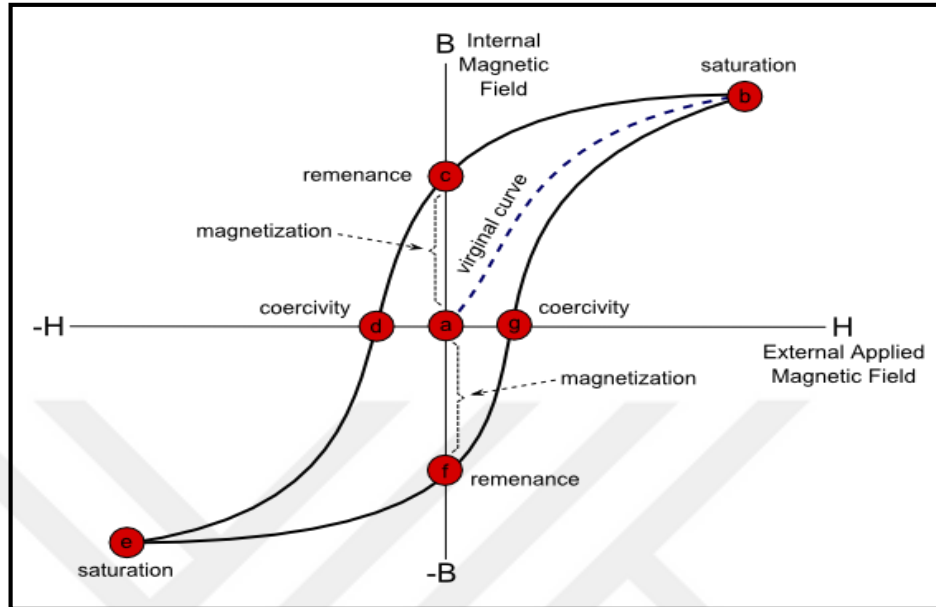


Figure 2.3. Magnetization M as a function of an applied magnetic field H [32]

Initially, the material has never been exposed to a magnetic field, so this leads to position (a) in the curve [32]. If the external magnetic field increases, magnetic domains inside the material align with the external field. At some point, all the dipoles and domains in the ferromagnetic material have been aligned with the external field.

At this point, (b), the material is reached saturation magnetization value and the internal magnetic field increases linearly with the external applied field. Thus, the substance begins to behave more like a paramagnetic or diamagnetic material [32].

At this point if we remove the external field, the internal magnetic field decreases to point (c) in the curve. At that point the substance has become magnetized and refers to have a magnetic remanence. The net magnetic dipole moments of the substance without an external field are not zero at this remanence point [32].

In order to remove this remnant magnetism, a magnetic field in the opposite direction is applied. So, if this opposite magnetic field is applied to continue, the internal magnetic field will continue to drop and at this point will attain a value of zero. This point, (d), implies as the coercivity of the substance. At this point, external applied magnetic field in the negative

direction continue to increase, and then eventually leads to saturation again as point (e). And then, the material starts linearly to increases in external applied magnetic field. Finally, this process going through points (f) and (g) by changing the direction of the external field again [32].

2.3. MAGNETITE

Magnetite also called magnetic iron ore is very common that is opaque, black, metallic mineral in the environment present in soils and pegmatites. It is one of the metal oxides that have the most interesting properties because of the containing both the Fe^{2+} and Fe^{3+} ions [22]. An ordinary synthesis reaction is shown as Figure 2.4.

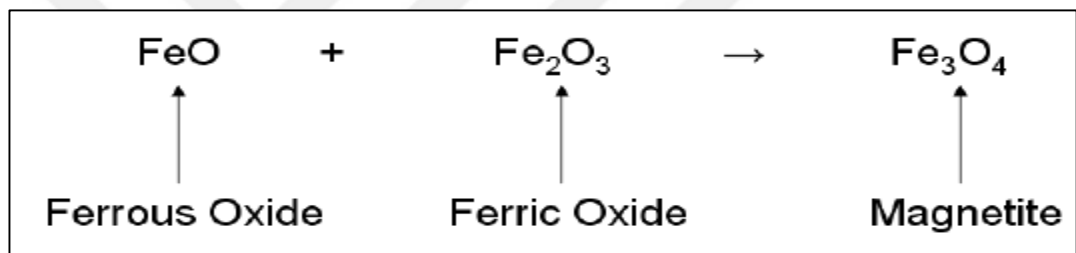


Figure 2.4. Oversimplified magnetite synthesis reaction [33]

A complex pattern of electrons between this two iron ions form magnetic nature. Additionally, it is important that magnetite is the only mineral that is magnetic due to other metallic minerals [28]. In nature, natural organisms are known as various magnetotactic bacteria have been using nano-scale (30-100 nm) magnetic particles in order to orient by using the directional sense of these organisms [22, 34].

2.3.1. Magnetite Synthesis Methods

Magnetic particles can be obtained under different synthesis conditions and many reports have described efficient synthesis approaches to produce the shape controlled, highly stable, biocompatible, and monodispersed iron oxide NPs. In the last decades, much research has been developed in order to prepare homogeneous nanoparticles of iron oxide a kind of

synthesis routes such as co-precipitation, thermal decomposition, hydrothermal synthesis and microemulsion [35-38].

2.3.1.1. Co-Precipitation Method

The most common method for obtaining iron oxides (Fe_3O_4 or $\gamma\text{-Fe}_2\text{O}_3$) is by co-precipitation. This method consists of mixing Fe^{3+} (ferric) and Fe^{2+} (ferrous) aqueous salt solutions by using basic medium such as sodium hydroxide (NaOH) or ammonium hydroxide (NH_4OH) at room temperature or at high temperature and schematic representation of co-precipitation method is shown as Figure 2.5. The co-precipitation method involves Fe^{3+} (ferric) and Fe^{2+} (ferrous) ions at a molar ratio of 1:2. The chemical co-precipitation reaction can be expressed as Eq. (1) [39].



The size, composition and shape of iron oxide NPs depend on the type of salts used (such as chlorides, sulfates, nitrates, perchlorates, etc.), the ferric and ferrous ions ratio, the reaction temperature, the pH, types of stabilization, ionic strength of the media, and the other reaction parameters (e.g. stirring rate) [39].

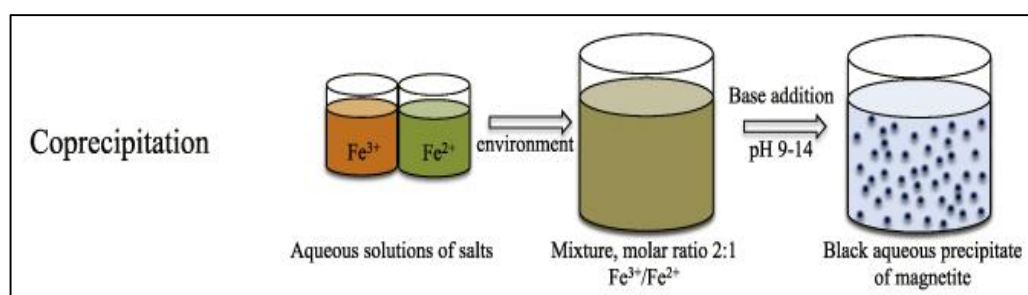
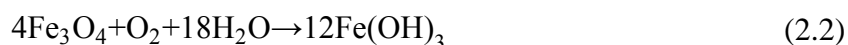


Figure 2.5. Schematic representation of Co-precipitation method [29]

After synthesis, a complete precipitation of magnetite occurs between pH 9 and 14, while sustaining a molar ratio of ferric:ferrous ions as 2:1 in an oxygen free environment. Magnetite NPs are not very stable under ambient conditions and may easily undergo

oxidation to α -Fe₂O₃ or Fe(OH)₃. Magnetite is sensitive to oxygen and in the presence of air as given Eqs. (2) and (3) [29, 40-43] ;

During the synthesis of magnetite NPs must be done in an anaerobic conditions (e.g. using N₂) in order to avoid possible oxidation with air.



Shortly, co-precipitation method is basic and simple large quantities of magnetic particles are got by using this method [36]. After synthesis, magnetic particles are not colloiddally stable and precipitate within seconds. However, various surface modifications can be used where a good control over size and magnetic properties is obtained while establishing colloidal stability. For instance, surfactants or other stabilizers (i.e polymer) can also be added in the reaction medium to generate stabilized nanoparticles [37].

However, the magnetite produced via co-precipitation method are relatively large, of broad size distribution, polydispersity, poor crystallinity, irregular in morphology and difficult to control their nanoparticle shape and size [44].

2.3.1.2. Thermal Decomposition Method

In this synthesis method, organic solution phase decomposition route is used. Thermal decomposition of organometallic compound in high boiling organic solvent in the presence of various stabilizing surfactants has become a improved technique in order to achieve monodisperse and uniform iron oxide nanocrystals [18, 44]. The iron precursors can be either, acetates [45], oleates [45], carbonyl [46] or oxalates [45], while high boiling solvents can be used such as benzyl ether or octadecene [36]. Various types of organic amines are used i.e. oleylamine, trioctylamine, oleylamine, and hexadecylamine. Additionally, alcohol, oleic acid

can be used as surfactants [37]. An illustration of magnetite nanoparticles synthesis by thermal decomposition method is shown as Figure 2.6.

The thermal decomposition technique is used in order to produce high quality iron oxide i.e. Fe_3O_4 nanoparticles [47]. The magnetite particles obtained by using thermal decomposition method are have high crystallinity [48], monodisperse [48] and can be can be obtained desired size and shape [36].

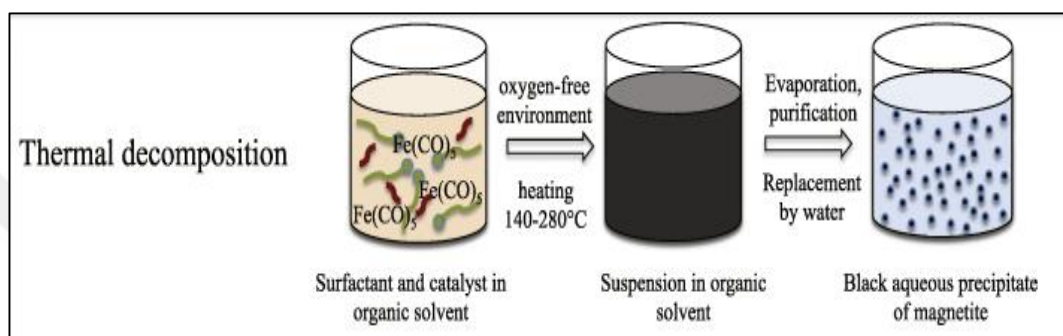


Figure 2.6. An illustration of magnetite nanoparticles synthesis by thermal decomposition method [37]

Although the thermal decomposition method has many advantages but, it has some disadvantages that require of relatively high reaction temperature [47], possible emission of toxic gases like CO [37], usage of not environmental friendly reagents [48], complicated procedures [47] and usage of multiple [47]. Moreover, obtained particles are usually insoluble in water or only soluble in some non-polar solvents.

2.3.1.3. Microemulsion Method

Microemulsion is a thermodynamically stable liquid mixture of two immiscible phases as water and oil under the surfactant present. Water and oil phases are stabilized by the arrangement of surfactant molecules that may form a monolayer at the interface between the oil and water, with the hydrophobic tails of the surfactant molecules dissolved in the oil phase and the hydrophilic head groups dissolved in the aqueous phase [48].

Particularly, water-in-oil (w/o) microemulsions are also called as reverse microemulsions formed by well-defined nanodroplets of the aqueous phase, dispersed by the assembly of

surfactant molecules in a continuous oil phase [48]. Magnetite nanoparticles can be synthesized by using reverse microemulsion method also is shown in Figure 2.7.

Microemulsions has some advantages such as environmental friendly synthesis method, economical and uniform nanoparticles. However, this method provide the major drawback is the usage of large amount of solvent to synthesize a significant amount of nanomaterials [49].

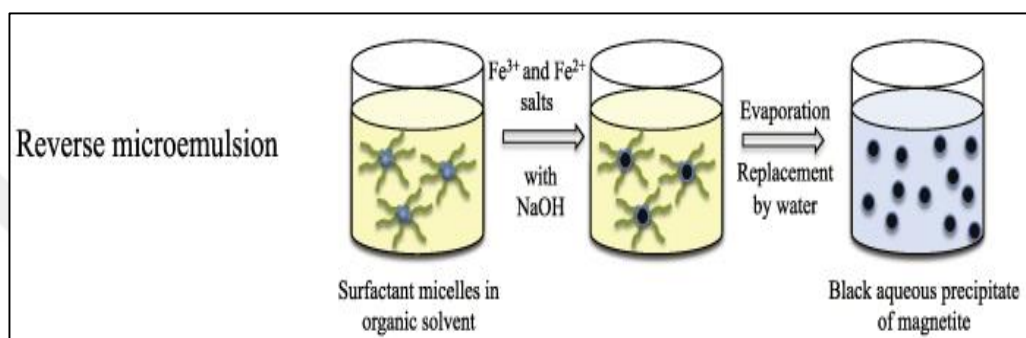


Figure 2.7. An illustration of magnetite nanoparticles synthesis by reverse microemulsion method [48]

2.3.1.4. Hydrothermal Synthesis

During the synthesis of iron oxide NPs, controlled size and shape are very significant because of the strong correlation between these parameters and magnetic properties. For the thermal decomposition and microemulsion method, relatively high temperatures are required or very complicated process are used [18]. Alternatively, water is used as a dispersion medium and organic compounds and polymers are used as stabilizer and dispersant in the hydrothermal process. For example, α -Fe₂O₃ nano structures have been synthesized hydrothermally using poly(vinyl pyrrolidone) as surfactant and sodium acetate as precipitation agent [50]. The purpose of the high heat energy and pressure during this synthesis is to increase the dissolution of iron precursors and fracturing from macronucleus to nanoscale particles.

Table 2.3. Comparison of the synthesis methods of magnetic nanoparticles [43]

Synthesis Method	Reaction Condition	Advantages	Disadvantages
Co-precipitation	Temperature : 20-90 °C Duration : minutes Solvent : water	Easy and low cost method Rapid synthesis with high yield	- Difficult to avoid nucleation - Obtained weak magnetic response particles - easily oxidation particles
Thermal Decomposition	Temperature : 100-320 °C Duration : hours-days Solvent : organic compound	High quality magnetite nanoparticles	- Require high temperatures - Complicated procedures - Required multiple reagents
Microemulsion	Temperature : 20 - 50 °C Duration : hours Solvent : organic compound	Very uniform particles	-Large amount of solvent
Hydrothermal	Temperature : 150-220 °C Duration : hours-days Solvent : water-ethanol	High yields of products Good morphology Relatively cost effective	-Slow kinetic due to the relatively low temperature

However, several researchers said that higher temperature can cause bigger particle size. After hydrothermal synthesis, the resulting nanoparticles had narrow particle size distribution, high degree of crystallinity as well as weak agglomerated powders [38].

The four above mentioned synthesis methods have some advantages and disadvantages. Thermal decomposition and hydrothermal synthesis route is the optimal method in order to control size and morphology of the iron oxide NPs. Co-precipitation method can be used to obtain water-soluble as well as biocompatible iron oxide NPs but, this methods shows synthesized particles have low control of the particle shape, aggregation of particles as well as broad distributions of sizes [36].

The advantages and disadvantages of the different methods of preparation of Superparamagnetic Iron oxide Nanoparticles (SPIONs) are mentioned briefly in Table 2.3.

2.5 APPLICATIONS OF MAGNETIC PARTICLES

The important property of magnetic particles is their response to the magnetic force. For biomedical applications, magnetic particles should have a high saturation magnetization because of the two reasons. Firstly, the movement of the magnetic particles can be controlled with applied external magnetic field. Secondly, the magnetic particles can be moved close to the tumour side. In addition, magnetic nanoparticles should be sufficiently small (10-50 nm), biocompatible, non-toxic, injectability and stable in aqueous medium at pH=7. Furthermore, iron oxide particles such as magnetite (Fe_3O_4) or its oxidized form maghemite ($\gamma\text{-Fe}_2\text{O}_3$) are most common for biomedical applications [51].

For biomedical applications, it is very important that nanoparticles have to be able to elude the reticuloendothelial system (RES). After nanoparticles are injected into the blood, they are coated with blood plasma protein. This process is called as opsonization. Hydrophilic nanoparticles (e.g. surface coating with dextran, PEG) oppose opsonization so, they increase the probability of achieving to target cells in the body [52, 53].

In almost all applications, the preparation and surface modification of magnetic particles affect the particle size and shape, the size distribution, the surface chemistry and consequently the magnetic properties of the particles, all parameters are very important for

application in biomedicine. Its application can be classified into two categories, that is, *in vitro* and *in vivo*. For *in vitro* applications, the main use is in diagnostic and separating of biomolecules, such as protein, cell, DNA/RNA, microorganism, and for *in vivo* applications can be further divided into therapeutic such as drug delivery and hyperthermia and diagnostic applications such as magnetic resonance imaging (MRI) [51].

2.5.1. Magnetic Resonance Imaging (MRI)

Nanoparticles, especially superparamagnetic iron oxide NPs have been used as contrast agents for *in vivo* and *in vitro* cellular and molecular imaging. Magnetic Resonance Imaging is a clinical diagnostic technique for mainly soft tissue or recent cartilage pathologies because of the different relaxation times of protons. In this way, superparamagnetic NPs increase the diagnostic specificity and sensitivity so, they are used to differentiate between healthy and diseased tissue in the human body [53].

Kim *et al.* synthesized ferrofluids which contains oleic acid (as a surfactant) coated magnetic nanoparticles for MRI contrast agents and then, these nanoparticles dispersed in the chitosan solution that is the convenient carrier for biomedical applications. MRI images of the ferrofluids with the images of Resovists® (a commercially available contrast agent for MRI) are compared. Their study showed that the ferrofluids exhibited enhancement of the MRI contrasts comparable to Resovist® *in vitro* [51].

2.5.2. Magnetic Hyperthermia

Another promising application of magnetic nanoparticles is hyperthermia treatment. Hyperthermia treatment can be used as a supplementary treatment for many applications such as chemotherapy, radiotherapy, and surgery in cancer therapy [54]. This opinion is based on the principle that a magnetic particle can generate heat by hysteresis loss under a magnetic field. Magnetic hyperthermia utilizes magnetic NPs as heat sources in order to raise tissue temperature to 43°C at tumour cells that is known to be more sensitive to heat than healthy cells [55]. In the below Figure 2.8. shows that the particles are first injected in

(a) tumour and, then, (b) an externally applied alternating magnetic field induces the hyperthermia.

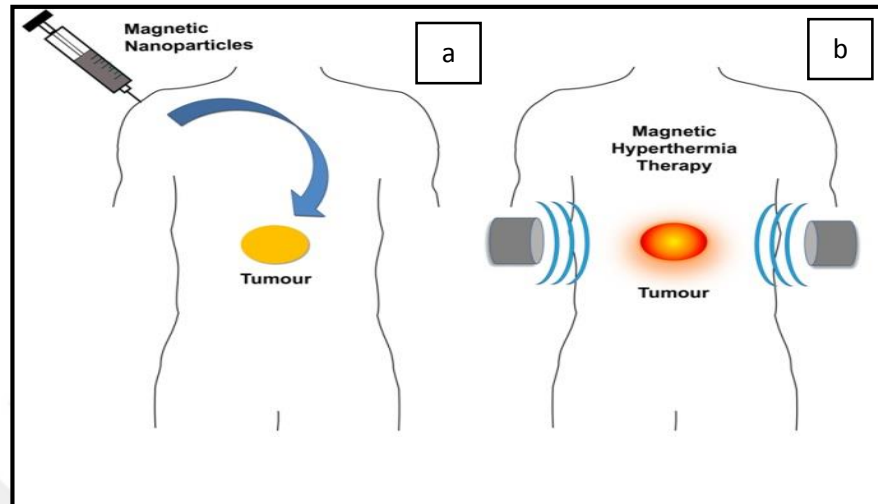


Figure 2.8. General Hyperthermia procedure for cancer therapy [55]

Magnetic particles embedded around a tumor site in the body and applied magnetic field then, heat up to a desired temperature. This desired temperature is dependent on the strength of the magnetic field, the magnetic properties of the material, and the cooling capacity of the blood flow in the tumor site of the human body. Thus, when a magnetic fluid is sustained to a various magnetic field magnetic nanoparticles become heat sources. Obtained powerful heat source is destroying only tumor cells whereas the normal cells can survive at temperatures higher than 43 °C [56, 57].

2.5.3. Drug Delivery & Targeting

The utility of many drugs is usually limited due to their potential to reach the specific site of therapeutic effect. Required drugs such as chemotherapy drugs are oriented for general system distribution often intravenously in human body. In many cases, only a very small amount of drug reaches the target site so, drug orientation causes many side effects as they attack the target cancer cells and also normal healthy cells. Therefore, a drug delivery system should be developed that optimizes the therapeutic action of a drug while reducing its deleterious side effects for human body [58].

Colloidal drug carriers can provide a targeted drug delivery associated with optimal drug release profiles. Among these many carriers, many types of micro/nanoparticles and liposomes have been the most extensively investigated. First of all, liposomes have some limitations for drug targeting such as poor stability and reproducibility, and low drug entrapment capability. However, many low molecular weight drugs are suitable to be delivered with this technique. In order to overcome these several problems, polymeric nanoparticles can be used as possible drug carriers because of the better stability and reproducibility than liposomes. The size of the NPs which are solid colloidal particles can be 1-100 nm. NPs can be used therapeutically as drug carriers in which the active compound is encapsulated, adsorbed, entrapped, dissolved and chemically attached. There are two types of drug loaded NPs for drug delivery based on preparation process [59]:

- Nanospheres
- Nanocapsules

Nanospheres have a matrix structure in which active ingredient are adsorbed or dispersed onto their surfaces of the particles. Nanocapsules possess a membrane-wall structure and active compound are adsorbed onto their exterior or entrapped in the core of the particles. These particles are shown as Figure 2.9.

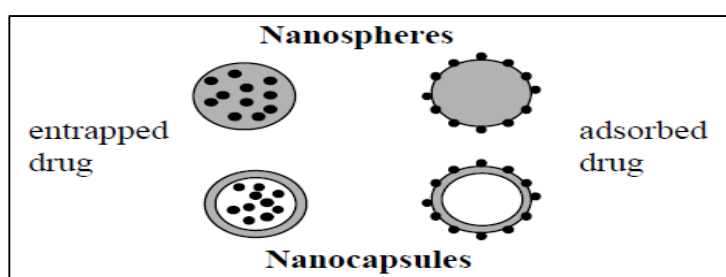


Figure 2.9. Types of drug loaded nanoparticles [59]

2.5.3.1. Drug Delivery with Nanoparticles

Nanoparticles (NPs) have been developed as an important strategy to deliver conventional drugs. NPs and other colloidal drug-delivery systems modify the kinetics, body distribution and drug release of an associated drug [54].

Nowadays, nanotechnology have an important impact on the drug delivery system and nanoparticles (NPs) can be used for many potential applications in biomedicine and research. Nanotechnology concentrate therapeutic agents nanocarriers for biomedical applications such as NPs, dendrimers and miceller systems. NPs have been developed as a significant approach in order to deliver many drugs, proteins and recently, nucleotides. NPs and other colloidal systems for drug delivery are very advantageous for modifying the kinetics and release of an associated drug [54].

Most of the drugs have some disadvantages such as their, high toxicity, high dosage, poor solubility, aggregation because of the poor solubility, nonspecific delivery, and short circulating half-lives but now, drug delivery system is developing rapidly in order to reduce drug dosage and side effects on healthy cells, increase patient compliance, provide product differentiation, reduce healthcare costs and extend the product life cycle [54].

Several types of NPs can be utilized for drug delivery system. Drugs can be loaded onto NPs by using some methods, such as surface attachment, encapsulation etc. NPs can pass through across barriers efficiently through small capillaries into individual cells because of their small size. In this manner, efficient drug accumulation is obtained at the target site in the body. Therefore, the undesirable side effects and the toxicity is decreased and the therapeutic efficacy is improved. Thus, nanoparticles can help to improve poor bioavailability or drug instability for therapeutic. In order to improve the stability of NPs, polymeric surfactants or modifiers can be used and are adsorbed to particles. After the NPs are coated with the polimeric surfactants, a layer forms and then, this layer generates an effective repulsive force between NPs so, this force prevents flocculation [60].

There are a lot of advantages of nanoparticles for drug delivery system. Advantages of nanoparticles are listed below.

Advantages of nanoparticles:

- Enhance the aqueous solubility of the drug
- Protect the drug from degradation
- Produce elongated release of the drug
- Enhance the bioavailability of the drug
- Target the drug to the specific site (e.g.tumour site)

- Reduce the toxic side effects of the drug

Many types of NPs can be used as drug-delivery systems. Types of NPs are Polymeric NPs, Solid-lipid NPs, Metal based NPs and Polymeric micelles etc [60].

Polymeric NPs: Almost polymeric NPs are biodegradable and biocompatible, in the past, researchers have had study for developing biodegradable NPs as a drug- delivery system. Moreover, they also display a good potential for surface modification and functionalization so, this property produce excellent pharmacokinetic control. Depending on their preparation technique, these can be NPs, nanospheres or nanocapsules. Nanospheres have a matrix, desired compounds or complexes can be dissolved in this matrix. Nanocapsules have two parts as a an inner core and polymeric shell. In this way, a desired compund can be adsorbed at their surface but, is usually dissolved in the core [58]. NPs should be small size and cells that is the most important advantage for drug-delivery applications due to the effective drug accumulation at the target areas [61].

Solid-lipid NPs: Solid lipid NPs were an alternative colloidal carrier system to liposomes and polymeric NPs for drug delivery system. These NPs are created from solid lipids and can be stabilized by different surfactant(s). Considering other carriers, solid lipid NPs has some advantages for controlled drug delivery. These advantages are biodegradability, a high bioavailability and good tolerability [62-64].

Metal based NPs: Metal NPs have very small sizes as approximately 40-50 nm that is the advantage for the carrying a higher dose of drugs. Au NPs are the most common metal and have many advantages for drug delivery system. For instance, it is very easy to synthesize and Au NPs are biocompatible and nontoxic [65].

Polymeric micelles: Polymeric micelles consists two monomer units as hydrophilic and hydrophobic. Micelle-forming surfactants improve the solubility of the poorly soluble drug in water. They also enhance their permeability across physiological barriers. In addition, they also decrease side effects and the toxicity associated with some drugs [66].

Magnetic Nanoparticles: The major drawback of many drugs are non-specificity for biomedicine. The non-specific technique cause many side effects because, cytotoxic effect of drug invade normal, healthy cells and also tumour cells. In order to overcome this

disadvantage iron oxides with core/shell structure can be used as sources of magnetic materials [56]. Iron oxides consists of some crystalline polymorphs known as especially hematite, maghemite, magnetite in spite of that only maghemite and magnetite are the most important materials for biomedical applications. These particles can be manipulated in aqueous medium by the application of an external magnetic field which make them attractive in targeting studies [21, 67].

Magnetic NPs are the most important materials in many sectors, especially are used for biomedical and biotechnological applications. For biomedical applications, size and magnetism of the nanoparticles are the critical properties. Moreover, field strength and geometry, the chemical properties of the drug-MNPs, depth of the target tissue, rate of blood flow, and vascular supply play a role in order to determine the effectiveness of drug delivery system. Furthermore, magnetic NPs can be used for cancer treatment in different ways. Firstly, magnetic NPs can be targeted for hyperthermia for cancer therapy, secondly, active compound can be loaded onto the magnetic NPs for drug targeting and finally, specific antibodies can be conjugated to the magnetic NPs in order to prevent tumour growth [68].

The biocompatibility and toxicity of magnetic NPs are other significant properties for biomedicine. They have a high magnetization thus, their movement can be controlled easily with external magnetic field in the blood flow. Increasing the magnetization is the very important advantageous to promote manipulation in drug delivery system [54]. The magnetic NPs must be small so, they can have superparamagnetic properties at room temperature in order to avoid agglomeration after removing magnetic field and to remain in circulation system without being removed by the body's natural filters such as the liver [69]. Superparamagnetic nanofluid is preferred because, it has great magnetization when nanofluid is subjected to an external magnetic field however, retain no permanent magnetism once the magnetic field is removed.

As an alternative to chemotherapy, anti-cancer agents adsorbed on the surface of the magnetic NPs is promising in magnetic drug targeting. The anti-cancer drug is loaded to the magnetic NPs and these magnetic NPs are injected into the vascular systems and then targeted to the desired site with external magnetic field and then finally, drugs are released on the target site as shown like Figure 2.10. [70]. Magnetic particles that are smaller than $4\mu\text{m}$ are eliminated by cells of the RES, especially in the liver (60–90%) and spleen (3–

10%). Additionally, the size of the magnetic particles that are larger than 200 nm are mostly filtered to the spleen, whose cut-off point extends up to 250 nm, while particles up to 100nm are mainly phagocytosed through liver cells [71]. In most studies the superparamagnetic particles employed are in the range of 10-20 nm which is a very appropriate size to be eliminated in the body.

In order to control the surface properties of magnetic NPs, particles can be coated with a biocompatible polymer during or after the synthesis. Coating of magnetic NPs with desired polymers is the most commonly used way partly because of the stability of magnetic NPs against oxidation and partly due to the ability of polymers to assist in drug carrying [71].

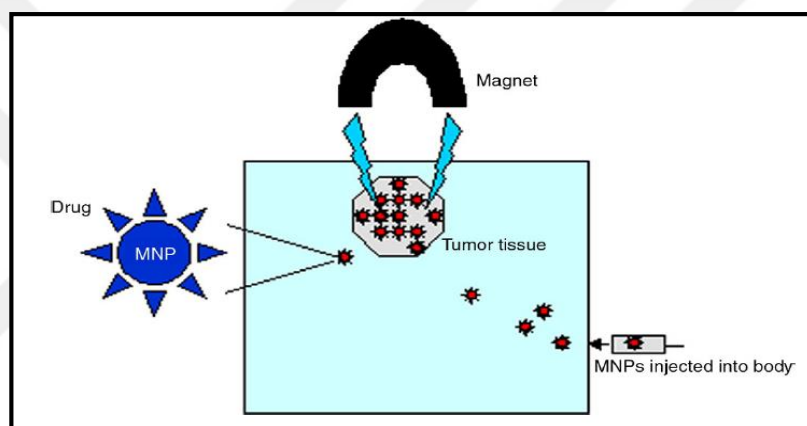


Figure 2.10. MNPs specifically targeted to the tumor tissue with the help of an external magnetic field [70]

2.5.3.2. Drug Delivery with Cyclodextrin

CDs have multifunctional characteristics so, they can use for some drug delivery systems like controlled and targeted drug delivery system, brain targeting, ocular drug delivery system, transdermal drug delivery system, nasal drug delivery system, oral drug delivery system etc [72].

Controlled and Targeted Drug Delivery System: Most of the works about the CDs shows that it can be used to improve the release rate of drugs and some current work demonstrates that CDs are used as carriers in controlled release and targeted drug delivery system. There are a lot of CD derivatives such as alkylated and acylated derivatives (hydrophobic CDs) are

used to extend the release of drugs, additionally hydrophilic derivatives of CD are used to improve the release rate [73]. Some drugs are formulated in order to enhance drug release like Prednisolone [74], Verapamil [75] and control release like Piroxicam [76], Diltiazem [77] using different CDs and derivatives [78].

Brain Drug Delivery (Brain Targeting): The concept of Bodor's chemical delivery system (CDS) (for example, covalent coupling of drugs to 1-methyl-1,4 dihydronicotinic acid through an enzymatically labile linkage, which improves drug lipophilicity) was utilized for targeting many drugs such as calcium channel antagonists, steroids, antitumor active agents to brain. Nevertheless, prodrug of CDs have poorly water soluble due to lipophilic moiety. H- β -CD enhance the solubility of CDs are because it helps to soluble drugs and also to improve the chemical stability of dihydronicotinic acid in aqueous medium [79-82].

Ocular Drug Delivery System: In an ocular drug delivery, dosage form for eye drop is very significant because of the instillation in the eye. However, some disadvantages are investigated about this dosage form such as its inadequacy to maintain high local concentration of active agent (drug) [83]. CDs have been used to enhance the solubility, stability, permeability and bioavailability of drugs and to decrease side effects of drugs like irritation and discomfort [84].

Transdermal Drug Delivery System: Outer layer stratum corneum is the first barrier for dermal drug absorption. In general, alcohols, fatty acids are used as penetration enhancers in order to reduce its barrier properties. In the topical preparations, CDs enhances solubility and stability of drugs, maintains the drug release, improves the transdermal absorption [85]. CDs do not enhance drug delivery through hydrophobic barriers like stratum corneum, but enhance through aqueous diffusion barrier. Additionally, CDs should not change the pH of the skin, cause skin irritation and interact with any substance of the skin [86].

Nasal Drug Delivery System: In order to increase the solubility of hydrophobic drugs in aqueous medium, CDs should be used in nasal formulations. The hydrophobic CDs behaves as penetration enhancers in nasal delivery of peptides . In nasal delivery, using CDs are very effective because, they should show ciliostatic effect, cause irritating and allergenic effect, and they should improve the permeation of some drugs across nasal epithelium [87].

2.5.3.3. Drug Delivery with Chitosan Nanoparticles

Some of the poorly soluble drugs involved in amphiphilic chitosan-based nanoparticles are anti-cancer drugs such as paclitaxel, camptothecin and doxorubicine. In addition to enhancing their solubility, the polymeric micelles help passive targeting in the tumor side due to improved retention (EPR) effect and permeability. This is “passive targeting”. For successful passive targeting, size and stability are very important parameters. If the particles circulate in the blood flow for longer period, particles reach tumor sites effectively. Furthermore, many therapeutic agents were investigated like anti-HIV, antifungal, and anti-inflammatory agents [88].

As a result, chitosan NPs have some advantages for drug delivery systems so, they can be used in systems such as parenteral, ocular, mucosal, brain targeting and control drug delivery.

In Parenteral Drug Delivery: The size, lipophilicity and surface charge effect biodistribution of NPs [89]. If the size of the particles are greater than 100 nm, they are absorbed rapidly by the reticuloendothelial system (RES), while smaller ones tend to extend circulation time. If the hydrophilic coating like polyethylene glycol (PEG) or nonionic surfactant are used on hydrophobic carriers, circulation time improves significantly [90]. Some studies show that chitosan NPs have a tendency to accumulate in many tumors [91]. The reason of this phenomenon can be the leakiness of tumor vasculature [92]. NPs can be controlled intravenously, because the diameter of the smallest blood capillary is approximately 4 μm [90]. It is investigated that Doxorubicin loaded chitosan NPs show improved survival rate of tumor after IV administration and regression in tumor growth [58].

In Ocular Drug Delivery: Ophthalmic formulation based on chitosan shows an excellent tolerance after using chitosan onto the rabbit's corneal surface due to the low toxic material chitosan [93]. Additionally to improve drug transport via ocular, chitosan NPs have the ability to improve the corneal penetration [94]. Some research shows that chitosan NPs attach to the rabbit's cornea and conjunctiva for 24 hours [95]. For topical ophthalmic delivery of antibiotic, gatifloxacin, the mucoadhesive chitosan-sodium Alg NPs have been studied as a new vehicle [96].

In Brain Targeting: Chitosan nanoparticles have been used after coating with Polysorbate 80 for brain targeting of the many drugs [97]. For treatment of central nervous system diseases, chitosan NPs can be utilized in order to enhance the brain targeting efficiency by the nose to brain pathway of the human body for many drugs. Chitosan NPs can combine the active drug and then, they target to the olfactory region with controlled release in order to maintain the desired active drug on the absorption site [98]. In addition, the estradiol chitosan NPs are an appropriate formulation for estradiol delivery to central nervous system because, they have higher estradiol concentration in cerebrospinal fluid (CSF) (which is the clear, colorless body fluid in brain) at each sampling time for intranasal delivery [99].

In Control Drug Delivery: Chitosan NPs are also applicable for controlled drug delivery. Colloidal chitosan particles can form easily by using some methods and entrap bioactive molecules. The mechanisms can be ionic crosslinking, ionic complexation and chemical crosslinking. In order to control drug release profile, chitosan is modified by some chemicals and chemical modification is utilized for the association of some bioactive molecules to polymer. Coating agents for liposome formulation is useful for the high chemical attraction of chitosan for cell membranes [100].

In Mucosal Drug Delivery: Many studies have shown that chitosan and their derivatives are used as safe absorption enhancers and are effective for the enhancement of mucosal delivery of peptide and protein drugs which are called as hydrophilic macromolecules [101, 102]. Mucus are highly hydrated glycoproteins which consist of salts, lysozyme and mucins and it has viscoelastic properties. Many reports shows that intercellular tight junctions open because of favouring the paracellular transport of many drugs [101, 103, 104]. The presence of mucus affects drug permeability freely and interaction electrostatically with cationic molecules like chitosan.

In this work, bare and three different types of CDs coated magnetite nanoparticles are synthesized by co-precipitation method. In addition, only chitosan nanoparticles and magnetite-chitosan beads are synthesized by ionic gelation method. An anti-cancer drug, TMZ is incorporated in the chitosan-magnetite beads to obtain a drug delivery system. Thereafter, targeting of anti cancer drug Temozolomide was carried out with magnetite-CD and magnetite-chitosan beads to simulate drug delivery systems, and optimum formulations for targeting are investigated.

3. MATERIALS AND METHODS

3.1. MATERIALS

Table 3.1. Chemicals for the synthesis of magnetite nanoparticles by co-precipitation method [100]

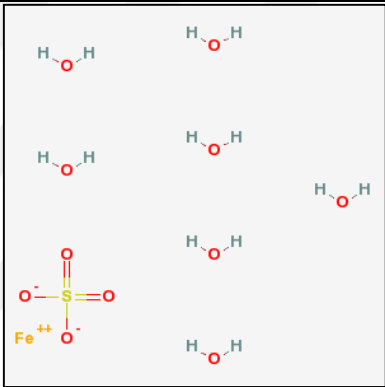
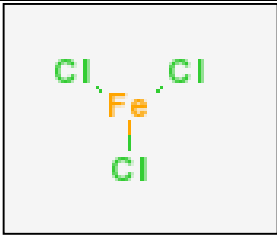
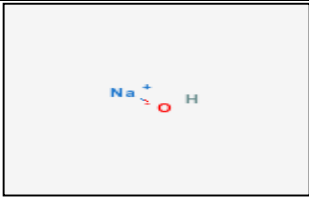
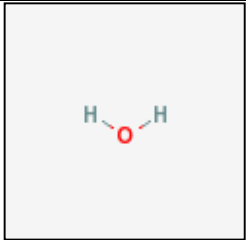
Chemical name	Formula	Structure	Provider	Purity
Iron (II) sulfate heptahydrate	$\text{FeSO}_4 \cdot 7\text{H}_2\text{O}$		Riedel-de Haen	90%
Iron (III) Chloride	FeCl_3		Riedel-de Haen	97%
Sodium Hydroxide	NaOH		Riedel-de Haen	99%
Water	H_2O		-	-

Table 3.2. Chemicals used for Tiron metal test

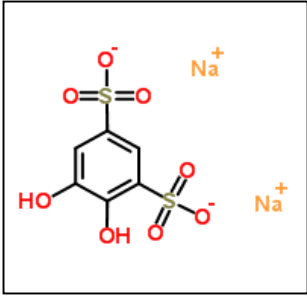
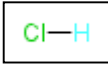
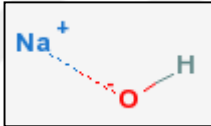
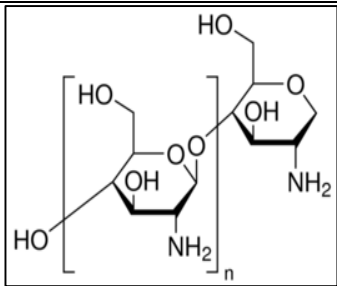
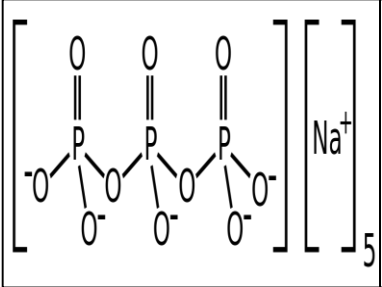
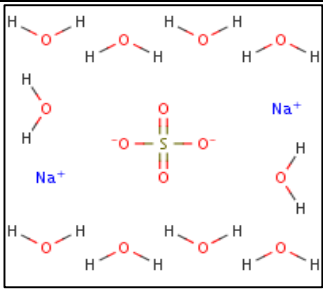
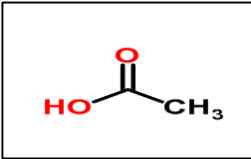
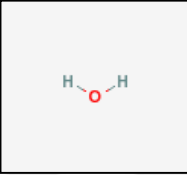
Chemical name	Formula	Structure	Provider	Purity
Tiron	$C_6H_4Na_2O_8S_2$		Riedel-de Haen	98.5%
Hydrochloric Acid	HCl		Merck	98.5%
Sodium Hydroxide	NaOH		Fluka	99%

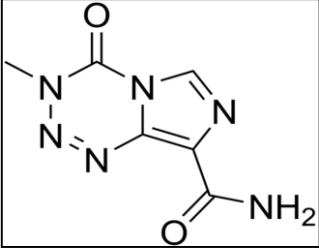
Table 3.3. Chemicals used for chitosan NPs synthesis

Chemical name	Formula	Structure	Provider	Purity
Chitosan	$C_6H_{11}NO_4$		Sigma Aldrich	-
Tripolyphosphate	$Na_5P_3O_{10}$		Sigma Aldrich	100%

Sodium Sulfate Decahydrate	$\text{Na}_2\text{SO}_4 \cdot 10\text{H}_2\text{O}$		Acros Organics	-
Acetic Acid	CH_3COOH		Sigma-Aldrich	$\geq 99.85\%$
Water	H_2O		-	-

3.1.1. Temozolomide

Table 3.4. Properties of Temozolomide

Chemical name	Formula	Structure	Provider
Temozolomide	$\text{C}_6\text{H}_6\text{N}_6\text{O}_2$		Koçak

Only 2% of all adults suffer from brain cancer, but brain tumours are debilitating malignant diseases. The most widespread type of brain tumours are malignant gliomas, among the most rapidly growth gliomas are high-grade gliomas. These types of tumours are leading to death rapidly in spite of surgery and radiotherapy[105].

Temozolomide (TMZ) has broad spectrum antineoplastic activity which is an anticancer active agent [106]. TMZ is the most common monofunctional alkylating agent prodrug of the many malignant brain tumours because it has perfect penetration to all cells into the body and also is able to pass the blood-brain barrier (BBB). So, TMZ is an impressive drug for malignant melanoma and other many several advanced cancers in human body [107].

Dacarbazine is the another active agent for brain cancers. Both Temozolomide and Dacarbazine converts to the active metabolite 5-(3-methyl)1-triazen-1-yl-imidazole-4-carboxamide (MTIC) as shown Figure 3.1. but, Temozolomide has many advantages over Dacarbazine [108].

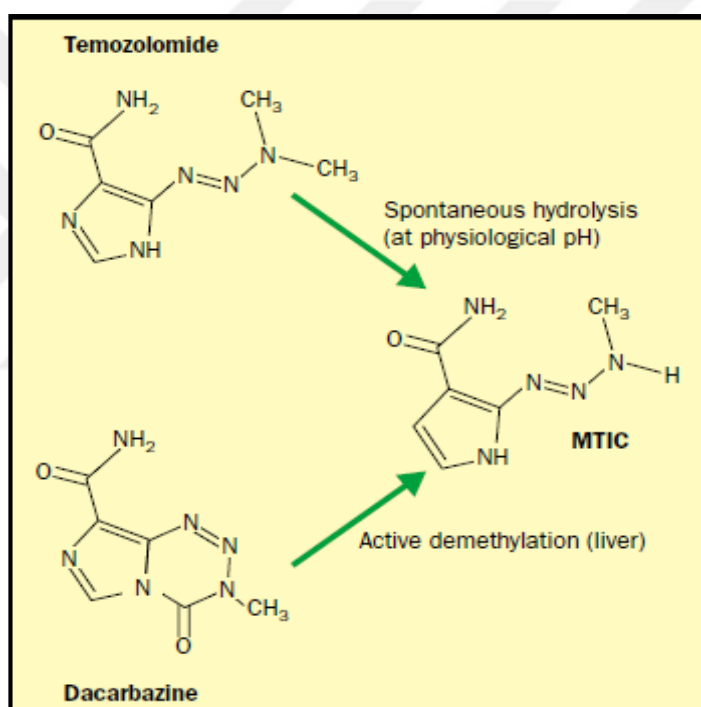


Figure 3.1. Temozolomide and dacarbazine and their common active metabolite, MTIC [105].

One of the advantages is that after oral administration, Temozolomide is activated into the reactive species which is completely and rapidly absorbed and converts spontaneously at physiological pH into the human body without any enzymatic demethylation [109]. However, Dacarbazine converts to MTIC due to the enzymatic demethylation of the liver in the body [110].

The antitumor active agent temozolomide (TMZ) decomposes in $\text{pH} \geq 7$ of aqueous medium but, it is more stable under acidic medium. Pure TMZ is observed as a white powder but, TMZ turns pink and brown when chemical degradation takes place as shown Figure 3.2. This color change is indicative of degradation to AIC upon storage, so active compound of TMZ is less effective. Figure 3.2. shows that color of pure TMZ turns from light pink to dark brown in the first week for 7 weeks experiment. Stability studies of TMZ in solid state shows that hydrolytic degradation is occurred at 40 °C and 75% relative humidity after one week which is determined by using Powder X-Ray Diffraction. TMZ is crystalline and nonhygroscopic material. The stability problem of TMZ is very important for brand name Temodar or Temodal which is the brand name of TMZ [111].

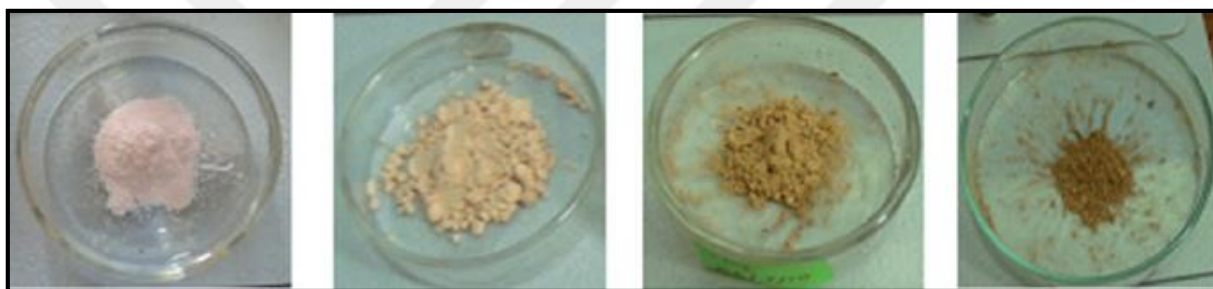


Figure 3.2. Physical stability and color comparison of pure TMZ 40°C and 75% Relative Humidity [111].

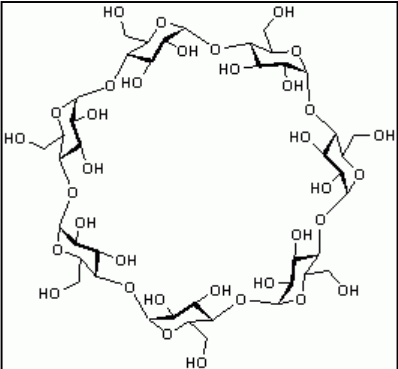
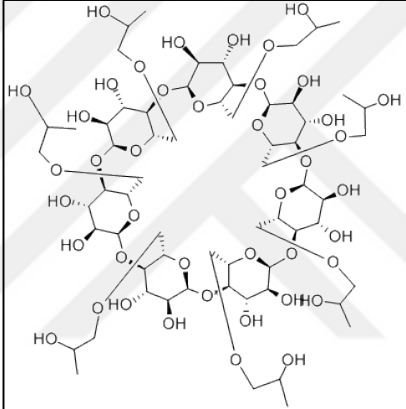
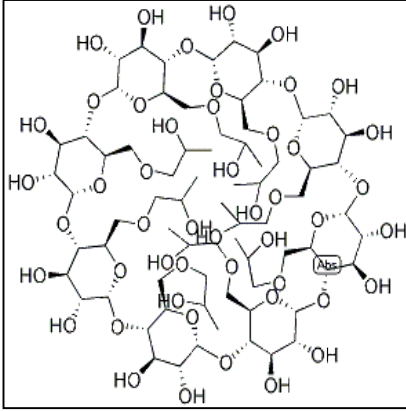
Therefore, some special storage precautions are very important such as humidity, desiccants, low oxygen and light levels in order to enhance the shelf life and stability of the TMZ. Pure white temozolomide can be stored at 45% relative humidity (RH) for after 24 hours.[108].

3.1.2. Cyclodextrins

Cyclodextrins are cyclic oligosaccharides which contain at least six D-(+) glucopyranose units attached by α -(1, 4) glucosidic as shown in Table 3.4. They are also called cyclomaltoses and cycloamyloses [113].

Shape of cyclodextrins are like cones because of the chair formation of the glucopyranose units which have primary and secondary hydroxy groups as shown Figure 3.3.

Table 3.5. Properties of Different Types of Cyclodextrins [112]

Chemical name	Formula	Structure	Provider	Purity
β -Cyclodextrin	$C_{42}H_{70}O_{35}$		Sigma-Aldrich	%97
2-hydroxy propyl β -Cyclodextrin	$C_{42}H_{70}O_{35}$		Sigma-Aldrich	-
2-hydroxy propyl γ -Cyclodextrin	$C_{42}H_{70}O_{35}$		Sigma-Aldrich	-

Primary hydroxy groups stretch from the narrow edge and secondary groups stretch from the wider edge due to this structure. As seen Figure 3.4, cyclodextrin molecules have a hydrophilic outer surface, while they have hydrophobic inner cavity [114].

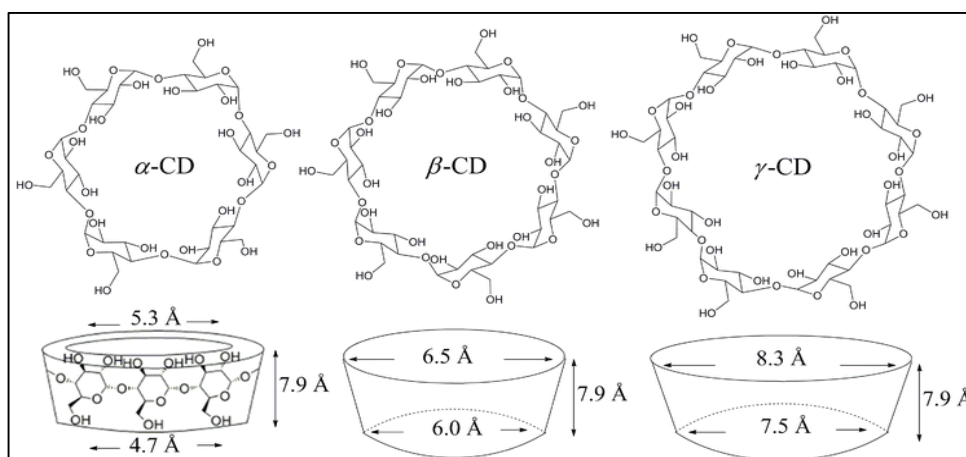


Figure 3.3. Different diameters of Cyclodextrins-Structures relations [116]

Cyclodextrins have strong intermolecular hydrogen bonding so, they have restricted solubility in the aqueous medium. Replacement of the H-bond of the structure forming –OH group help to enhance their solubility [117]. Therefore, various derivatives of cyclodextrin are investigated such as hydroxyl propyl derivates of β , γ and methylated β -cyclodextrins, sulfo butyl ether β -cyclodextrin etc [118].

Table 3.6. Properties of Cyclodextrins

Property	α -cyclodextrin	β -cyclodextrin	γ -cyclodextrin
Number of glucopyranose units	6	7	8
Molecular weight(g/mol)	972	1135	1297
Solubility in water at 25°C	14.5	1.85	23.2
Outer diameter(Å)	14.6	15.4	17.5
Cavity diameter(Å)	4.7-5.3	6.0-6.5	7.5-8.3
Height diameter(Å)	7.9	7.9	7.9
Cavity volume(Å ³)	174	262	427

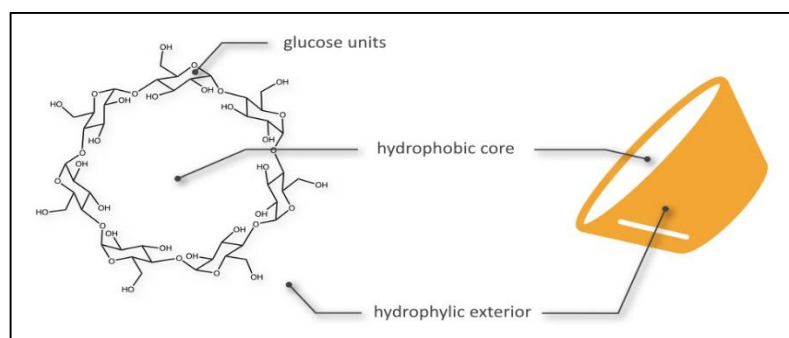


Figure 3.4. Hydrophilic outer surface and hydrophobic inner core of cyclodextrins [114]

The most important property of cyclodextrins is the ability to form inclusion complexes because of its structure. Inclusion complex is a stoichiometric molecular phenomenon which only one guest molecule interacts with the cavity of the cyclodextrin host molecule as shown Figure 3.5. This complexation is a dimensional fit between guest molecule and host cavity. If the size of the guest molecule is wrong, it will not be entrapped into the cyclodextrin cavity [119]. In order to form a complexation, thermodynamic interactions between cyclodextrin, guest and solvent is very critical. Moreover, for the formation of a stable complex, hydrophobic interactions, a variety of non-covalent forces, such as Vander Waals forces, and other forces are liable [118].

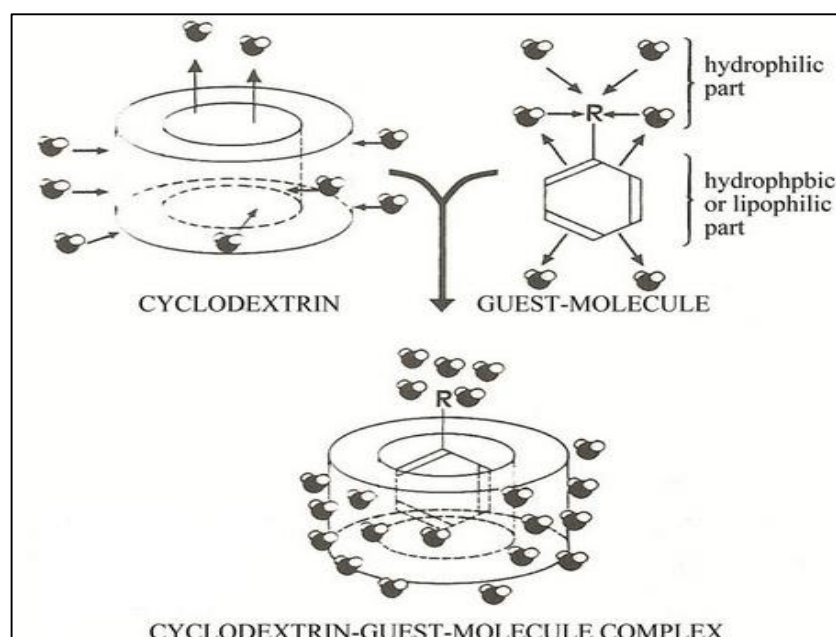


Figure 3.5. Inclusion complex between cyclodextrin and guest molecule

As a result, CDs have been used to form inclusion complex in order to increase solubility of poorly soluble drugs and enhance their bioavailability and stability. There are many advantages of cyclodextrin of inclusion complexation [83].

Some advantages are:

- i. Enhancement of solubility: CDs increase the solubility of many drugs which can fit in the hydrophobic CD cavity [120].
- ii. Enhancement of bioavailability: CDs increase the bioavailability of poorly soluble drugs by increasing drug permeability on mucosal membranes and improve drug absorption [121].
- iii. Improvement of stability: Functional group and nature are very significant effect for stability. Cyclodextrins enhance the stability of many drugs against oxidation, hydrolysis, photodecomposition so, also improve the shelf life of drugs [122].
- iv. Reduction of irritation: Drug can irritate the skin or stomach but, if complexation with CDs decrease the local concentration of the drug, irritation can reduce [83].
- v. Odor and taste masking: Drugs or functional groups can make unpleasant odors or taste, but if drug is encapsulated within the CD cavity, much more acceptable odor and taste to the patient are obtained [83].

Several techniques are used to form complexes with cyclodextrins, like complex preparation in aqueous phase, kneading, co-precipitation, freeze drying, co-evaporation, etc.

- Complex preparation in aqueous phase: initially, CD is dissolved in an aqueous medium, and then active agent (drug) is added. Mixture is stirred at a specific temperature to form complex for a specific period of time [123, 124].

In this work, inclusion complex solutions between TMZ and CDs is obtained using this method to explore the enhancement of solubility of TMZ after complex formation.

- Kneading method: Paste of cyclodextrin is prepared with small amount of water to make homogeneous paste in mortar and then, the drug is added slowly without a solvent. After grinding paste, solvent of the mixture is dried by rotary evaporator, and the obtained powder is the complex [125] and procedure of this method is shown as Figure 3.6.

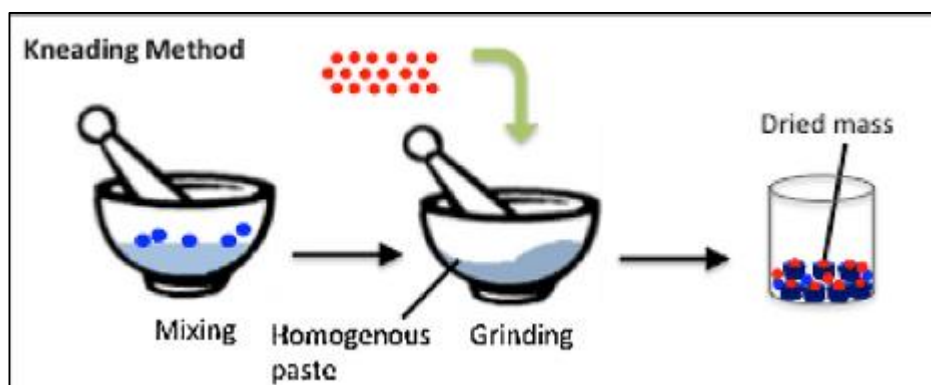


Figure 3.6. Kneading method CD/drug inclusion complex [126]

- Co-precipitation: Cyclodextrin is dissolved in an aqueous medium and while cyclodextrin solution is stirred, drug is added to the solution. CDs and drug solution are stirred and then, precipitate is formed. The precipitate is collected by centrifugation and then, washed [127].
- Lyophilization/ Freeze drying technique: The drug and CD are dissolved in water or ethanol respectively or both in the aqueous phase [128]. The mixture is stirred for a specific time at a desired temperature to reach equilibrium and then, solution is filtered, frozen and lyophilized to obtain dried complex particles [129] and the procedure of this method is shown as Figure 3.7.

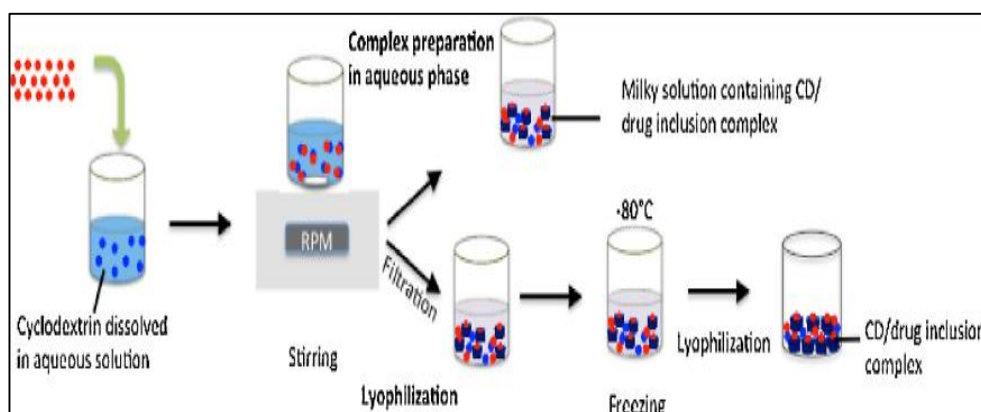


Figure 3.7. Lyophilization method CD/drug inclusion complex [126]

In this work, this technique is employed to obtain inclusion complex particles between TMZ and CDs to be investigated by DSC, TGA and SEM for the characterization of the inclusion complex.

- Co-evaporation method: is also called as solvent evaporation method. In this technique, drug is dissolved in an organic phase and CD is dissolved in the aqueous phase by stirring in order to obtain successful dispersion [130]. And then, suspension is centrifuged to remove the excess amount of drug and then, evaporated to obtain dried mass under vacuum [131, 132] the procedure of this method is shown as Figure 3.8.

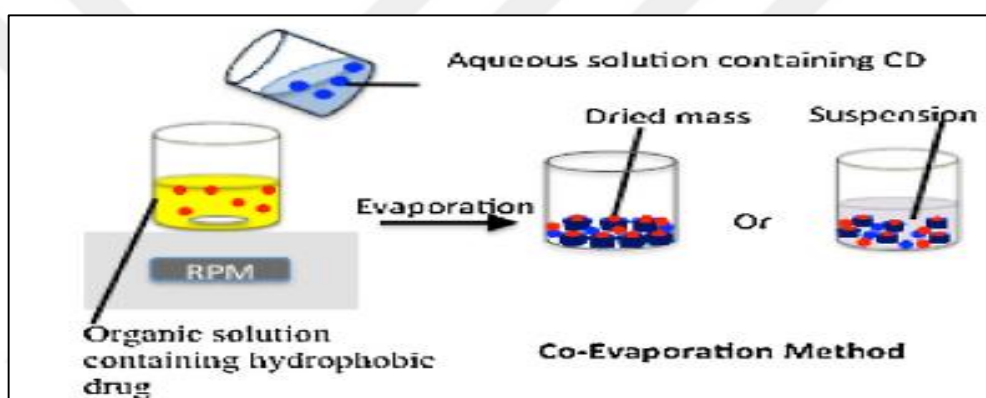
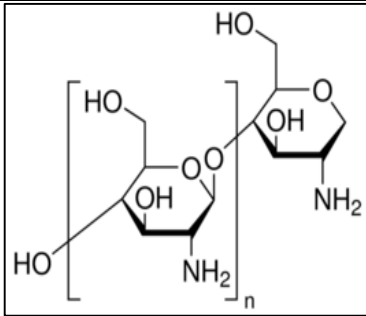


Figure 3.8. Co-evaporation method CD/drug inclusion complex [126]

3.1.3. Chitosan

Chitosan is a natural polymer prepared by the partial N-deacetylation of biopolymer chitin from some crustacean shells such as shrimps and reef lobsters. Chitin is very similar to cellulose that it is a glucose-based unbranched polysaccharide consisting of (1-4)-linked 2-acetamido-2-deoxy-b-D-glucopyranose. In addition, in nature chitin is known to be the most abundant biopolymer after cellulose and it is non-toxic and biocompatible. The chemical structure of chitin is similar to cellulose in the arrangements of inter- and intrachain hydrogen bonding. Chitosan is obtained by a partially deacetylated polymer of acetyl glucosamine made through alkaline deacetylation of chitin and production process is shown in Figure 3.10. [133]

Table 3.7. Properties of Chitosan

Chemical name	Formula	Structure	Provider
Chitosan	$C_6H_{11}NO_4$	 <p>The diagram shows the repeating unit of chitosan, which is a linear polysaccharide of 2-amino-2-deoxy-D-glucopyranose. It consists of two pyranose rings linked by a (1-4) glycosidic bond. The left ring is enclosed in brackets with a subscript 'n'. The right ring has an amino group (-NH₂) at the C2 position. Hydroxyl groups (-OH) are shown at the C2, C3, and C6 positions of both rings.</p>	Sigma Aldrich

Chitosan does not refer to an unique compound that contains compound polymer of N-acetyl glucosamine and glucosamine. Thus, chitosan is a linear polysaccharide consisting of (1-4)-linked 2-amino-2-deoxy-b-D glucopyranose. Moreover, chitosan is found in cell walls of yeast, fungi and some microorganisms [135].

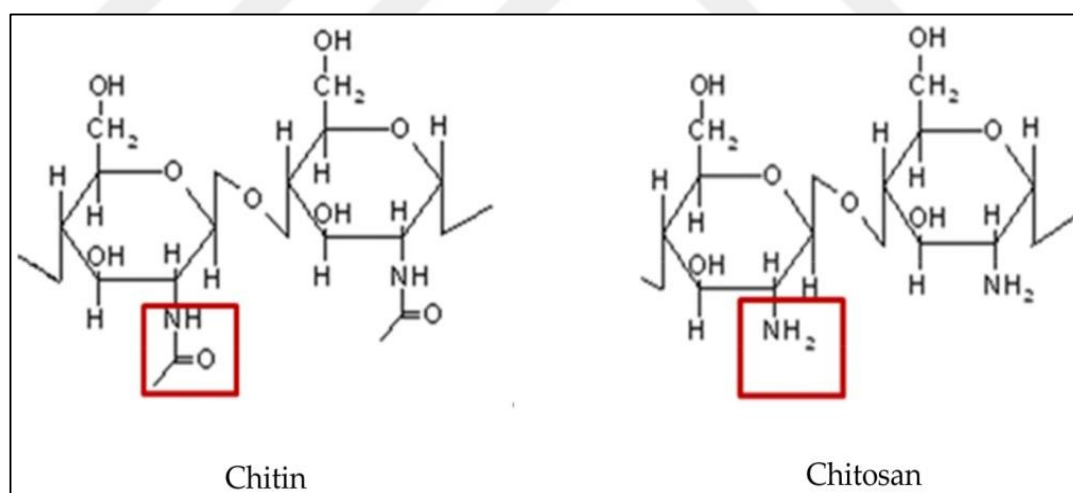


Figure 3.9. Structure of the chitosan and chitin [136]

Chitin is insoluble in many solvents but, chitosan is soluble in many organic acidic solutions at pH less than 6.5 containing acetic, tartaric, and citric acid and it is insoluble in sulfuric and phosphoric acid. Structure of the chitosan and chitin are compared as seen Figure 3.9.

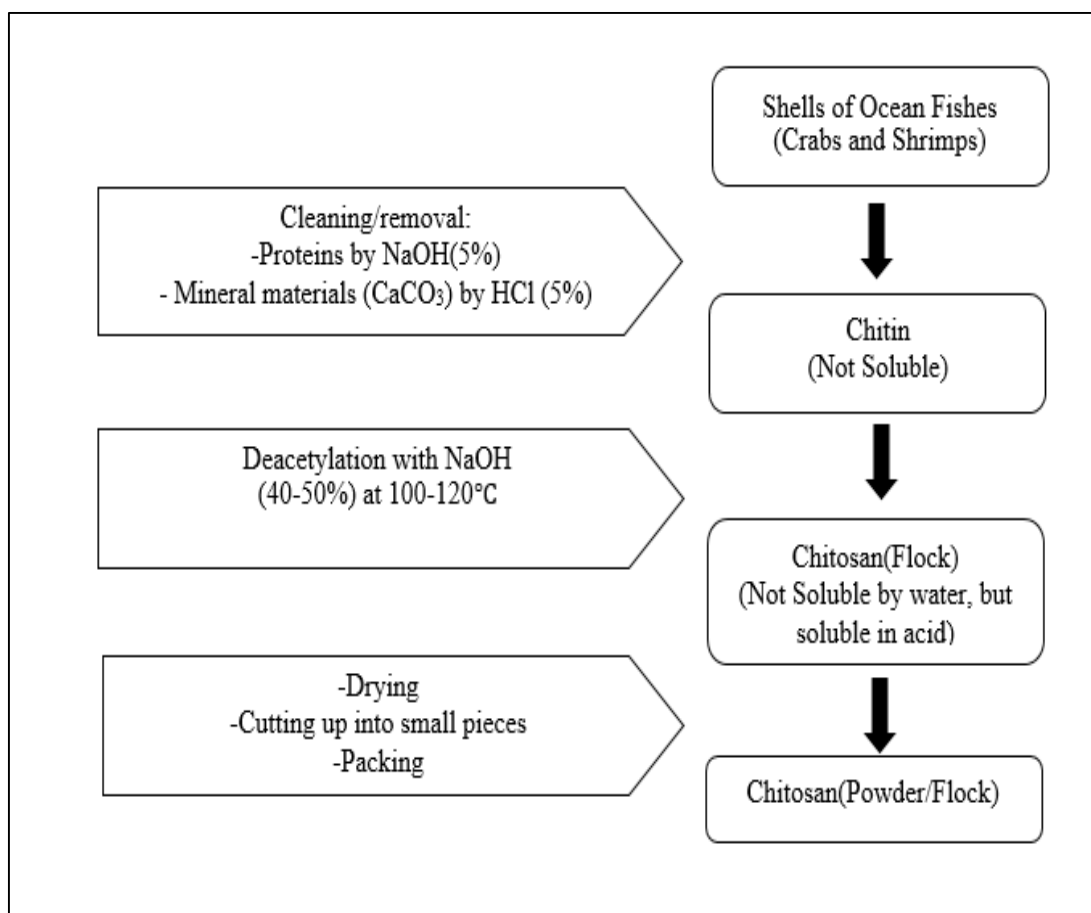


Figure 3.10. Schematic presentation of chitosan production [134]

Molecular weight, viscosity and degree of deacetylation are very significant in order to determine the properties of the chitosan. The molecular weight effect is very important so, lower molecular weight and lower DA of chitosan display good solubility and degradation faster than its high molecular weight of chitosan. [136]

In addition, pK_a of chitosan on the amine groups is approximately 6.5. At pH less than 6, chitosan shows polycationic behaviour so, chitosan is soluble in many organic solutions. If the chitosan is soluble in neutral and basic conditions, it can be developed to obtain trimethyl chitosan derivatives [134].

There are at least four methods are available in order to prepare chitosan nanoparticles: ionotropic gelation, microemulsion, emulsification solvent diffusion and polyelectrolyte complex formation.

3.1.3.1. Preparation methods for Chitosan Nanoparticles

Ionotropic gelation method: Ionotropic gelation is also called as Ionic gelation technique is based on electrostatic interaction between macromolecules. In this method, chitosan has amine groups that are positively charged and negatively charged small anionic molecules is needed such as phosphate, citrate, sulfate etc. TPP is very useful in order to prepare chitosan NPs because it is nontoxic, multi-valued and able to consist gelate through conjugation of oppositely charged between negatively charged TPP and positively charged amino groups of chitosan [137].

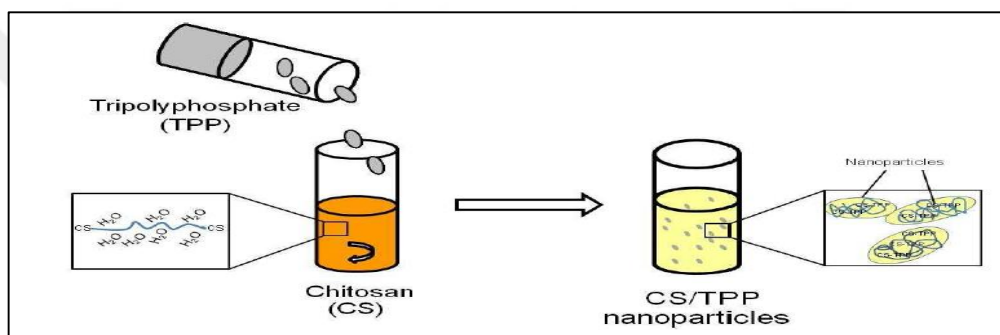


Figure 3.11. Preparation of chitosan NPs with ionic gelation method

If the ratio of chitosan and the anionic molecule is changed, the size and surface charge of nanoparticles can be altered. Moreover, if solution temperature is increased during the preparation, the mean particle size of NPs decreases. Also, if physicochemical conditions such as pH of the medium or volume change, phase transition occurs [138].

In this technique, firstly, chitosan should be dissolved in acetic acid and then, chitosan solution is added to the polyanion and NPs are formed spontaneously under mechanical stirring at room temperature [139]. This preparation process is shown as Figure 3.11. This method is preferred being of a simple preparation technique in the aqueous medium.

In this work, ionotropic gelation method is used with slight modifications in order to obtain chitosan NPs and magnetite-chitosan beads for encapsulation and targeting studies.

Emulsion Cross-linking method: In this technique, a surfactant can be dissolved in n-hexane. Chitosan is dissolved in acidic acid solution and then, chitosan solution and glutaraldehyde

as an appropriate cross-linking agent are added to surfactant and hexane mixture under continuous mechanical stirring at room temperature.

In this manner, chitosan NPs are obtained in the presence of a suitable surfactant. Under continuous stirring overnight in order to accomplish cross-linking process that the free amino group of chitosan conjugates with cross-linking agents glutaraldehyde [58]. This preparation process is shown in Figure 3.12.

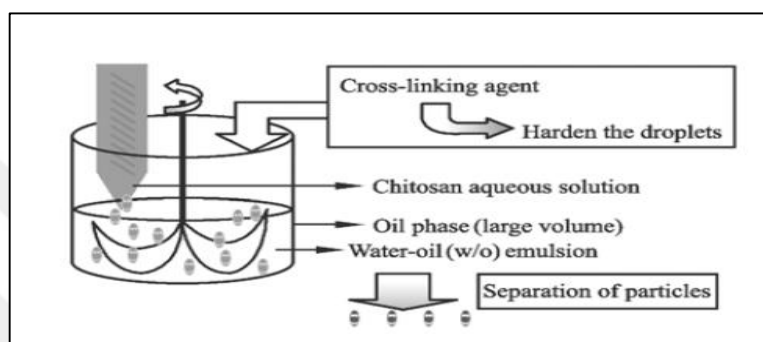


Figure 3.12. Preparation of chitosan NPs with emulsion cross-linking method [140]

Reverse Micellar Method: The preparation of chitosan nanoparticles from reverse micelles was studied as a plan for targeted drug delivery. In this technique, lipophilic surfactant such as cetyl trimethylammonium bromide (CTAB) or sodium bis(ethyl hexyl) sulfosuccinate (AOT) is dissolved in a proper organic solvent thus, water-in-oil microemulsion is prepared. The aqueous phase contains chitosan, whereas glutaraldehyde and the drug are added in the organic phase under stirring continuously at room temperature. After solvent evaporation, nanoparticles can be extracted [141]. Procedure of this method is shown as Figure 3.13.

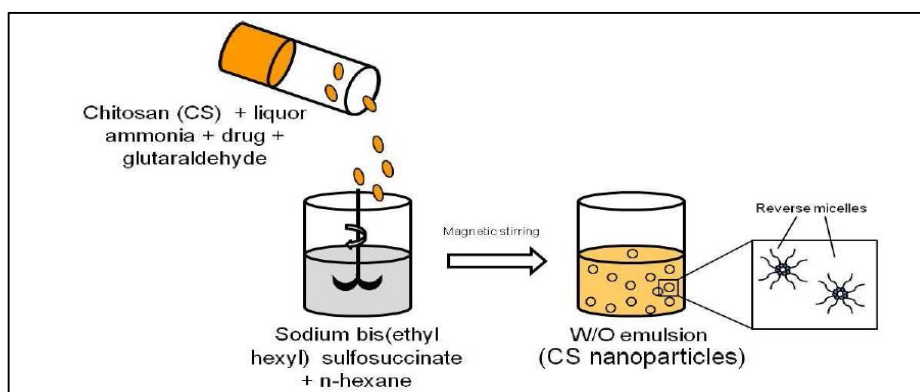


Figure 3.13. Schematic diagram of the method of reverse micellisation [142]

Reverse micellar method has some advantages for example, size of the nanoparticles are around 100 nm or even less. However, one of the disadvantage of this technique is the requirement for large amounts of solvent [143].

Emulsion Droplet Coalescence Method: This method was derived from cross-linking method and was first published for microparticle preparation. And then, some researchers have developed chitosan nanoparticles loaded with gadolinium by using this method as a strategy for cancer therapy [144].

Initially, chitosan is dissolved in the aqueous solution of gadolinium and 1 mL of this solution is added to 10 mL of liquid paraffin which contains sorbitan sesquiolate (Span® 83). The mixture is stirred with a high-speed stir, and then water in oil emulsion is formed. At the same time, same water-in-oil emulsion is prepared with NaOH as the aqueous phase. When both these emulsions are then mixed using a high-speed stir, droplets of emulsions collide and then coalesce and finally precipitation is observed [137]. As a result, chitosan nanoparticles are formed within the emulsion droplets as seen Figure 3.14.

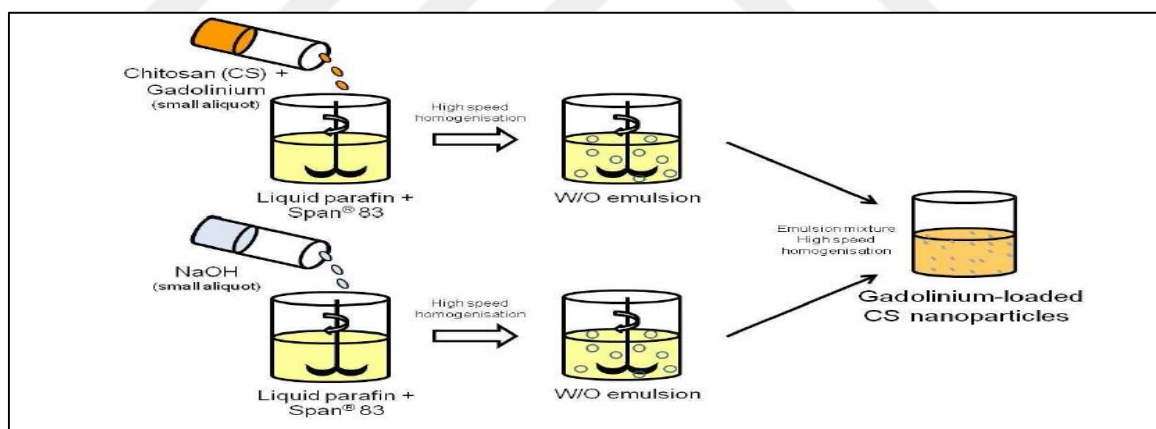


Figure 3.14. Schematic diagram of the method of emulsion droplet coalescence [142]

3.2. METHODS

3.2.1. Thermogravimetric Analysis (TGA)

Thermogravimetric Analysis is a method in which the mass of material (increase or decrease) is observed upon heating. Chemical reactions such as combustion, reduction of metal oxides

etc. and physical transitions like vaporization, evaporation etc. causes weight loss and are detected by TGA curves [145]. The Thermogravimetric Analyzer (TGA) is a laboratory tool used to characterize materials in various applications such as environmental, food, pharmaceutical etc.

It can be seen as Figure 3.15, sample's weight is measured by a precision balance of TGA while sample is heated or cooled in the furnace which is carried out in Helium or Argon as an inert atmosphere or only in an air [145].



Figure 3.15. Thermogravimetric analysis (TGA) instrument

In this project, TGA is used to determine the amount of different types of Cyclodextrin that coats the magnetite surface. TGA is also used to indicate complexation between TMZ and β -CD by using onset temperature presence of chitosan in chitosan-magnetite beads are also shown using TGA. TGA of the magnetite particles with and without cyclodextrins and only TMZ, only β -CD, TMZ- β -CD complex and TMZ- β -CD physical mixture are performed using a Perkin Elmer thermogravimetric analyzer at a heating speed of 10°C/min under nitrogen where the temperature is changes from 25 °C to 600 °C. All samples are dried in a vacuum oven or by a freeze-dryer (SCANVAC, coolsafe) overnight.

3.2.2. Differential Scanning Calorimetry (DSC)

DSC is a thermoanalytical method than can indicate a lot of characteristics of materials which is based on the difference in the amount of required heat to increase the temperature

between sample and references as a function of temperature. There are many applications of DSC like phase transition (melting points, glass transition..) crystallization times and temperatures, heat capacity, percent cure, purities, percent crystallinity, thermal stabilities, etc [146]. The Differential Scanning Calorimeter and its accessories used during the experimental study can be seen in Figures 3.16. and 3.17.

In this project, Differential Scanning Calorimetry is used to compare the endothermic and exothermic peaks of only TMZ, three different CDs, TMZ-CD complexes and TMZ-CD physical mixtures. These samples are performed using Setaram instrumentation, DSC 131 at a heating speed of 10°C/ min under nitrogen where the temperature is changed from 20 °C to 400 °C.



Figure 3.16. Differential Scanning Calorimeter

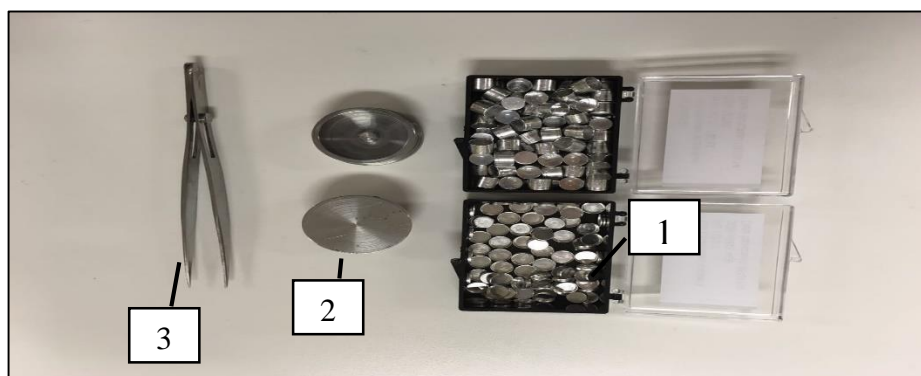


Figure 3.17. Accessories used for DSC

(1-Creusets 2-Crimping Tool 3-Tweezers)

3.2.3. Dynamic Light Scattering (DLS)

Dynamic Light Scattering (DLS) is a method for measuring the average hydrodynamic diameter of sub micron particles, the device is shown as Figure 3.19. DLS measurement relates Brownian motion which is the random movement of the particles in the solvent molecules with the size of the particles taking into consideration the viscosity based on Stoke's Einstein Equation;

$$d(h) = \frac{kT}{3\pi\eta D} \quad (3.1)$$

where $d(h)$ is hydrodynamic diameter, D is translational diffusion coefficient, k is Boltzmann's constant, T is absolute temperature and η is viscosity assuming spherical particles [147].

DLS is a useful tool for determining the agglomeration of nanoparticles as a function of time. When DLS measurement is compared to TEM images, the aggregation stage of the nanoparticles can be determined. If the particles have unagglomerated suspension, the diameter which measured with DLS will be very similar the TEM size. If the particles are susceptible agglomeration, DLS measurement is much larger than the TEM measurement [147]. This is schematically shown in Figure 3.18.

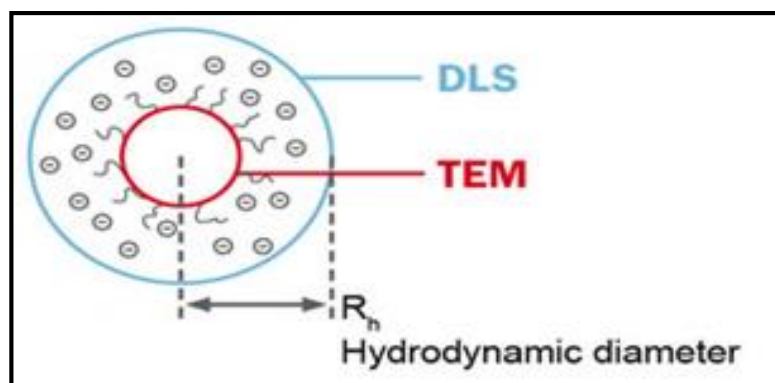


Figure 3.18. Hydrodynamic diameter for TEM and DLS



Figure 3.19. Dynamic Light Scattering

In this project, Dynamic Light Scattering (DLS) that is used to measure the size of magnetite with and without cyclodextrins and also, the size of the chitosan nanoparticles and magnetite- chitosan beads which is typically in the nanometer region.

3.2.4. UV-Visible Spectroscopy

A spectrum is a graphical representation which is the amount of light transmitted or absorbed by material as a function of the wavelength. UV-Vis spectrophotometry can produce many qualitative informations such as identification of pure substances, identification of carbonyl bands, enzyme activities etc. A UV-Vis Spectrophotometer is shown in Figure 3.20. [148].



Figure 3.20. UV-Visible Spectrophotometer [148]

In general, liquid sample is used for visible and ultraviolet spectroscopy. This sample must be placed in a transparent cuvette in order to allow measurement. Different cuvettes possess different optical properties. There are generally three different types of cuvettes like plastic, glass, or quartz. Glass cuvettes should be used if wavelengths in the visible range from 380

nm to 780 nm is necessary for the experiment. However, quartz cuvettes should be used if wavelengths below 380 nm is requirement and are shown as Figure 3.21. [148].



Figure 3.21. Quartz Cuvette [148]

In this project, UV-Vis Spectroscopy is used to quantify the complexation of TMZ with different types of Cyclodextrins. UV-Vis Spectroscopy of the TMZ solutions with and without cyclodextrins are performed using a Perkin Elmer UV/Vis Spectrophotometer. It is known that typical maximum absorbance value of TMZ is 330 nm. In our measurements, an absorbance range of 200-450 nm is used. Therefore, quartz cuvettes are employed for all experiments.

3.2.5. High Pressure Liquid Chromatography (HPLC)

High Pressure Liquid Chromatography is very important method for analytical chemistry. This technique is used in order to quantitative, identify and separate the substances which is dissolved in the liquid. HPLC can be applied for many industries such as nutraceuticals, cosmetics, environmental, food, etc [149]. In HPLC, the sample (liquid) is passed through a column using an appropriate mobile phase. The column is chosen depending on the polarity of the sample. The chemical of interest in the sample passes the column in a specific time and appears as a peak. The calibration curve prepared by the standards is used to quantify the chemical.

In this work, high performance chromatography is used for the determination the amount of the temozolomide. HPLC system consists of 1525 Binary Pump, 2487 UV-Vis Detector, 717 Autosampler and a thermal column manager unit was equipped. X-Bridge 150 x 4.6, .5 μ m column was used and also computer was used to perform process of the raw data.

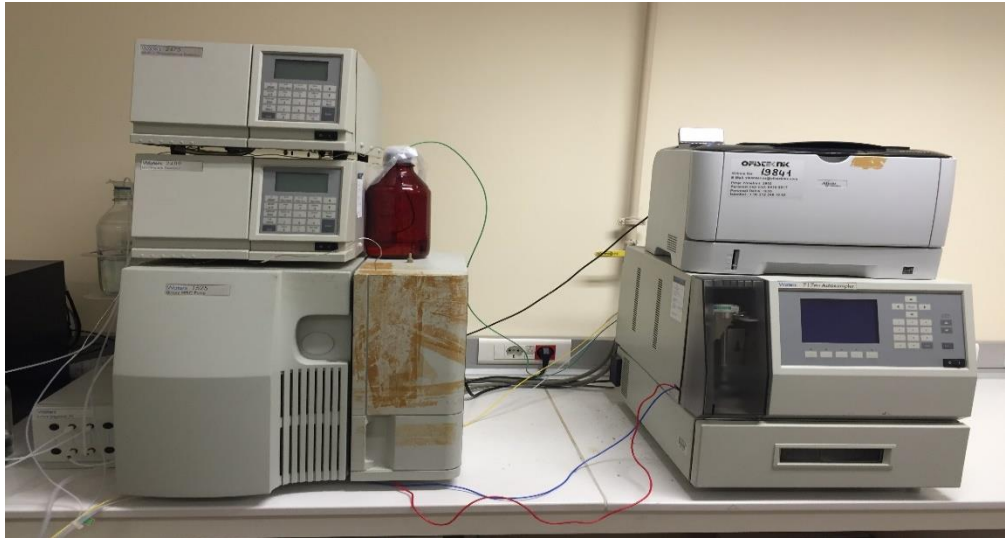


Figure 3.22. High Performance Liquid Chromatography

In HPLC reverse phase C18 column (X-Bridge 150mmx .6cm, .5 μ m, Waters) was used. Water that contained 0.5% acetic acid / methanol (80:20 v/v) was prepared for mobile phase. Standard calibration curve was obtained by five different temozolomide concentrations and for each measurement three sample was used and 3 injections were applied for each sample. An image of the high performance chromatography instrument in this project is given in Figure 3.22.

3.2.6. Scanning Electron Microscopy (SEM)

Scanning Electron Microscope focuses electron beam over a surface of the material in order to create a three dimensional image.



Figure 3.23. Scanning Electron Microscopy

In this project, Scanning electron microscopy (SEM, JEOL Ltd., JSM-5910LV) is used to show morphology changes that occur upon complex formation between TMZ and different types of cyclodextrins. In addition, this technique is also used to obtain images of chitosan beads with and without magnetite.

4. SYNTHESIS OF MAGNETITE NANOPARTICLES AND CHARACTERIZATION

In this chapter, preparation technique of magnetite nanoparticles with and without cyclodextrins are given describing co-precipitation method. Size determination of magnetite nanoparticles, coating amount of cyclodextrins on the surface of the magnetite and magnetic properties are investigated. In addition, colloidal stability of magnetic nanoparticles with cyclodextrins are illustrated.

4.1. SYNTHESIS OF MAGNETITE NANOPARTICLES

4.1.1. Synthesis of Bare Magnetite Nanoparticles

Magnetite particles are prepared by using co-precipitation method. In this method, iron sulfate heptahydrate and iron chloride (anhydrous) are used to synthesize magnetite nanoparticles. Initially 80 mL distilled water is de-aerated which is done by passing nitrogen gas through the reaction medium for ½ hours. The solution is heated up to 80°C in a reactor while stirring mechanically. It is important that the synthesis should be carried out 80°C .

After ½ hour, required amounts of iron sulfate and iron chloride are dissolved in the reaction medium under nitrogen gas. After 15 minutes, 20 mL .. M NaOH is added as a base. Upon this addition, blackening of the solution is observed immediately, which suggests the formation of magnetite nanoparticles. These chemicals are mixed for another ½ hour and then, the mixture is cooled down to room temperature. The amounts of all chemicals for the preparation of bare magnetite nanoparticles are shown in Table 4.1.

After synthesis, magnetite nanoparticles are collected by magnetic separation the precipitate is washed once with water. And then, magnetic nanoparticles are dried in a 60 °C vacuum oven.

Table 4.1. Amounts of chemicals for bare magnetite nanoparticle

Ingredients	Amounts
NaOH	0.65 M
Distilled water	80 mL
FeSO ₄ .7H ₂ O	0.242 g
FeCl ₃	0.282 g

4.1.2 Synthesis of Magnetite Nanoparticles with Cyclodextrins

In the synthesis of magnetite nanoparticles with different types of cyclodextrins, procedure of the preparation is the same of the bare magnetic nanoparticles. The only additional step is that following the addition of distilled water, desired amount of cyclodextrin is also added to the reaction medium. The amounts of all chemicals for the preparation of magnetite nanoparticles with cyclodextrin are shown in Table 4.2. After synthesis, magnetite nanoparticles are collected by magnetic separation the precipitate is washed once with water. And then, magnetic nanoparticles are dried in a 60 °C vacuum oven.

Table 4.2. Amounts of chemicals for magnetite nanoparticles with cyclodextrin

Ingredients	Amounts
NaOH	0.65 M
Distilled water	80 mL
Cyclodextrins	1, 0.5, 0.25 g
FeSO ₄ .7H ₂ O	0.242 g
FeCl ₃	0.282 g

4.1.3 Tiron Metal Test to Determine Magnetite Concentration

Tiron metal test is based on the fact that Fe ions and tiron forms a colored complex. By using this test, corresponding Fe ions and tiron forms a complex which has a maximum absorbance value is intensity at 480 nm. This absorbance value is measured in order to obtain the concentration of magnetite by using Equation 4.1.

$$C \left(\frac{\text{g}}{\text{ml}} \right) = \frac{(\text{ABS@480nm}) \times (\text{Dilution factor}) \times 231.52 \times 25}{39986 \times 162.15 \times 3 \times 0.1} \quad (4.1)$$

In this test, 0.1 mL magnetic fluid is mixed with concentrated (37%) hydrochloric acid and then, this solution is heated with a heat gun until the color of the solution changes to yellow. After color change, obtained solution is mixed with the tiron solution. 3 mL sodium hydroxide solution is added to the solution where the solution turns to red immediately. Finally, water is added until the final volume reaches 25 mL. In order to measure the absorbance of the final solution, dilution is needed because of the high absorbance of the complex (high Fe amount). Thus, the final solution may be diluted by 5, 10 or 15 factors in order to obtain absorbance values lower than 1.5 at 480 nm. Amounts of chemicals of the Tiron metal test are given in Table 4.3.

Table 4.3. Amounts of chemicals for Tiron Metal Test

Ingredients	Amounts
Magnetic Fluid	0.1 mL
Hydrochloric Acid (Concentrated, 37%)	0.4 mL
Tiron Solution	0.083 g/mL
Sodium Hydroxide Solution	4 M

4.2. CHARACTERIZATION OF MAGNETIC NANOPARTICLES

4.2.1. Dynamic Light Scattering Measurements

Magnetite nanoparticles are prepared by co-precipitation method and then characterized by dynamic light scattering (DLS) technique. DLS is used for obtaining the average size distribution of magnetite nanoparticles with and without different cyclodextrins. The size distribution by number graph is the most significant result to determine the size of the nanoparticles. The size measurement for magnetite nanoparticles solution was repeated thrice to provide more accuracy.

Table 4.4. Size distribution of the magnetite NPs after 1st and 3rd measurements

Sample	for first measurements	for third measurements
	Size (nm)	Size (nm)
Bare magnetite	47	63
Magnetite with β -Cyclodextrin	57	58
Magnetite with 2-hydroxy propyl β -Cyclodextrin	60	66
Magnetite with 2-hydroxy propyl γ -Cyclodextrin	61	67

As a result of the measurements, three different results were obtained for size distributions because of the agglomeration during the measurements. There is a significant difference in the size obtained from the first to the third measurement of bare particles. As these particles are uncoated, they have a tendency to aggregate and finally precipitate. This can be followed from the increase in the hydrodynamic radius values as more time passes from the 1st and 3rd measurement. The particle sizes between different CDs is not significant.

Thus, size obtained from the first measurement of the magnetite solutions is always smaller than the third measurement of the magnetite solutions as shown Table 4.4. This agglomeration can be followed from Figure 4.1 and Figure 4.2. Cyclodextrins are attached onto the surface of the magnetite nanoparticles. Therefore, these figures also shows that the

size of the bare magnetite nanoparticles are smaller than the magnetite nanoparticles coated with cyclodextrins.

According to the Table 4.4., it can be said that sizes of magnetic nanoparticles changed between 45 nm to 75 nm. However, it is known that the bare magnetic nanoparticles core size was 10 nm by using the co-precipitation method [151] and when the cyclodextrins were attached to the surface the diameter of magnetite nanoparticles should increase to nearly 13 nm. Therefore, the obtained results can be explained as aggregation, where clusters of nanoparticles with a hydrodynamic diameter of nearly 10 particles are predominant in solution.

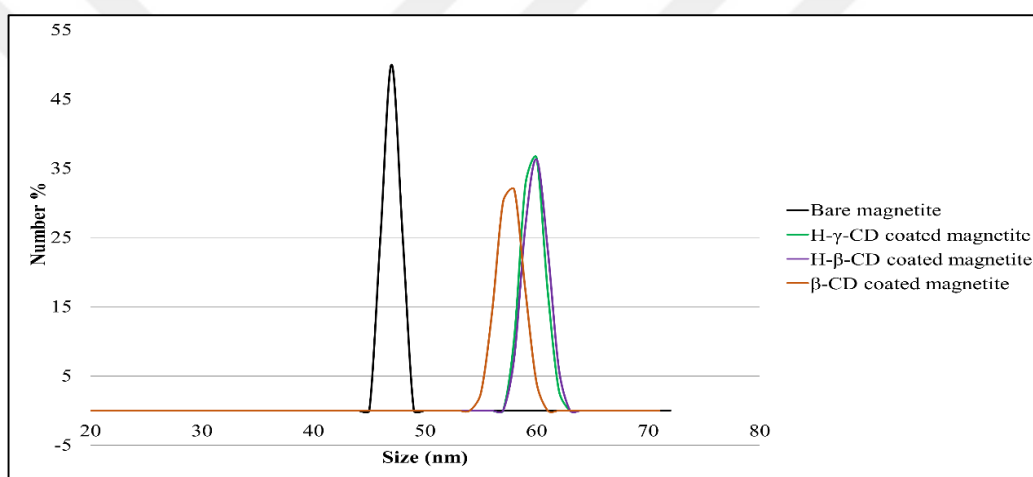


Figure 4.1. Size distribution of magnetite NPs for first measurement

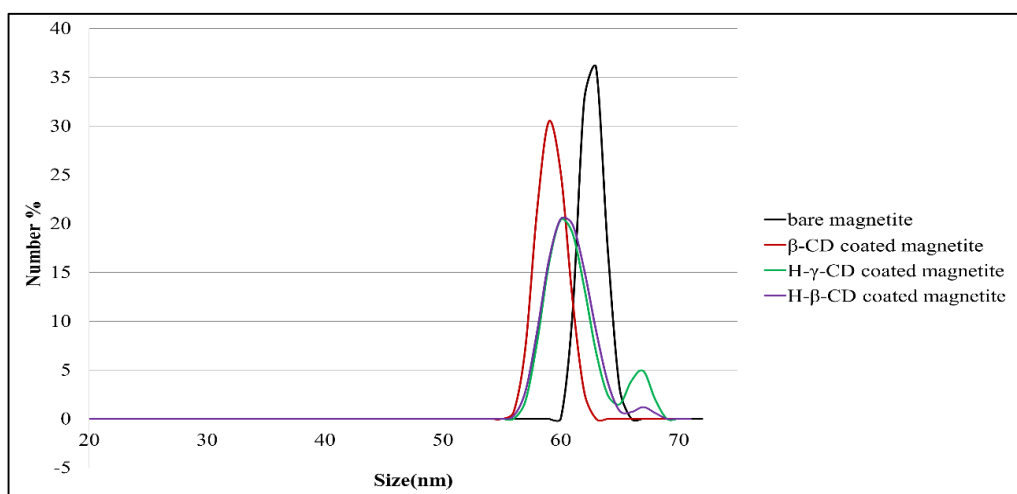


Figure 4.2. Size distribution of magnetite NPs for third measurement

4.2.2. Thermogravimetric Analysis Measurements

Cyclodextrin amount on the surface of the magnetite nanoparticles was determined by thermogravimetric analysis in air atmosphere. The nanoparticles are washed once and then dried in a vacuum oven at 60°C at 20 mbar. For TGA scan, temperature is increased from 25 °C to 600 °C. It was expected that cyclodextrins can hold onto the surface of magnetic nanoparticles and also provide colloidal stability of magnetic nanoparticles. Thermogravimetric analysis is employed to determine the weight of CDs with respect to total weight of the sample, indicating the amount of CD present on the magnetite surface. This instrument measures the weight loss as a function of rising temperature as seen Figure 4.3.

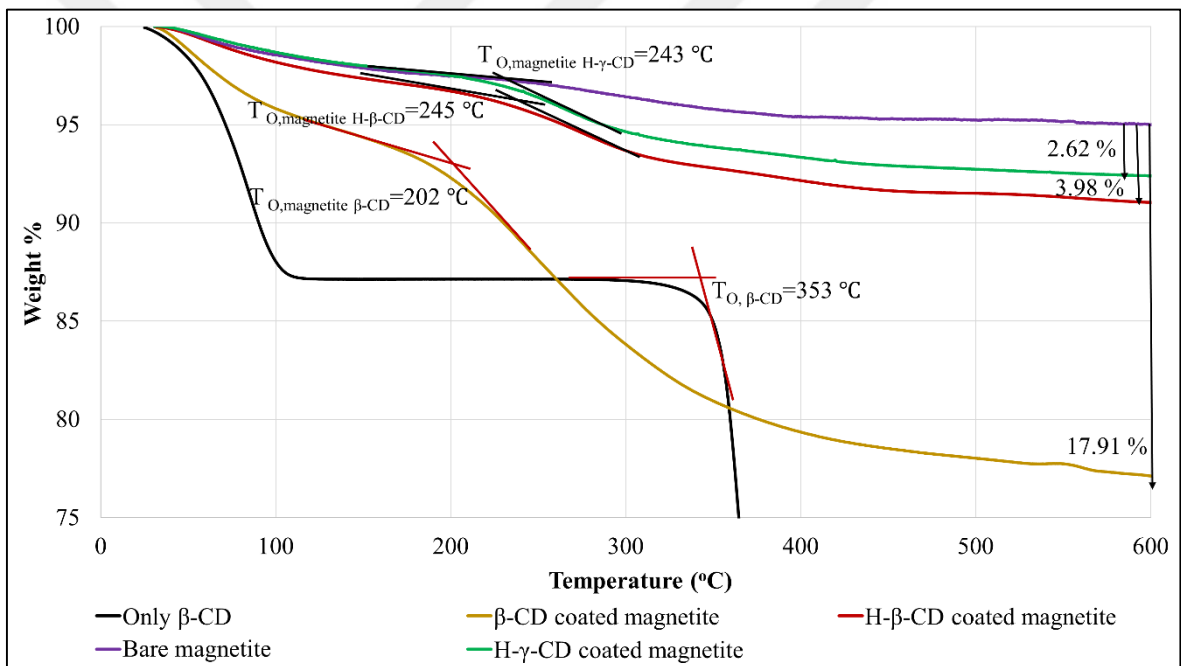


Figure 4.3. Thermogravimetric Analysis for magnetite with and without CD's

As seen in Figure 4.3. the thermal degradation curve of bare magnetite shows a small initial loss of approximately 1.74 wt % loss until 150 °C which is attributed to water evaporation that remains as residual water after drying of the sample. Further decrease of 2.63 wt % until temperature reaches 600 °C may be attributed to the impurity.

The thermal degradation curve of magnetite coated with CD's shows an initial water loss of about 2-5 wt % until temperature reaches 150 °C and the most important degradation step is

observed in the temperature range of 150-600 °C which is the organic layer around the NPs. For each coated particle, weight loss obtained between 150 °C and 600 °C is attributed to the CD coating. The wt % difference between the two plateau's at 150 °C and 600 °C is tabulated in Table 4.5. as % coating of magnetite NPs with different type of CD's.

In addition, onset temperature can be used as a verification of the compound. For three different types of CD coated magnetite nanoparticles as shown in Figure 4.3, black line shows the weight loss profile of only β -CD, with the onset temperature of 353 °C. Dark yellow line is the weight loss profile of β -CD coated magnetite nanoparticles, with the onset temperature of 202 °C. And, green and red line shows the weight loss profile of H- γ -CD and H- β -CD coated magnetite nanoparticles, with the onset temperatures of 243 °C and 245 °C respectively. These results shows that there are temperature shifts of CD coated magnetite nanoparticles with respect to the CD alone. This is very significant, indicating attachment of CDs onto the surface of the magnetite nanoparticles. It should be noted that the highest amount of CD coating is achieved with β -CD (17 wt% loss as opposed to 4 and 2.6 wt% for H- β -CD and H- γ -CD, respectively) where the highest shift in onset T is also observed. As more CD resides on magnetite surface, the change in onset T becomes more pronounced.

Table 4.5. % coating of magnetite NPs with different CD's

Type of cyclodextrins	wt % (150 °C-600 °C) according to the bare magnetite nanoparticles
β -Cyclodextrin	17.09
2-hydroxy propyl β -Cyclodextrin	3.98
2-hydroxy propyl γ -Cyclodextrin	2.62

Finally, these results show that we were able to successfully coated the magnetite particles with all types of CD's however at varying coating densities.

4.2.3. Colloidal Stability of Magnetic Nanoparticles

In order to determine the colloidal stability of magnetite NPs with and without different CD coatings, solutions are placed in vials and are left at room temperature without any mixing or shaking and then, time to precipitation is observed by naked eye.

The photographs in Figure 4.4. show that bare nanoparticles settle within 15 minutes whereas the settling time of different cyclodextrin coated magnetic nanoparticles are tabulated in Table 4.6.

These results were also in line with the colloidal stability as magnetite – cyclodextrin complex could be dispersed in aqueous medium regardless of the type of cyclodextrin used. However it was shown that 2-hydroxy propyl β -Cyclodextrin coated magnetite nanoparticles had the longest colloidal stability.

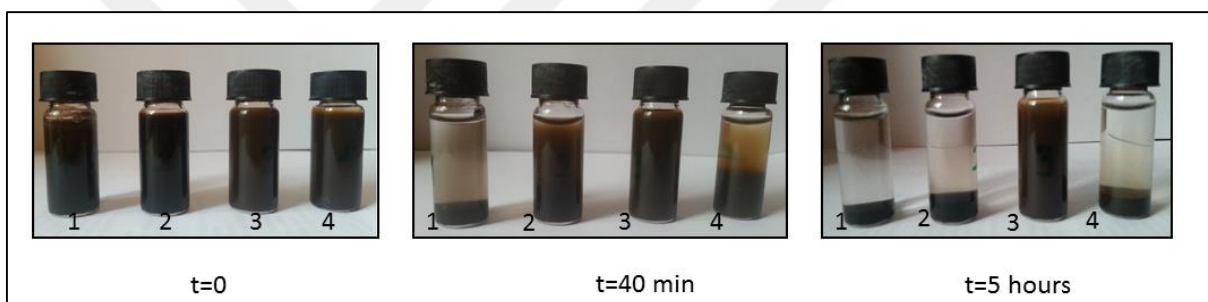


Figure 4.4. Magnetite nanoparticles with and without CD's at t=0, t=40 min and t=5 hrs

(Magnetic Nanoparticles 1= Bare, 2= β -CD coated, 3= H- β -CD coated, 4= H- γ -CD coated)

Table 4.6. Time to Precipitation for synthesized magnetic NPs

Sample	Time to Precipitation
Bare magnetite	15 minutes
Magnetite with β -Cyclodextrin	55 minutes
Magnetite with 2-hydroxy propyl β -Cyclodextrin	> 5 hours
Magnetite with 2-hydroxy propyl γ -Cyclodextrin	40 minutes

5. PREPARATION METHODS OF INCLUSION COMPLEX BETWEEN CYCLODEXTRINS AND TEMOZOLOMIDE AND CHARACTERIZATIONS

In this chapter, firstly, solubility of Temozolomide is investigated in 0.1 M HCl to be used in complexation studies. Preparation techniques of inclusion complexes between TMZ and three different cyclodextrins (β -Cyclodextrin (β -CD), 2-Hydroxy propyl- β -Cyclodextrin (H- β -CD), 2- Hydroxy propyl- γ -Cyclodextrin (H- γ -CD)) are presented to analyze the complex formation. These complex formations are investigated using DCS, TGA, HPLC and UV and also are illustrated with SEM.

5.1 DETERMINATION OF SOLUBILITY OF TEMOZOLOMIDE

It is known that Temozolomide has low stability and solubility in aqueous medium. Both the stability and solubility of Temozolomide are enhanced in acidic medium [111] therefore, all experiments were carried out in 0.1 M HCl. In order to determine if presence of cyclodextrins increase the solubility of TMZ, initially the solubility of TMZ was determined in 0.1 M HCl.

Arbitrary amount of excess TMZ is added to 5 mL 0.1 M HCl in order to determine saturation concentration of TMZ. After vortex mixing followed by sonication for 2 minutes, the excess TMZ is removed by 6000 rpm 15 min centrifugation. The amount of TMZ in the supernatant of the solution is determined by UV-Vis Spectroscopy which measures characteristic absorbance of TMZ at 330 nm. Firstly, this concentration is determined which is the solubility of TMZ, TMZ solutions that are below this concentration are prepared by dissolving different amounts of drug again in 5 mL 0.1 M HCl and measuring their absorbance values by UV-Vis Spectroscopy.

5.2. PREPARATION OF TMZ-CYCLODEXTRIN INCLUSION COMPLEX SOLUTIONS AND PARTICLES

The complexations of TMZ were formed with three different cyclodextrins (β -cyclodextrin (β -CD), Hydroxy propyl- β -cyclodextrin (H- β -CD), Hydroxy propyl- γ -cyclodextrin (H- γ -CD) that contain six (β -CD) to eight (H- γ -CD) membered rings.

5.2.1. Preparation Method of TMZ-CD Inclusion Complex Solution

In order to show the complexation of different types of cyclodextrin with TMZ, TMZ solutions are mixed with CD solutions at different molar ratios as 1:1, 1:2 and 1:5. Firstly, cyclodextrin is weighed and 0.1 M HCl solution is added to obtain 0.5 g solution. Separately, excess amount of TMZ (7.25 mg, i.e. approximately two times higher than its solubility) is weighed. Cyclodextrin solutions are prepared as 0.0265 g β -CD in 0.5 mL 0.1 M HCl and is added to the weighed solid TMZ. The resulting solution is vortex mixed for a few seconds. After vortex mixing, sufficient 0.1 M HCl is added to the solution in order to obtain a total of 1 g solution. And then, this solution is again vortex mixed for a few seconds and shaken at 250 rpm at 37 °C using an Orbital shaker (LABWIT, ZWYR-240).

After required amount of times, final solutions are centrifuged (Hettich, EBA 21) at 6000 rpm for 5 minutes and the supernatant is diluted 200 times with 0.1 M HCl.

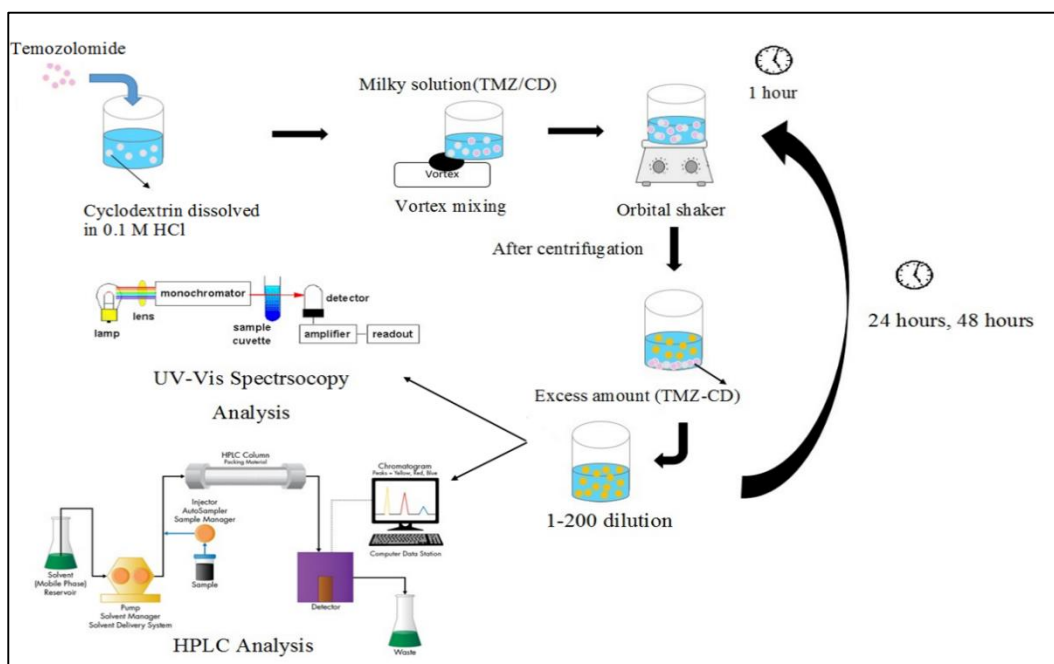


Figure 5.1. Preparation process of TMZ-CD inclusion complex solution

The absorbance values are measured by using UV-Vis Spectroscopy between 200-450 nm for only first day and only at 330 nm by using HPLC for zeroth, first and second days. Preparation process of TMZ-CD inclusion complex solutions to be analyzed with UV-Vis Spectroscopy and HPLC is schematically is shown in as Figure 5.1.

5.2.2. Preparation Method of TMZ-CD Inclusion Complex Particles

After the centrifugation step described in Section 5.2.2., the supernatant is freeze-dried (SCANVAC, coolsafe) to obtain TMZ-CD complex particles. Preparation process of TMZ-CD inclusion complex particles is shown in Figure 5.2.

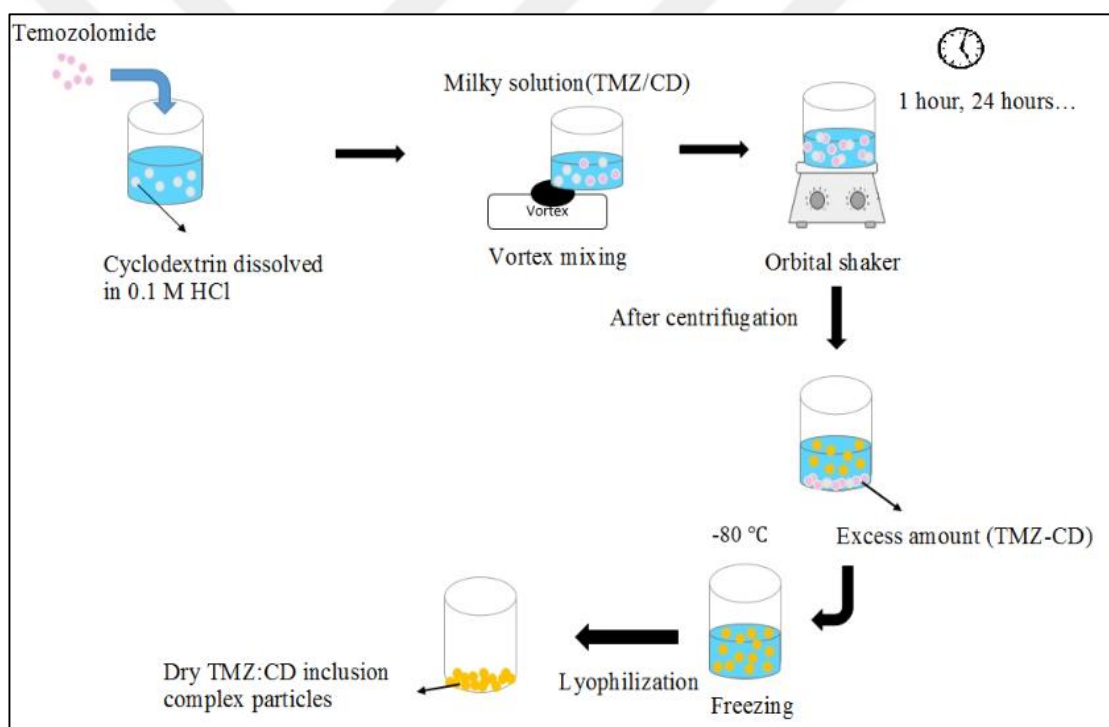


Figure 5.2. Preparation process of TMZ-CD inclusion complex particles

5.2.3. Preparation method of TMZ-CD physical mixtures

Excess amount of TMZ (7.25 mg) is mixed with three different types of CDs (1:5 mol ratio) in the solid phase using a spatula and this mixture is kept at 4 °C until measurements.

5.3. ULTRAVIOLET-VISIBLE SPECTROSCOPY MEASUREMENTS

5.3.1. Calibration Curve of TMZ

In order to obtain calibration curve of the TMZ, different six concentrations of TMZ are prepared in 0.1 M HCl solution. After preparation of TMZ solutions, prepared solutions are diluted and absorbance values are measured between 200 and 450 nm by using UV-Vis Spectroscopy. It is known that characteristic TMZ peak is observed at 330 nm. Absorbance values at 330 nm for different concentrations of TMZ and related concentrations of TMZ is used and then, calibration curve of TMZ are plotted as shown in Figure 5.3.

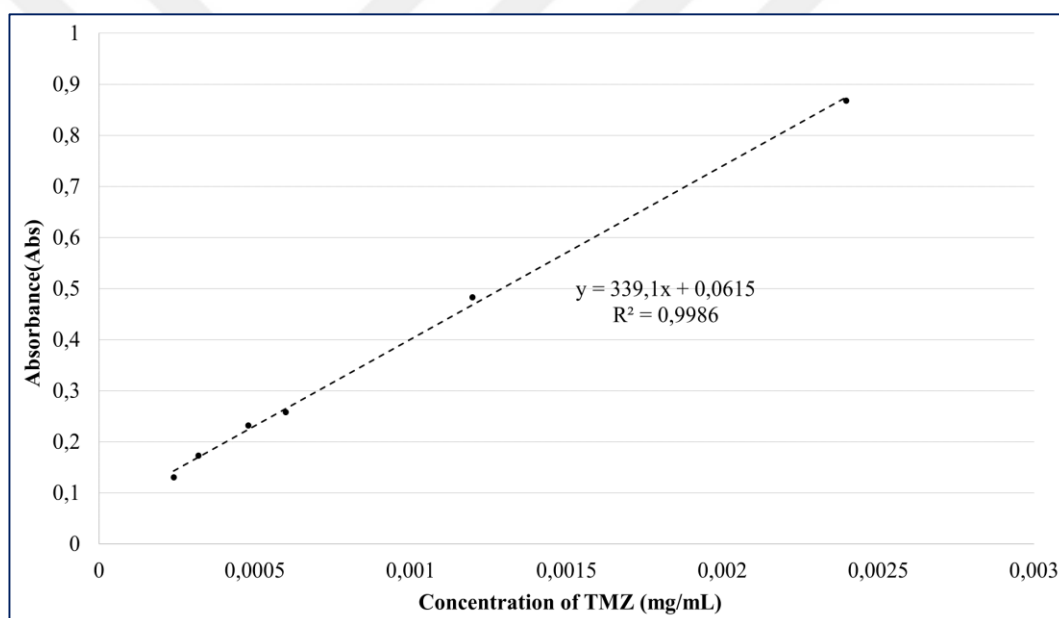


Figure 5.3. Calibration curve of TMZ

The measured amount of TMZ are calculated based on this calibration curve.

5.3.2. Solubility Curve of TMZ

Solubility curve of TMZ is shown as Figure 5.4. Thus, the solubility of TMZ was found as 3.46 mg/mL.

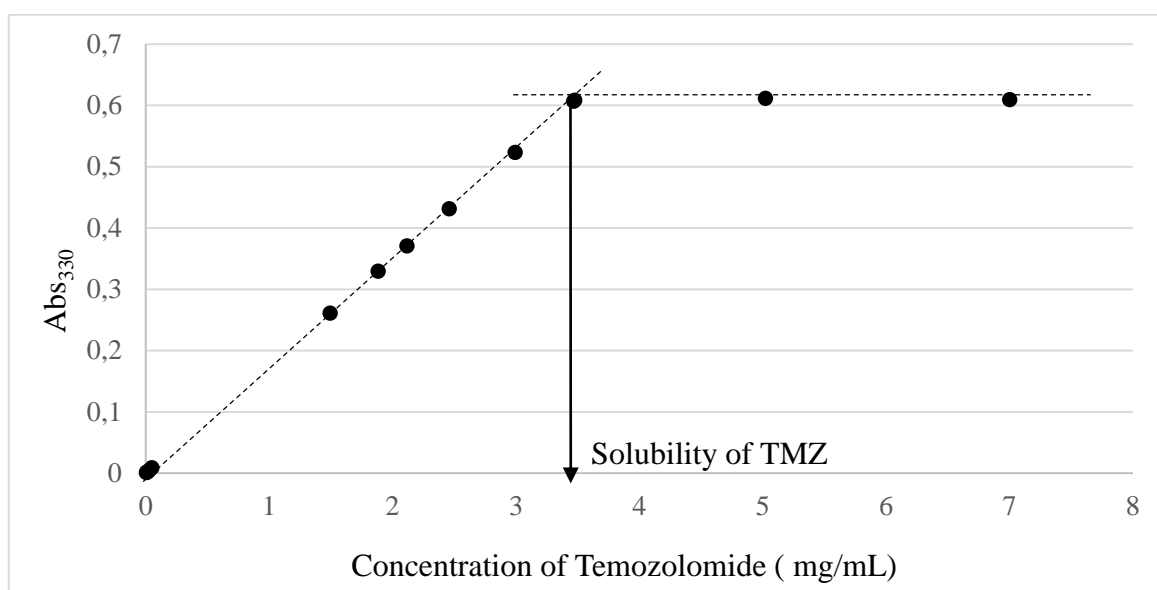


Figure 5.4. The solubility curve of Temozolomide

5.3.3. Enhancement of the Solubility of Temozolomide

If the TMZ and different types of CD's formed a complex, solubility of the TMZ should increase in 0.1 M HCl. After mixing TMZ and CD solutions with molar ratio as TMZ: CD 1:1, the mixtures are shaken continuously at 250 rpm for 24 hours.

After 24 hours, amounts of solubilized TMZ in TMZ-CD complexes are measured using a spectrophotometer, taking the data at 330 nm, where the signature peak of TMZ exists. CD does not have a peak in the UV region, so all the signal comes from TMZ.

In Figure 5.5 shows that the peak height at 330 nm is increased with rising dissolved temozolomide amount because of relations between absorbance and concentration. The signature peaks of TMZ in each solutions with three different cyclodextrins are higher than solution which contains only temozolomide. Thus, for 24 hours measurements, absorbance of the only TMZ solution is found to be lowest which indicates lowest solubility for only TMZ in 0.1 M HCl.

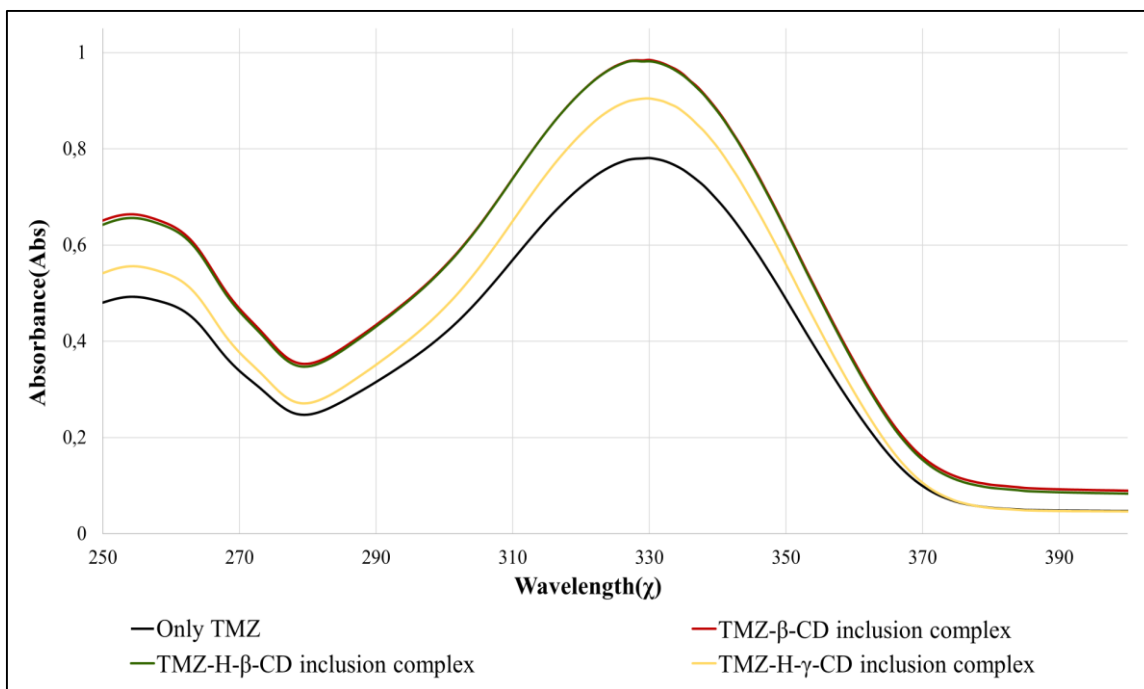


Figure 5.5. Absorbance of TMZ in the presence of different CD's and only TMZ in 1:1 ratio after the formation of inclusion complex after 24 hours

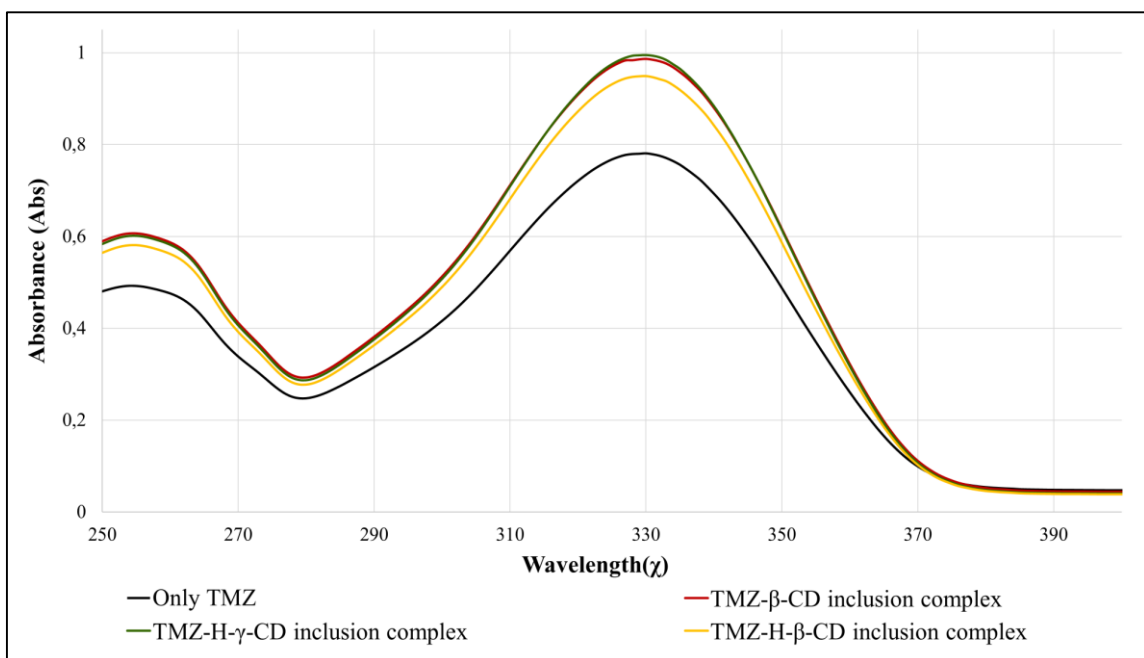


Figure 5.6. Absorbance of TMZ in the presence of different CD's and only TMZ in 1:2 ratio after the formation of inclusion complex after 24 hours

Hence, it could easy be said that temozolomide forms a complex with three different cyclodextrins namely β -cyclodextrin, hydroxy β -cyclodextrin, hydroxy γ -cyclodextrin in 0.1 M HCl and, inclusion complex enhances the solubility of temozolomide. The positive effect of cyclodextrins on temozolomide solubility is continued to be investigated with increasing the amount of cyclodextrins in complexation to obtain an ideal temozolomide-cyclodextrin ratio. For that purpose TMZ:CD complexes with 1:2 and 1:5 ratios are formed and their UV spectrums are shown in Figure 5.6. and 5.7.

The amounts of solubilized TMZ in all CD mixtures and in only TMZ solution after 24 hours are calculated by using the calibration curve of TMZ in Figure 5.3 and are tabulated in Table 5.1. Individual absorbance scans comparing the change in solubility from three different molar ratios for each solution show that the amount of solubilized TMZ is higher in the presence of CD's regardless of the type of CD used however at varying degrees.

The amounts of solubilized TMZ in only TMZ solution and in all molar ratios of TMZ: CD complexes in decreasing order for the 24 hours is given below :

TMZ-H- β -CD inclusion complex > TMZ- β -CD inclusion complex > TMZ-H- γ -CD
inclusion complex > only TMZ

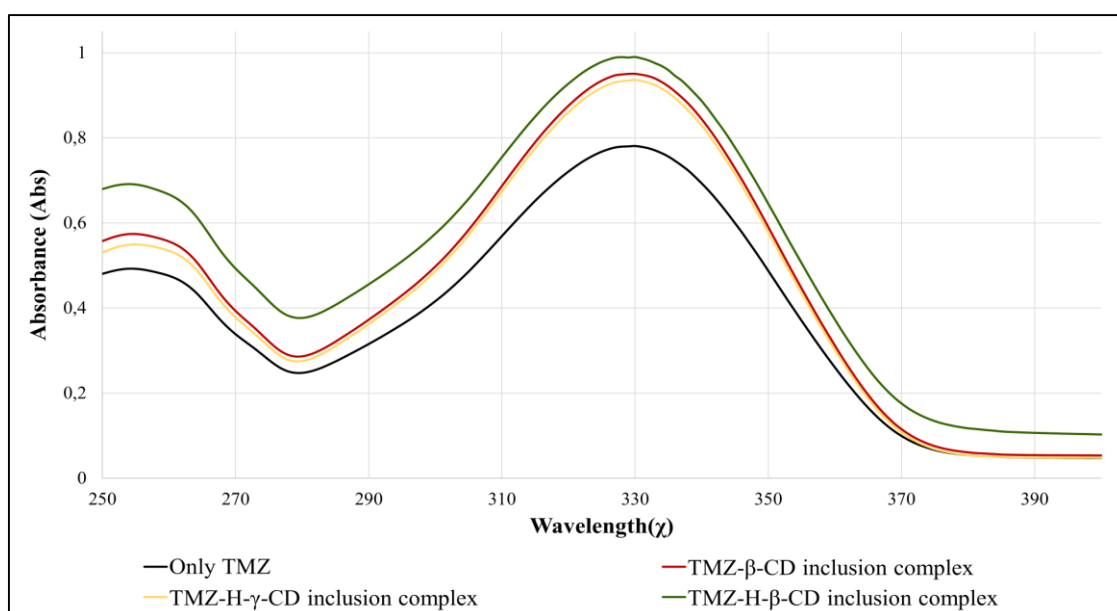


Figure 5.7. Absorbance of TMZ in the presence of different CD's and only TMZ in 1:5 ratio after the formation of inclusion complex after 24 hours

Table 5.1. Amounts of solubilized TMZ in mg/mL in 0.1 M HCl after the formation of inclusion complex after 24 hours

	1 mol TMZ : 1 mol CD (mg/mL)	1 mol TMZ : 2 mol CD (mg/mL)	1 mol TMZ : 5 mol CD (mg/mL)
Only TMZ	3.46±0.006		
TMZ- β-CD inclusion complex (mg/mL)	4.34±0.06	4.35±0.12	4.33±0.04
TMZ- H-β- CD inclusion complex (mg/mL)	4.97±0.12	4.39±0.05	4.36±0.06
TMZ- H- γ- CD inclusion complex (mg/mL)	4.32±0.06	4.17±0.08	4.12±0.15

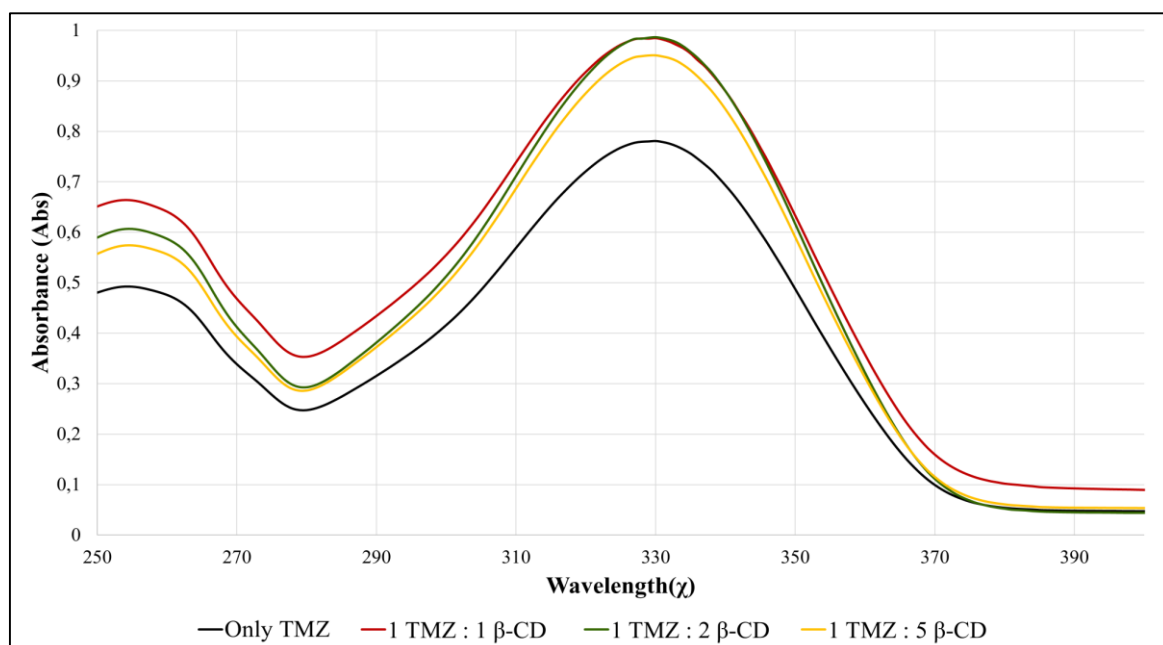


Figure 5.8. Absorbance of TMZ in the presence of β-CD and only TMZ in all molar ratios after the formation of inclusion complex after 24 hours

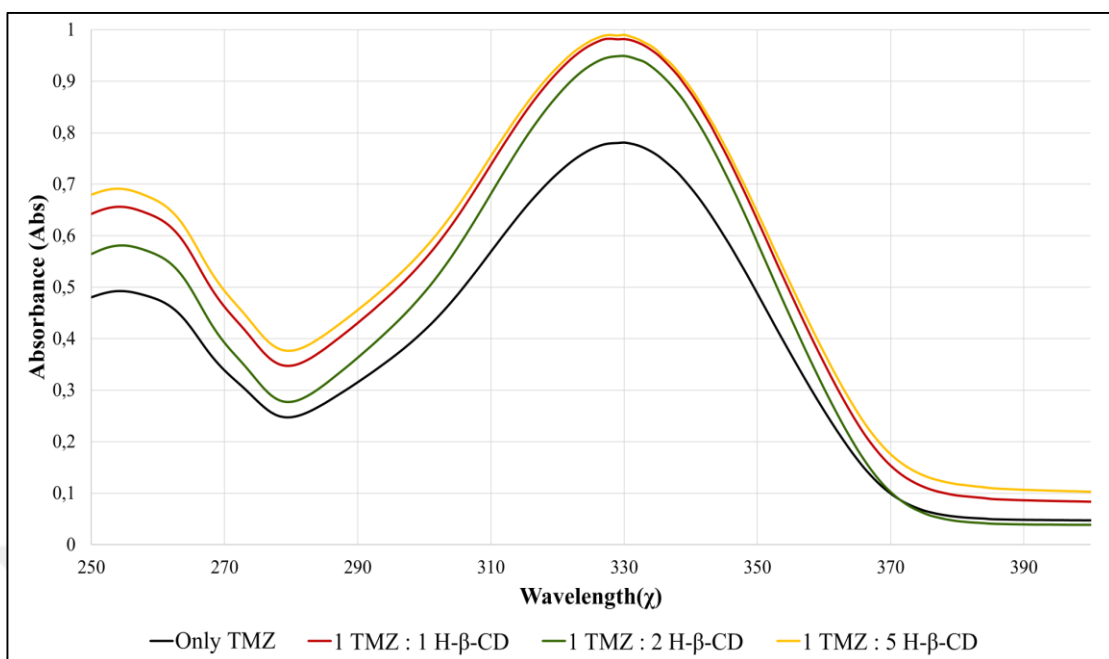


Figure 5.9. Absorbance of TMZ in the presence of H- β -CD and only TMZ in all molar ratios after the formation of inclusion complex after 24 hours

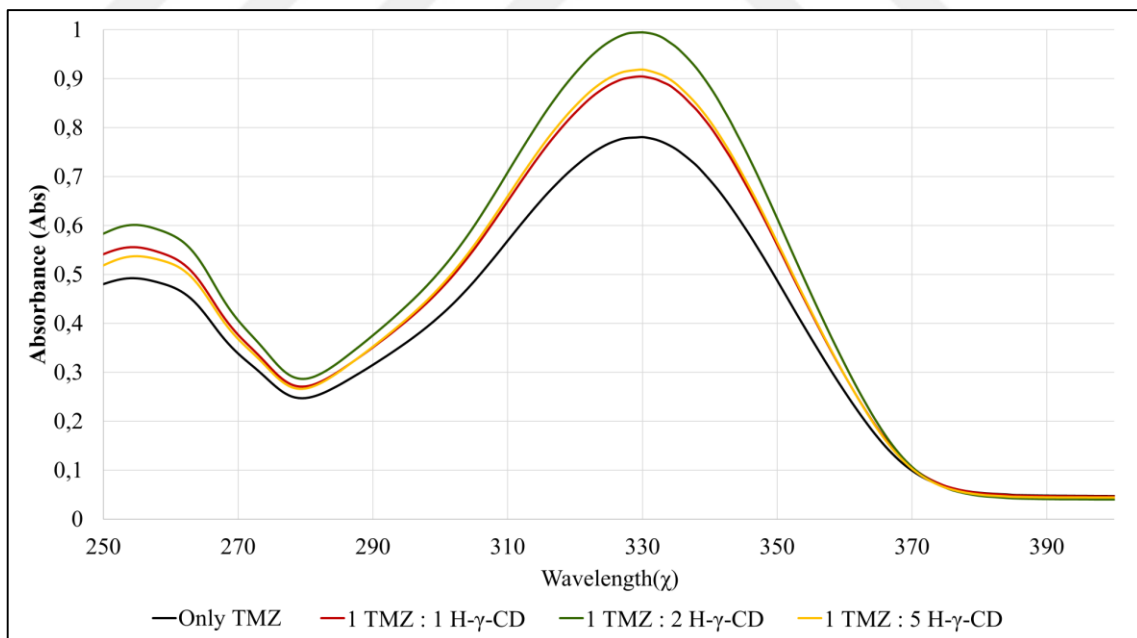


Figure 5.10. Absorbance of TMZ in the presence of H- γ -CD and only TMZ in all molar ratios after the formation of inclusion complex after 24 hours

In addition, Figure 5.8, 5.9 and 5.10 also show individual absorbance scans comparing the change in solubility of TMZ from three different molar ratios for each CD solutions and only TMZ solution. According to these Figures, the amount of solubilized TMZ is higher in the presence of CD's regardless of the type of CD used however, this increase is not proportional to quantity of cyclodextrin. In summary, solubilized amount of TMZ with and without CDs are plotted for all molar ratios as Figure 5.11.

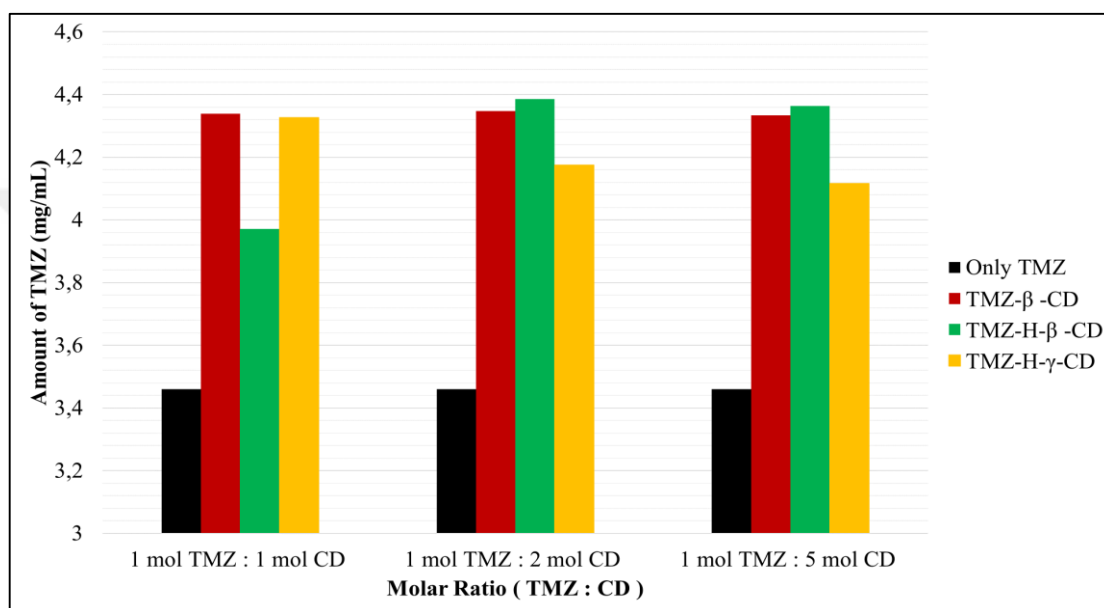


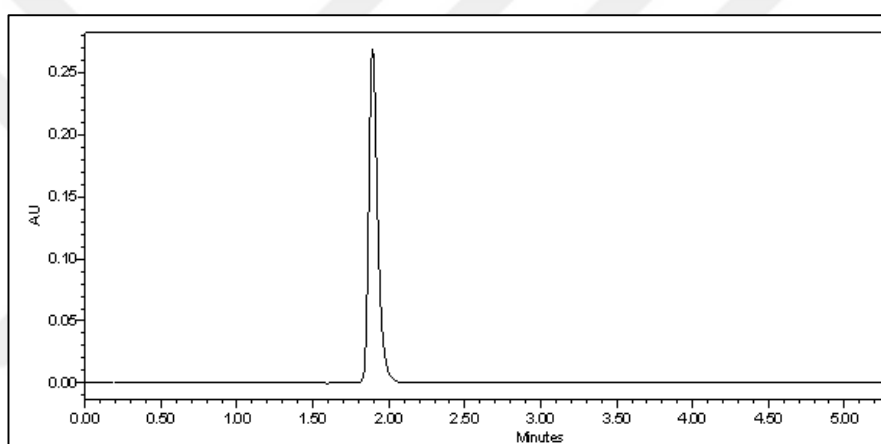
Figure 5.11. Amount of solubilized TMZ in the presence of CDs and only TMZ in all molar ratios after the formation of inclusion complex after 24 hours

5.4. HIGH PRESSURE LIQUID CHROMATOGRAPHY MEASUREMENTS

In order to more accurately measure the concentration of solubilized TMZ in the presence of different CD's as well as in their different mixing ratios after one hour, 24 hours and 48 hours HPLC method is used. To measure the amount of TMZ, five different known concentrated standard solutions is given to the system and correlation of these obtained data is used in the evolution of peak areas from which, the concentration of unknown samples can be calculated. Therefore, the height of temozolomide peaks will give the raise to dissolved temozolomide amount quantitatively.

In HPLC reverse phase C18 column (X-Bridge 150mmx .6cm, .5 μ m, Waters) was used. Water that contained 0.5% acetic acid / methanol (80:20 v/v) was prepared for mobile phase. Standard calibration curve was obtained by five different temozolomide concentrations and for each measurement three samples were used and three injections were applied for each sample.

Like UV-Vis Spectroscopy measurements, after mixing TMZ and CD solutions with molar ratio as TMZ: CD 1:1, 1:2 and 1:5 the mixtures are shaken continuously at 250 rpm for 1 hour, 24 hours and 48 hours. And then, solutions are centrifuged at 6000 rpm for 15 min to remove excess amount of TMZ and supernates are diluted 200 times.



5.12. Typical TMZ scan in HPLC analysis (All data is shown in Appendix)

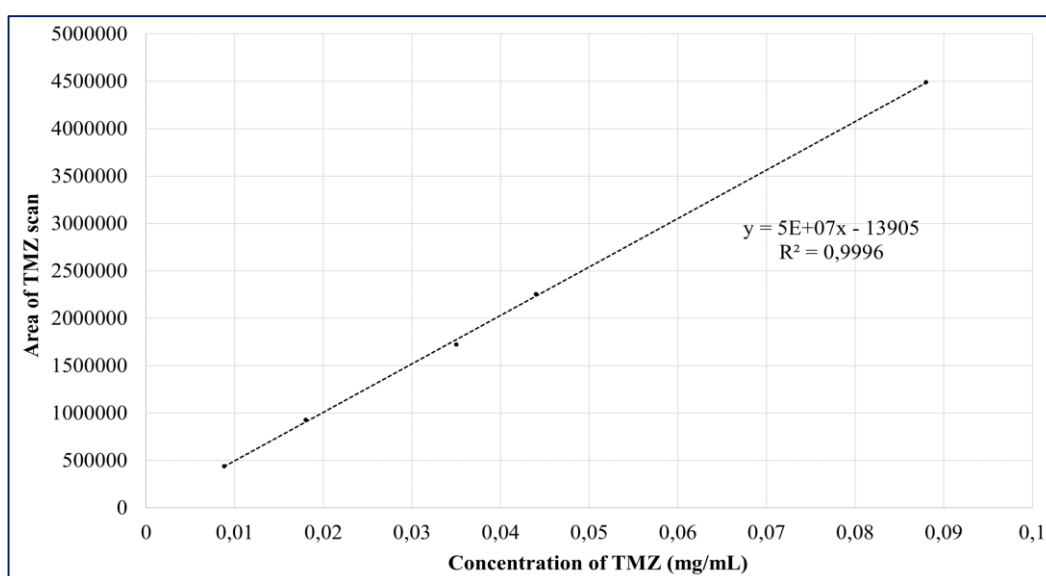


Figure 5.13. Calibration curve of Temozolomide for HPLC analysis

The peak area of TMZ at approximately 2 min which is the retention time at 330 nm is increased with rising dissolved temozolomide amount because of relations between area and concentration and the typical TMZ scan in HPLC analysis is shown in Figure 5.12. Solubilized amount of TMZ for each sample is calculated by using calibration curve in Figure 5.13.

Table 5.2. Amounts of solubilized TMZ in mg/mL in 0.1 M HCl after the formation of inclusion complex after one hour and 24 hours

	1 mol TMZ : 1 mol CD (mg/mL)		1 mol TMZ : 2 mol CD (mg/mL)		1 mol TMZ : 5 mol CD (mg/mL)	
	One hour	24 hours	One hour	24 hours	One hour	24 hours
Only TMZ	3.46±0.006					
β-CD-TMZ	4.23±0.16	4.23±0.40	4.43±0.14	4.31±0.49	4.59±0.07	4.51±0.07
Hydroxy-β-CD-TMZ	4.13±0.14	4.29±0.04	4.3±0.09	4.26±0.4	4.43±0.4	4.25±0.1
Hydroxy-γ-CD-TMZ	4.33±0.16	4.29±0.04	4.35±0.07	4.43±0.02	4.53±0.5	4.52±0.8

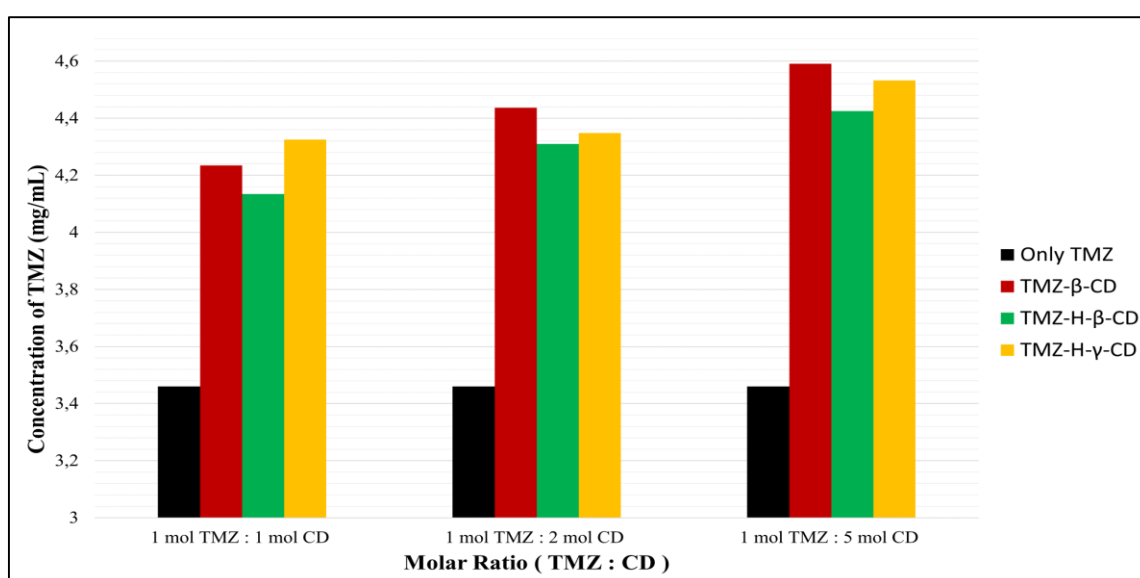


Figure 5.14. Amounts of solubilized TMZ in mg/mL after the formation of inclusion complex after one hour

The amount of temozolomide is obtained for each complex (1 mol TMZ:1 mol CD, 1 mol TMZ:2 mol CD, 1 mol TMZ:5 mol CD) after 1 hour, 24 hours and 48 hours are shown in Table 5.2 and Table 5.3 and graphically presented in Figure 5.14., 5.15. and 5.16. respectively.

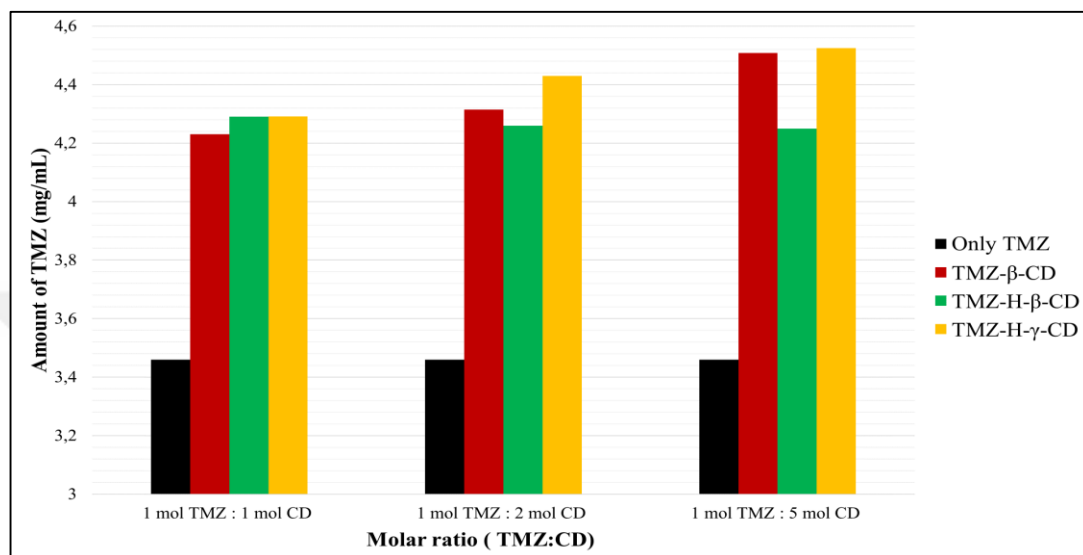


Figure 5.15. Amounts of solubilized TMZ in mg/mL after the formation of inclusion complex after 24 hours

Table 5.3. Amounts of solubilized TMZ in mg/mL in 0.1 M HCl after the formation of inclusion complex after 48 hours

	1 mol TMZ : 1 mol CD	1 mol TMZ : 2 mol CD	1 mol TMZ : 5 mol CD
Only TMZ (mg/mL)	3.46±0.006	3.46±0.006	3.46±0.006
TMZ- β-CD inclusion complex (mg/mL)	4.28	4.33±0.38	4.57±0.45
TMZ- H-β-CD inclusion complex (mg/mL)	4.52	4.46±0.18	4.53±0.1
TMZ- H- γ-CD inclusion complex (mg/mL)	4.56	4.5±0.31	4.67±0.17

Table 5.2 and Table 5.3 show that the amount of TMZ solubilized in the presence of cyclodextrins or not, does not significantly change from one hour to 24 hours but, a slight increase after 48 hours is observed. Figure 5.14, Figure 5.15 and Figure 5.16 clearly shows that TMZ solubility increases with increasing the three different CD's amount in the different mixing ratio, however this increase is not proportional with the added CD's.

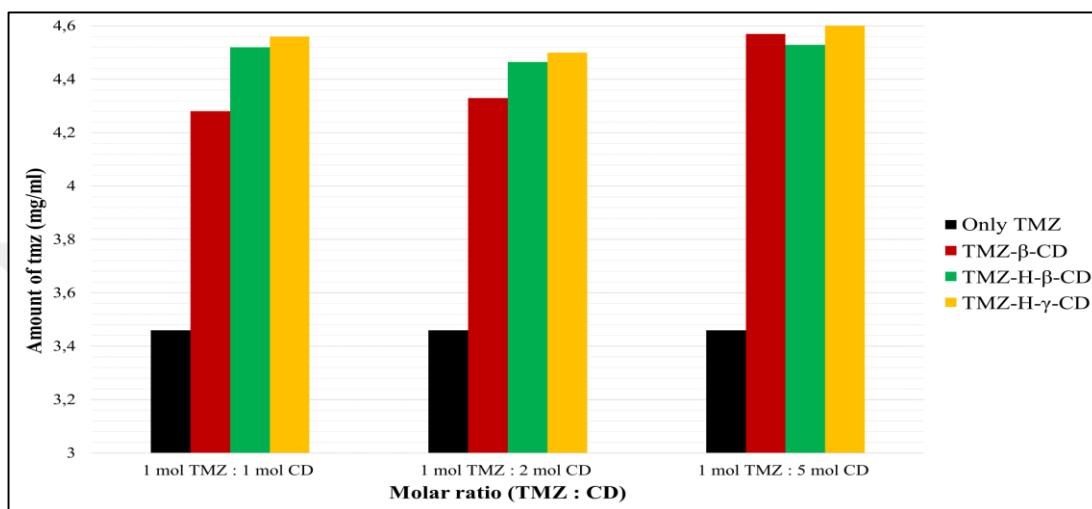


Figure 5.16. Amounts of solubilized TMZ in mg/mL after the formation of inclusion complex after 48 hours

5.5. HEAT PROFILES OF INCLUSION COMPLEXES

To show that inclusion complex actually forms heat profiles of inclusion complexes with between TMZ and CDs, the first technique employed was DSC. Differential Scanning Calorimeter measures the heat flow with respect to temperature. When a complex forms the interaction between the molecules should lead to a different heat profile than that of a physical mixture of the two components, therefore only TMZ, only β-CD, TMZ-β-CD inclusion complex particles and TMZ-β-CD physical mixing are investigated using DSC. In Figure 5.17, the temperature scan in the range of 25 °C and 250 °C, exhibit an exothermic peak around 209 °C for only TMZ, which shows the heat released upon decomposition of TMZ. In this temperature range, an endothermic peak around 140 °C for only β-CD is observed which is related to the dehydration of β-CD.

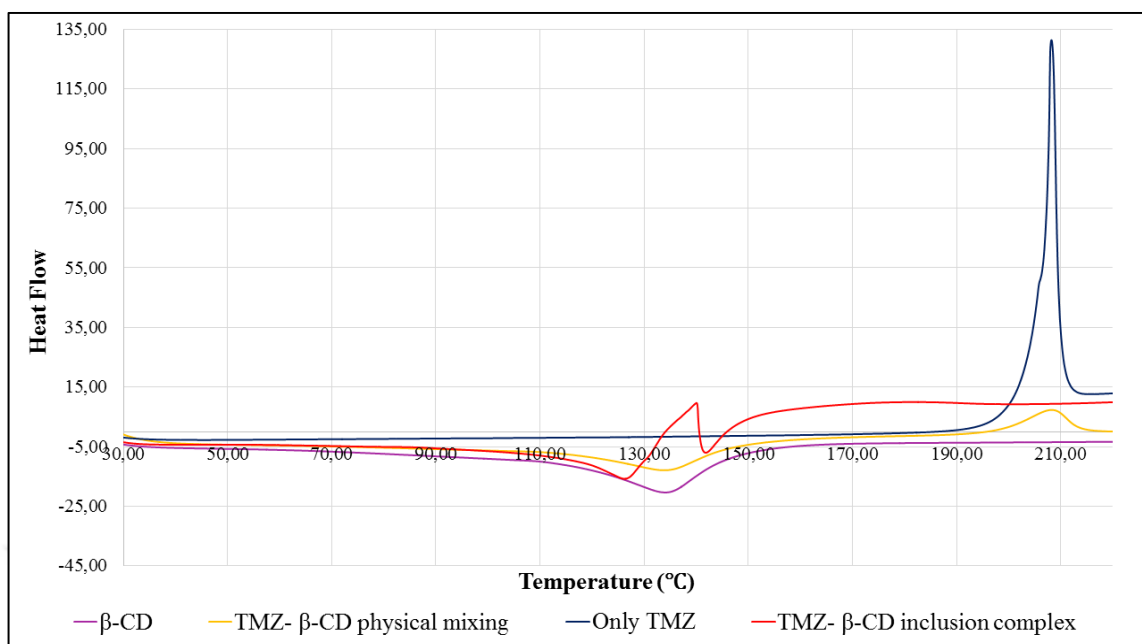


Figure 5.17. DSC curves of TMZ- β -CD inclusion complex and physical mixing

In the physical mixture of TMZ- β -CD, both the endothermic peak of dehydration from β -CD and exothermic peak from the decomposition of TMZ are present in the exact temperature locations of only TMZ and only β -CD. However, in the inclusion complex, neither of these peaks is visible, indicating the formation of a new complex. Many experimental studies reported that according to the results of DSC experiments, the obtained inclusion complexes had different physicochemical characteristics compared to the physical mixture of free substances [152-154]

5.6. THERMOGRAVIMETRIC ANALYSIS OF COMPLEXES

TGA is another technique employed to show that inclusion complex and physical mixture of TMZ and CDs exhibit different thermal behavior. TGA shows the weight loss (weight %) of materials upon heating (Temperature, °C).

In general, weight loss occurs due to the decomposition of the material and the onset temperature of this decomposition is particular point to the compound, therefore onset temperature can be used as a verification of the compound. Many experimental research showed that TGA was used to determine characterization of inclusion complex between

some drugs and cyclodextrins [155,156]. In TGA measurements, prepared inclusion complex particles and physical mixing particles are compared with TMZ only and CD only.

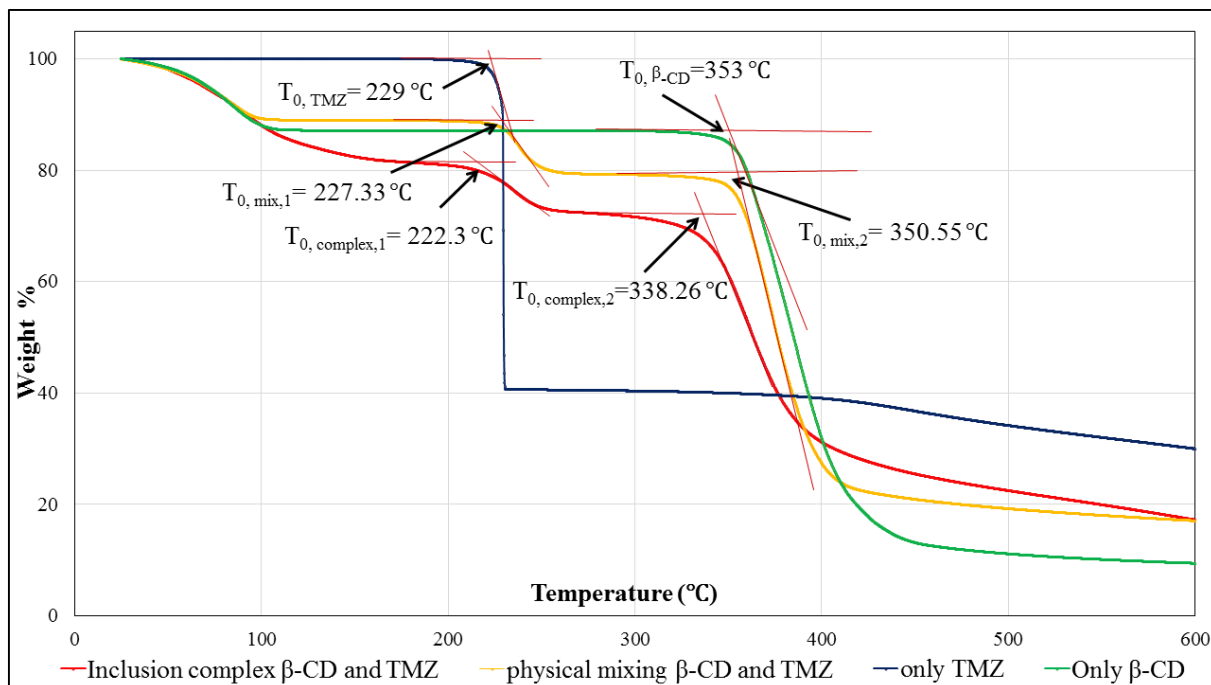


Figure 5.18. TGA curves of only TMZ, only β -CD, TMZ- β -CD inclusion complex and physical mixing

For TMZ- β -CD inclusion complex as Figure 5.18., dark blue line shows the weight loss profile of only TMZ, with the onset temperature of 229 °C. Green line is the weight loss profile of only β -CD, with the onset temperature of 353 °C. The initial weight loss observed until about 150 °C is due to water loss in the structure. In the physical mixture (yellow line), two onset temperatures are observed in the graph, one can be associated with TMZ (227 °C) and the other can be β -CD (351 °C). The onset values are very similar to those of pure TMZ and β -CD, which is expected from the physical mixture. However, in the TMZ- β -CD inclusion complex, although two onset temperatures from TMZ and β -CD did not disappear, are still observed, there is a temperature shift of 7 and 15 °C respectively, which is quite important, indicating interaction of TMZ and β -CD at the complexation level.

5.7. MORPHOLOGY OF THE INCLUSION COMPLEX

In order to observe the formation of inclusion complex between TMZ and β -CD, morphology changes are very important for each particles. Morphology of the particles of this size are best observed by using SEM. In Figure 5.19 and 5.20 it is clearly said that TMZ and β -CD morphologies are very different each other.

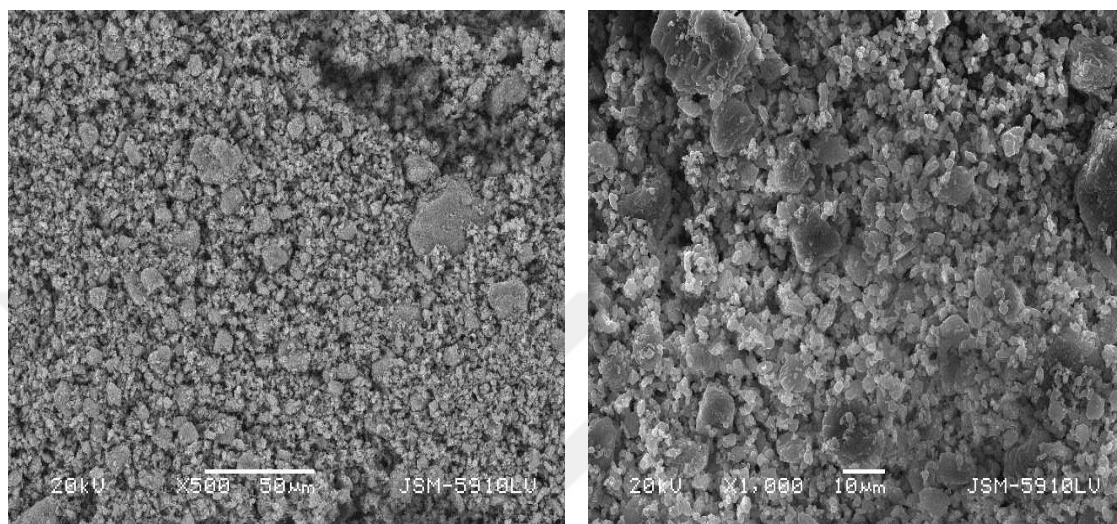


Figure 5.19. SEM images of only TMZ

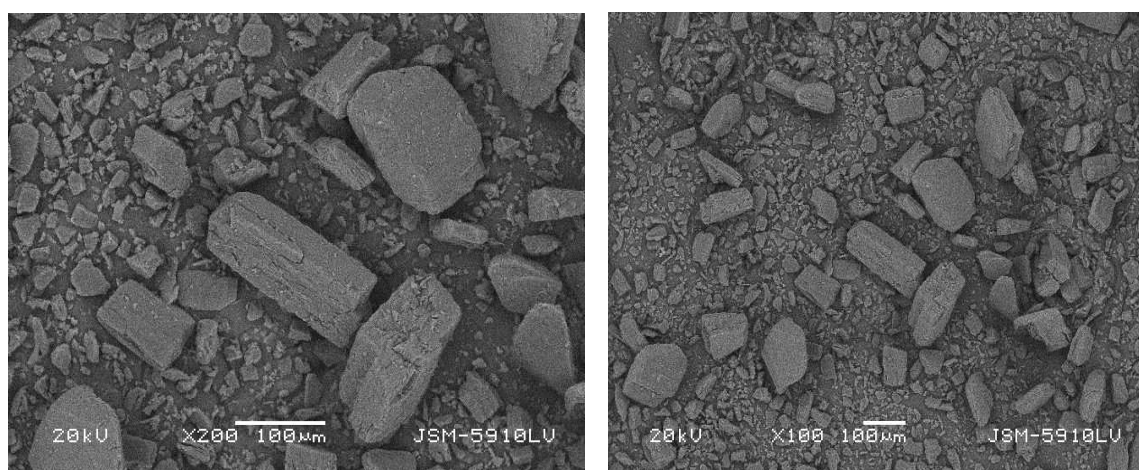


Figure 5.20. SEM images of only β -CD

In the physical mixture as Figure 5.21, the individual only TMZ and only β -CD morphologies can be identified. However, upon formation of a inclusion complex between TMZ and β -CD as Figure 5.22, a new morphology is observed where neither TMZ nor the β -CD is distinguished.

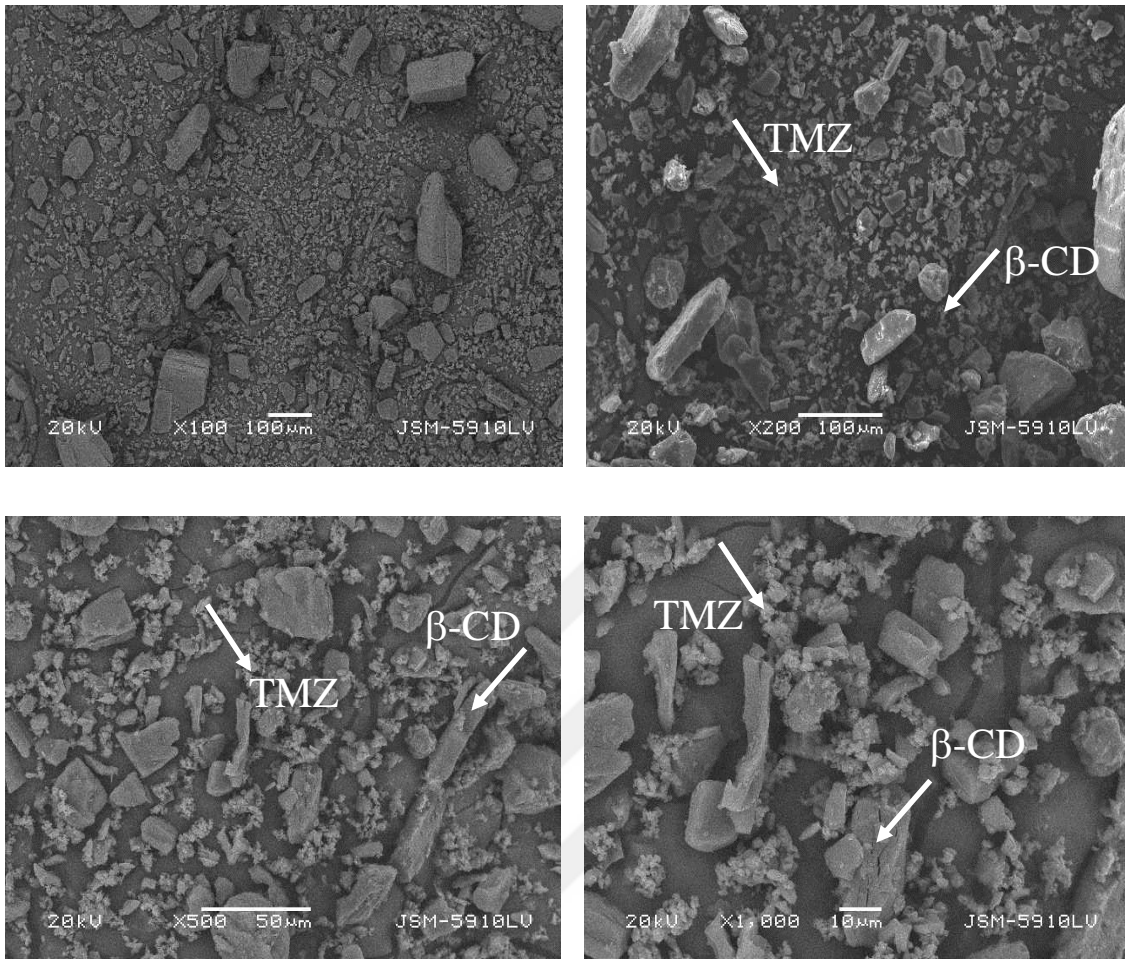
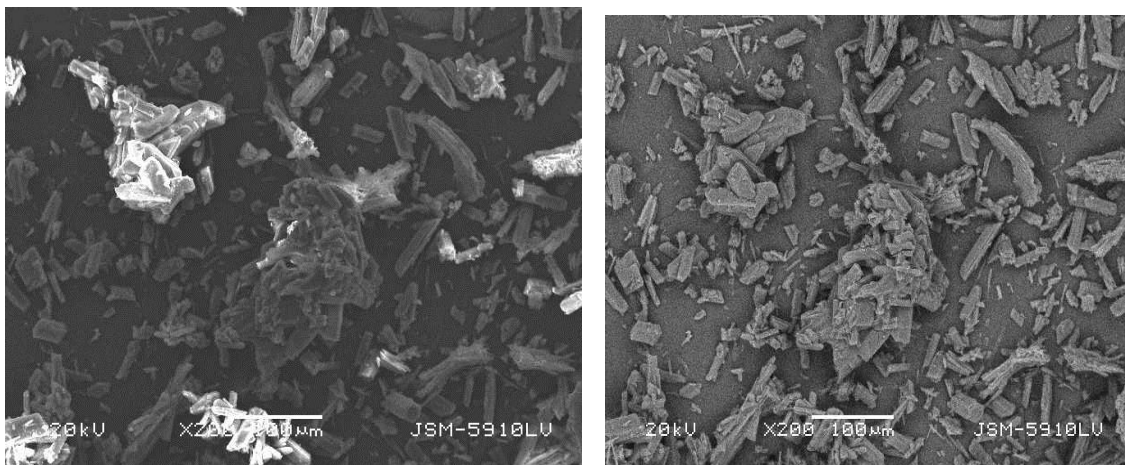


Figure 5.21. SEM images of TMZ- β -CD physical mixing



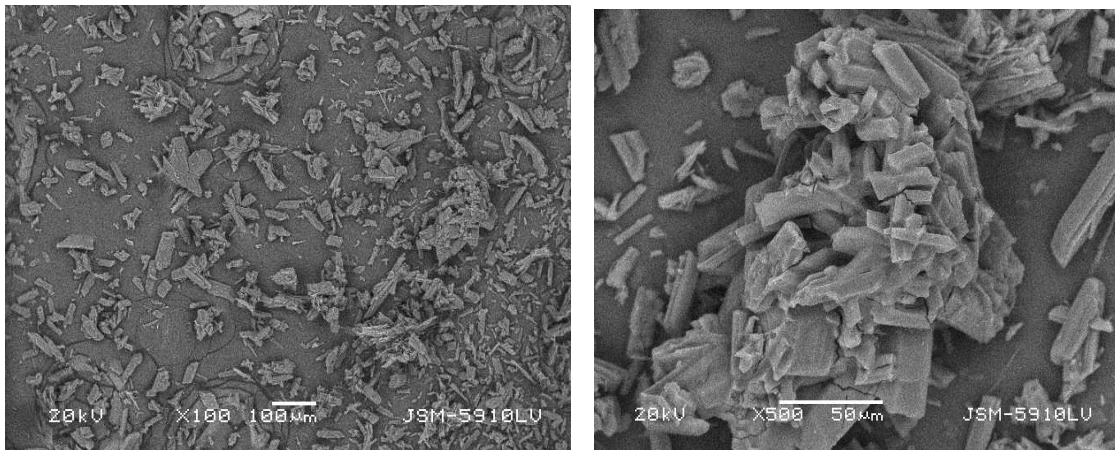


Figure 5.22. SEM images of TMZ- β -CD inclusion complex

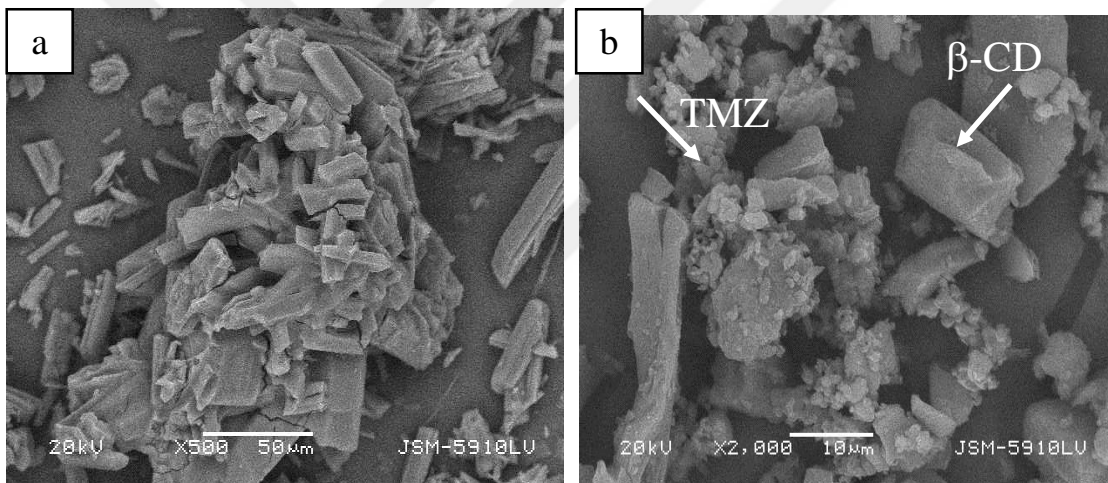


Figure 5.23. SEM images of TMZ- β -CD inclusion complex (a) and physical mixing (b) comparison

It can be seen clearly Figure 5.23 (b) shows that only TMZ and only β -CD is directly observed but, inclusion complex between TMZ and β -CD in Figure 5.23 (a) has different morphology from physical mixture where neither TMZ nor β -CD can be distinguished. There are a lot examples for SEM images of inclusion complex using different types of cyclodextrins with some medically relevant substances such as Ropivacaine [157], Chlorzoxazone [158], ellagic acid [159], Benzocaine [160], Oxaliplatin [161], Omeprazole [162]. For all, a clear difference between inclusion complex and physical mixture was evident, similar to what we have observed.

6. TARGETING OF TEMOZOLOMIDE USING MAGNETIC NANOPARTICLES

This chapter gives the optimization of the synthesis method of magnetite chitosan beads. Characterization of these particles are illustrated with SEM and DLS. In addition, preparation technique of chitosan nanoparticles and magnetite-chitosan beads with TMZ are given. Encapsulation of TMZ in these particles and beads are investigated using HPLC. Targeting studies of with magnetite-CD-TMZ and magnetite-chitosan-TMZ are presented in order to collect maximum amount of TMZ in a desired area.

6.1. FORMATION OF CHITOSAN NANOPARTICLES

Three different methods are used in order to synthesize chitosan nanoparticles.

First method (with TPP): 10 mL 0.5 wt % Chitosan in 1% acetic acid solutions and 10 mL 1 wt%, 1.5 wt% TPP solutions in water are prepared. While 10 mL TPP solutions are magnetically stirred, chitosan solution is drop wise added to the salt solution over one minute and the final solution is stirred with 500 rpm another 30 minutes. Procedure for the preparation of chitosan nanoparticles are shown in Figure 6.1 for the above-mentioned method.

Second method (with $\text{Na}_2\text{SO}_4 \cdot 10\text{H}_2\text{O}$): In the same way, 10 mL 0.2, 0.25, 0.5, 0.75 and 1 wt% chitosan in 1% acetic acid solutions and 10 mL 2.5, 5 wt% $\text{Na}_2\text{SO}_4 \cdot 10\text{H}_2\text{O}$ solutions are prepared. While 10 mL $\text{Na}_2\text{SO}_4 \cdot 10\text{H}_2\text{O}$ solutions are magnetically stirred, 10 mL chitosan solution is added dropwise to the salt solution and the obtained solution is stirred with 500 rpm another 30 minutes. Procedure for the preparation of chitosan nanoparticles is shown in Figure 6.1 for the above-mentioned method.

After the synthesis of the chitosan nanoparticles using both methods, the obtained solutions are centrifuged at 6000 rpm for 15 minutes. It is expected that the precipitates are the chitosan nanoparticles.

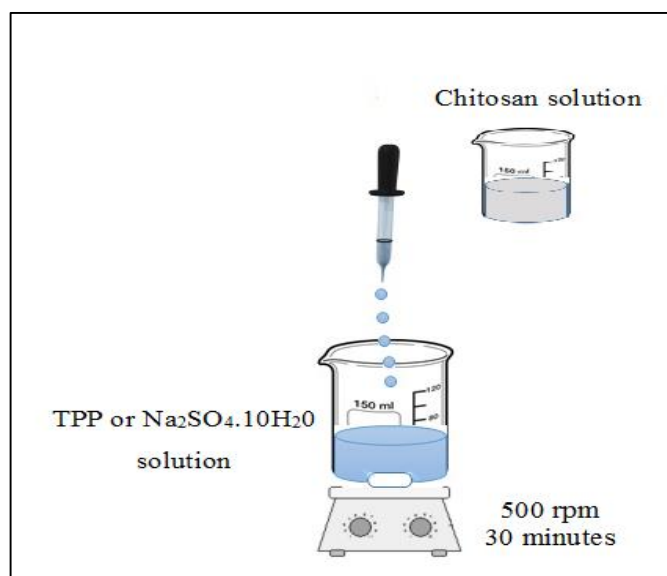


Figure 6.1. Chitosan formation procedure (first and second method)

6.2 FORMATION OF MAGNETITE-CHITOSAN BEADS

First method (Chitosan-magnetite solution): 10 mL 0.25, 0.5, 0.75 and 1 wt% chitosan in 1% acetic acid solutions are prepared and 3 mL 3.91 mg/mL aqueous magnetite solution is added to the prepared chitosan solution. 10 mL 5 wt% and 2.5 wt% $\text{Na}_2\text{SO}_4 \cdot 10\text{H}_2\text{O}$ in water are prepared and then, 13 mL chitosan-magnetite solution is added dropwise to the 10 mL salt solution over one minute and the final solution is stirred another 30 minutes. Procedure of this method is shown in Figure 6.2.

Second method (Salt-magnetite solution): 10 mL 0.25, 0.5, 0.75 and 1 wt% chitosan in 1% acetic acid solution is prepared and then, 3 mL 3.91 mg/mL aqueous magnetite solution is added to 10 mL 5 wt% and 2.5 wt% aqueous $\text{Na}_2\text{SO}_4 \cdot 10\text{H}_2\text{O}$ solution to obtain the final desired salt concentration (magnetite-salt solution). While being magnetically stirred, chitosan solution is drop wise added to the magnetite-salt solution over one minute and the final solution is stirred another 30 minutes. Procedure of this method is shown in Figure 6.3.

6.3. FORMATION OF CHITOSAN NPs AND MAGNETITE-CHITOSAN BEADS WITH TMZ

Two different ways are used in order to prepare chitosan NPs and magnetite-chitosan beads with TMZ.

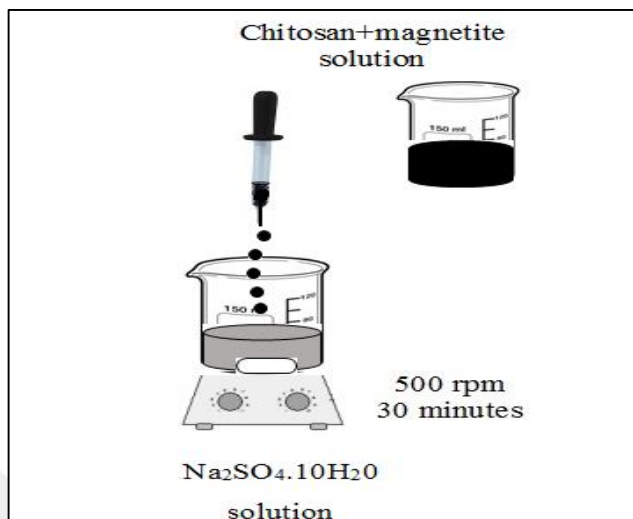


Figure 6.2. Formation of magnetite-chitosan beads with first method

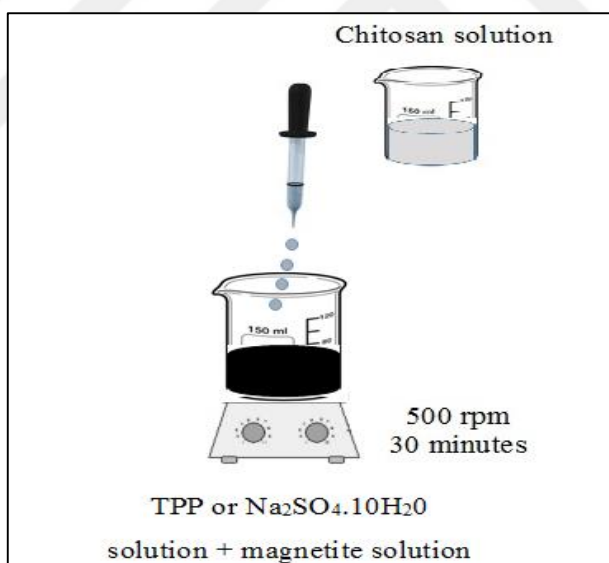


Figure 6.3. Formation of magnetite-chitosan beads with second method

First way (TMZ addition during the formation): The required amount of TMZ is added to the prepared chitosan solution and then the solution is magnetically stirred with 350 rpm for 30 minutes (chitosan-TMZ solution). Afterwards, chitosan-TMZ solution is added drop wise to the salt solution and the final solution is stirred another 30 minutes. Thus, magnetite-chitosan beads are obtained with TMZ.

Second way (TMZ addition after the synthesis): The required amount of TMZ is added after the synthesis of chitosan NPs and magnetite-chitosan beads and then is stirred approximately 30 minutes. Thus, magnetite-chitosan beads are obtained with TMZ.

6.4. ENCAPSULATION OF DRUGS IN MAGNETITE-CHITOSAN BEADS AND ONLY CHITOSAN NANOPARTICLES

After the synthesis of the magnetite-chitosan beads and only chitosan particles, the obtained solution is centrifuged at 6000 rpm for 15 minutes. It is expected that the precipitates are the chitosan-magnetite beads and chitosan nanoparticles. The amount of TMZ in the beads and particles are calculated from measuring the remaining TMZ in the supernatant using HPLC.

6.5. TARGETING OF TMZ WITH MAGNETIC PARTICLES

Firstly, the targeting experiments are carried out with magnetite-CD-TMZ nanofluid and then, magnetite-CD-chitosan-TMZ nanofluid for optimization.

6.5.1. Targeting of TMZ with magnetite-CD and magnetite-chitosan beads

In order to target TMZ using magnetite-CD nanoparticles to the desired area in the body, some in vitro experiments were carried out. For the experiments, 55 mL/min flow rate a flow system with 2.51 mm diameter tubing of 103 cm length, 5 Neodymium magnets generating 0.5 T magnetic field in a specific part of the tube (i.e. the test section) and a peristaltic pump is used with 40 rpm to simulate targeting studies. A schematic diagram for targeting magnetite-CD-TMZ and magnetite-chitosan-TMZ is shown in Figure 6.4. After the flow is stopped, only air is passed in the tube in order to collect magnetite-CD-TMZ nanofluid in the desired area (test section). And then, magnets are removed and captured magnetite nanoparticles are collected with 1 M HCl solution.

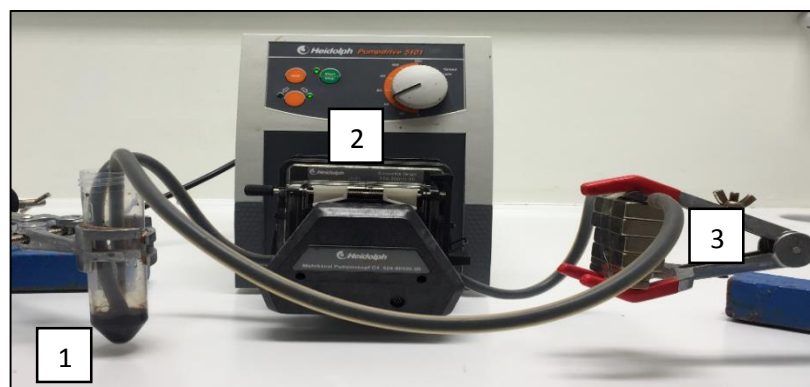


Figure 6.4. Schematic Diagram of Targeting Study

(1-magnetic fluid, 2-peristaltic pump and 3-test section)

Also, targeting of TMZ using magnetite-chitosan beads experiments were carried out using the same procedure and set-up.

For magnetite-CD and magnetite-chitosan beads targeting experiments, the concentration of magnetite captured in the desired area is calculated after carrying out Tiron chelation test and the amount of TMZ captured in the desired area is determined using HPLC.

6.5.2. HPLC Analysis for Targeting Studies

Prior to measurements, magnetite in the system should be removed as the presence of nanoparticles would interfere with the HPLC measurements and clog the column. After targeting experiments, in order to remove the magnetite prior to HPLC measurements, 1 M HCl is used to convert all $\text{Fe}_3\text{O}_4(\text{s})$ to $\text{Fe}^{+3}(\text{aq})$, which takes place overnight. 1 M HCl is also required for the chemical stability of TMZ alone until the HPLC measurements are performed.

6.6. DRUG ENCAPSULATION AND TARGETING

6.6.1. Targeting of magnetite-CD-TMZ particles

Firstly, 1 wt% β -CD coated magnetite nanoparticles are synthesized by co-precipitation method. And then, β -CD coated magnetic nanoparticles are collected with magnetic separation as shown Figure 6.5 and 50 mL 0.1 M HCl solution was added to magnetic nanoparticles to ensure the stability of TMZ. 10 mg TMZ was added into the magnetic nanofluid and then, solution was vortexed and sonicated for 1 minute to dissolve TMZ completely to obtain magnetite-CD-TMZ solution.



Figure 6.5. Magnet Separation of Magnetic Nanofluid

The magnetite-CD-TMZ nanofluid was passed continuously through the system with 40 rpm for 5 hours. After the flow is stopped, only air was passed in the tube in order to collect magnetite-CD-TMZ nanofluid but, it was seen that particles did not collect in the test section because of the colloidal stability of the nanofluid. Therefore, concentration of the β -CD in the magnetite solution was decreased as 0.5 wt% and 0.25 wt%. The same procedure was repeated however again, magnetite-CD-TMZ nanofluid collected was too little as shown Figure 6.6 a and b. It can be seen that the collection of the nanofluid is not successful in the desired area.

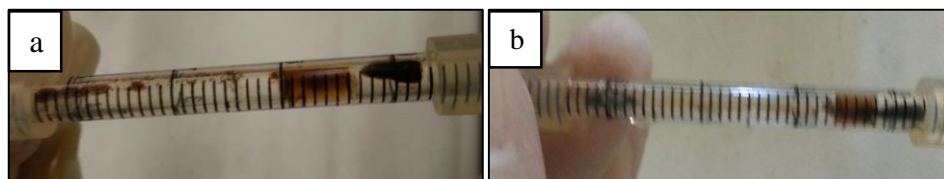


Figure 6.6. Captured magnetite-CD-TMZ nanofluid in the test section using (a) 0.5 %wt CD (b) 0.25 %wt CD after 5 hrs

These results show that successful collection of magnetic nanofluid was not achieved in the test section. It is known that when concentration of CD is decreased in the magnetic nanofluid in water, colloidal stability of the nanofluid is decreased. However, these experiments were carried out in 0.1 M HCl so, colloidal stability of 0.5 wt% CD magnetite solution in water and in 0.1 M HCl after 5 hours is shown in Figure 6.7.

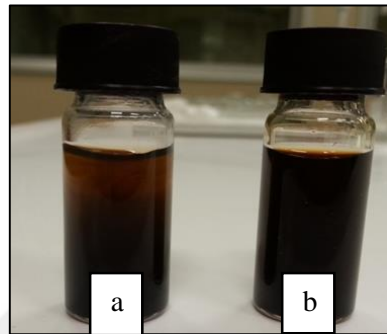


Figure 6.7. Colloidal stability of magnetite nanofluid in water (a) and in 0.1 M HCl (b) after 5 hours

Figure 6.7. shows that magnetite nanofluid in 0.1 M HCl more stable colloiddally than magnetite nanofluid in water after 5 hours. Highly colloidal particles cannot be collected by a magnet during flow. The colloidal stability of particles increase over time in the presence of 0.1 M HCl, therefore the duration of the experiment is shortered to 1 hr to be able to capture more particles.

Thereafter, magnetite-CD-TMZ nanofluid which contain 0.25 wt% β -CD and 10 mg TMZ was passed continuously through the system with 40 rpm for 1 hour. After the flow is stopped, only air was passed in the tube in order to collect magnetite-CD-TMZ nanofluid, it was seen that captured amount of magnetite was increased as shown in Figure 6.8(a).

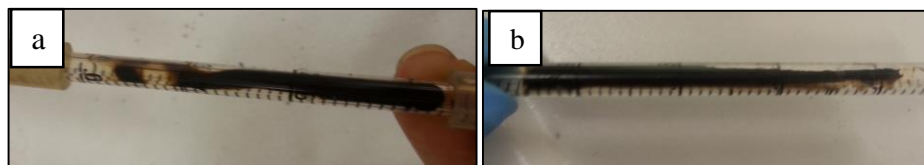


Figure 6.8. Captured magnetite-CD-TMZ nanofluid in the test section using (a) 0.25% wt CD and (b) 0.125% wt CD after 1 hr

And then, HPLC was used in order to calculate the collected amount of TMZ in captured magnetite-CD-TMZ nanofluid. For HPLC results, 0.01 mg TMZ was targeted to the desired area (test section).

In addition, same experiments were repeated with magnetite-CD-TMZ nanofluid which contain 0.125 wt% β -CD and 10 mg TMZ was passed continuously through the system with 40 rpm for 1 hour. After targeting study, only air was passed in the tube in order to collect magnetite-CD-TMZ nanofluid, it can be seen that magnetite-CD-TMZ nanofluid was collected in the test section as shown Figure 6.8(b).

The amount of collected TMZ in the test section was 0.01 mg which is 1% of the initial amount of TMZ in the magnetic fluid. The low amount of TMZ collected indicates that magnetite-CD system is not successful in targeting TMZ in desired area.

In the previous section, the inclusion complex formation between TMZ-CD was shown. CDs were also shown to stabilize magnetite NPs and TGA results had shown the presence of CD's with the particles. In this section, the magnetite was shown to be collected in the desired area. With all these three successful pairings, TMZ should have been collected in the test section. However, this step failed for reasons that were not further investigated. In an attempt to form particles that will contain TMZ and still can be directed by a magnetic field, magnetic beads with chitosan are prepared.

6.6.2. Encapsulation and Characterization of Chitosan Nanoparticles

6.6.2.1. Morphology of the Chitosan Nanoparticles

To explore the morphology of chitosan nanoparticles formed, SEM is used. Initially, chitosan nanoparticals were synthesized with TPP as a salt by using first method as mentioned in Section 6.1. SEM images show that chitosan nanoparticles which are synthesized with two different concentrations of salt (final concentration of TPP to be 0.5 wt% and 0.75 wt%) are not spherical particles, they have only smooth surface. Chitosan gels were obtained using TPP as shown in Figures 6.9 and 6.10.

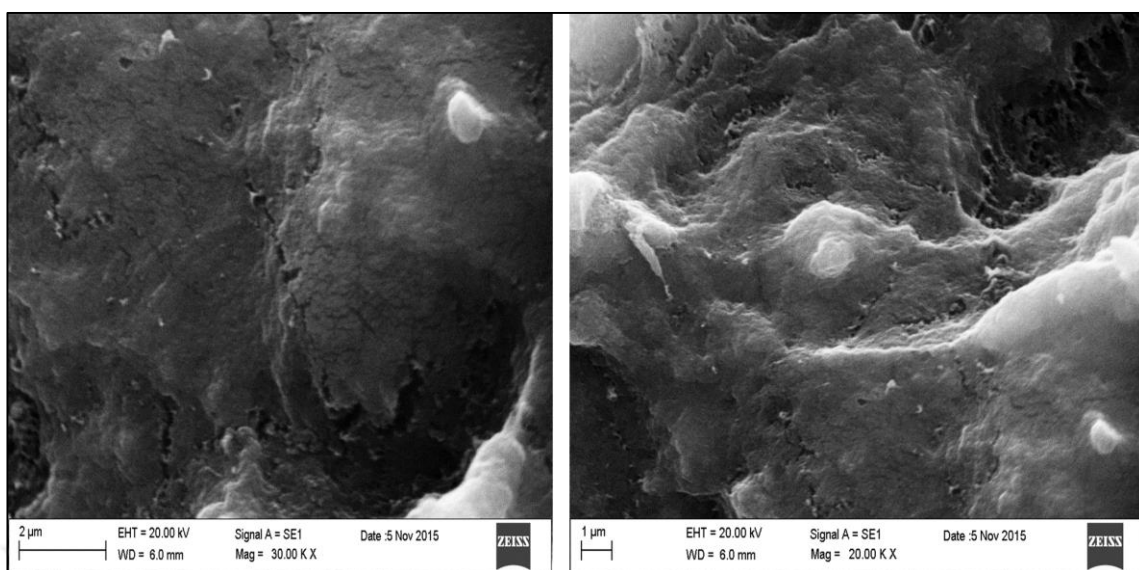


Figure 6.9. SEM images of chitosan NPs

([TPP]_{final} = 0.5wt% ; [chitosan]_{final} =0.25 wt%)

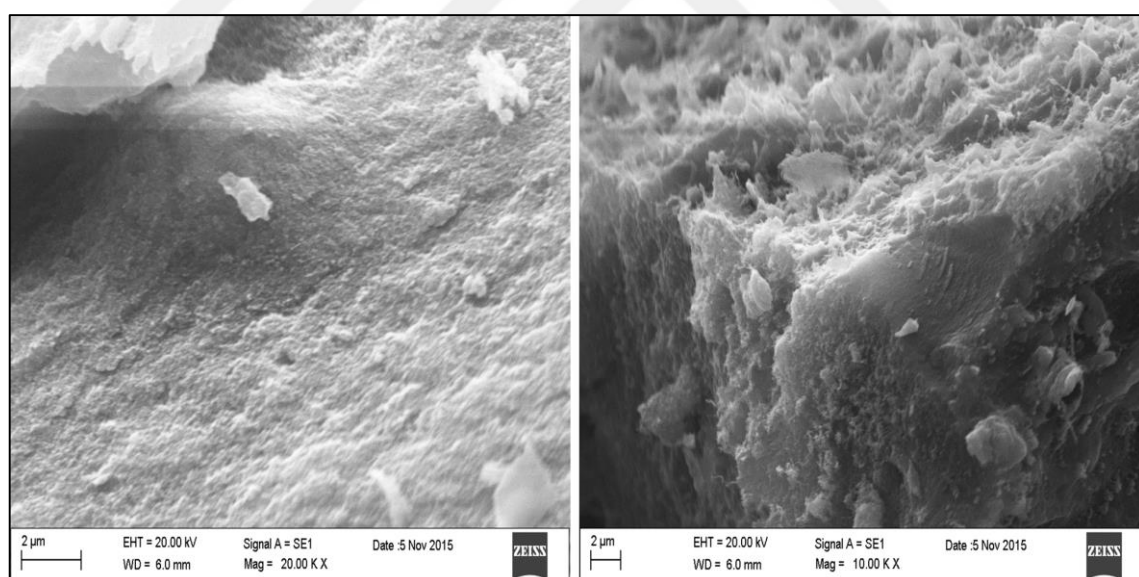


Figure 6.10. SEM images of chitosan NPs

([TPP]_{final} = 0.75wt% ; [chitosan]_{final} =0.25 wt%)

Therefore, chitosan nanoparticles were synthesized with $\text{Na}_2\text{SO}_4 \cdot 10\text{H}_2\text{O}$ by using second method as mentioned in Section 6.1. Chitosan NP prepared by iontopric gelation method with TPP was first reported by Calvo et al. (1997) [163], and has been widely examined and

developed by Janes et al. (2001) [164], and Pan et al. (2002) [165]. Using this method, average size of the obtained spherical chitosan NPs are approximately 200 nm [163, 164], 150 nm [165], 100 nm [166] and 75 nm [167]. However, in our work, Figures 6.11 and 6.12 show that chitosan nanoparticles are formed by using 5 wt% $\text{Na}_2\text{SO}_4 \cdot 10\text{H}_2\text{O}$ as a salt and 0.2 wt% and 0.25 wt% chitosan. Based on these results, experiments to optimize the nanoparticles are continued with $\text{Na}_2\text{SO}_4 \cdot 10\text{H}_2\text{O}$ salt. It can be seen that spherical chitosan nanoparticles were not obtained homogeneously and further studies are required.

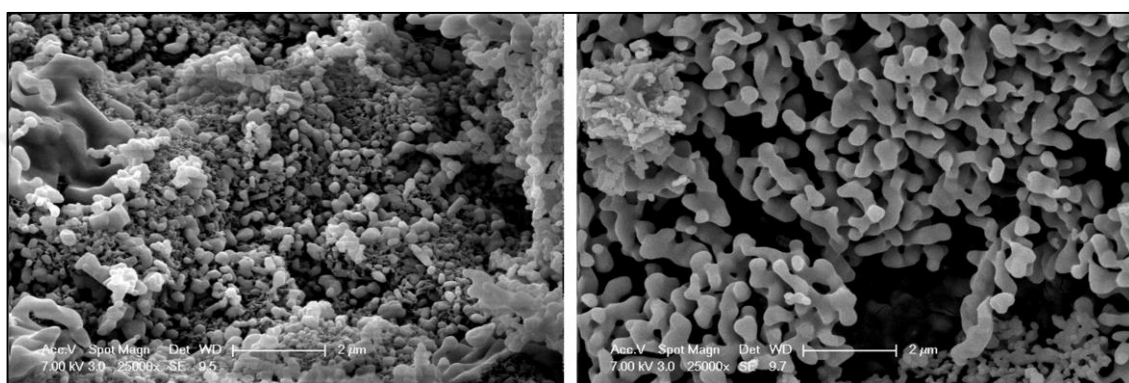


Figure 6.11. SEM images of chitosan NPs

($[\text{Na}_2\text{SO}_4 \cdot 10\text{H}_2\text{O}]_{\text{final}} = 2.5 \text{ wt\%}$; $[\text{chitosan}]_{\text{final}} = 0.10 \text{ wt\%}$)

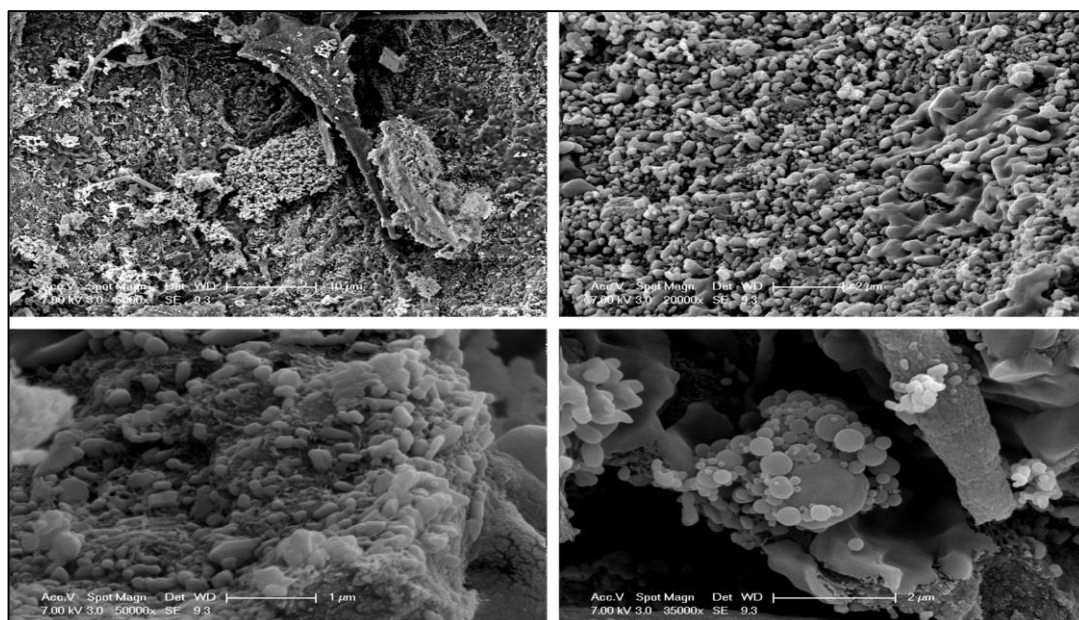


Figure 6.12. SEM images of chitosan NPs

($[\text{Na}_2\text{SO}_4 \cdot 10\text{H}_2\text{O}]_{\text{final}} = 2.5 \text{ wt\%}$; $[\text{chitosan}]_{\text{final}} = 0.125 \text{ wt\%}$)

First the salt concentration was increased. When concentration of $\text{Na}_2\text{SO}_4 \cdot 10\text{H}_2\text{O}$ was increased to 7.5 wt% in the second method of formation of chitosan nanoparticles better, chitosan nanoparticles are formed by using 5 wt% $\text{Na}_2\text{SO}_4 \cdot 10\text{H}_2\text{O}$ rather than 7.5 wt% $\text{Na}_2\text{SO}_4 \cdot 10\text{H}_2\text{O}$.

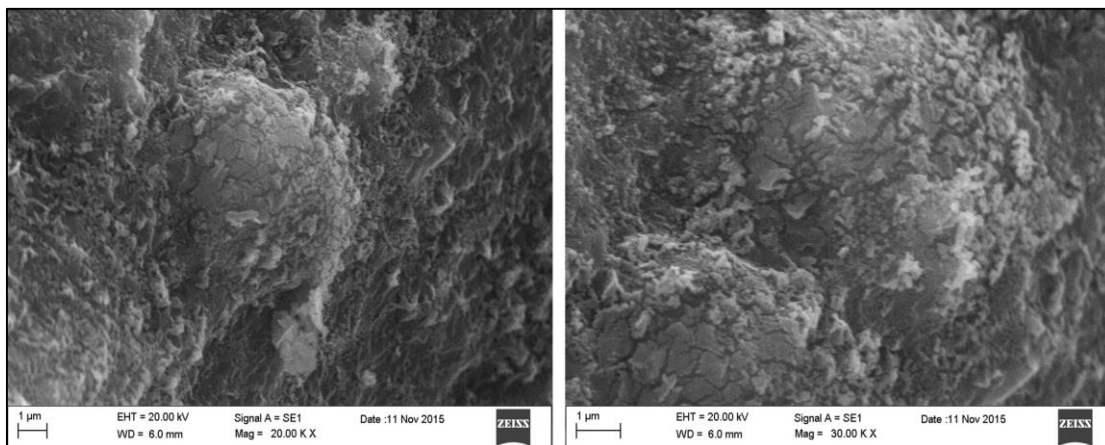


Figure 6.13. SEM images of chitosan NPs

($[\text{Na}_2\text{SO}_4 \cdot 10\text{H}_2\text{O}]_{\text{final}} = 3.75 \text{ wt\%}$; $[\text{chitosan}]_{\text{final}} = 0.125 \text{ wt\%}$)

Figure 6.13 and 6.14 clearly show that if the concentration of salt is increased, smooth surfaces as opposed to particles are obtained.

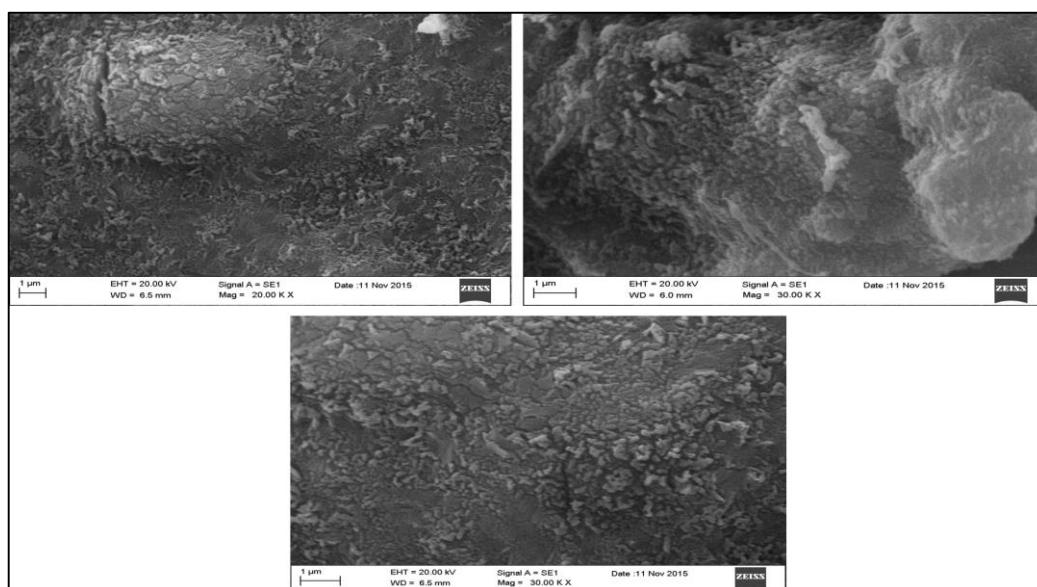


Figure 6.14. SEM images of chitosan NPs

($[\text{Na}_2\text{SO}_4 \cdot 10\text{H}_2\text{O}]_{\text{final}} = 3.75 \text{ wt\%}$; $[\text{chitosan}]_{\text{final}} = 0.25 \text{ wt\%}$)

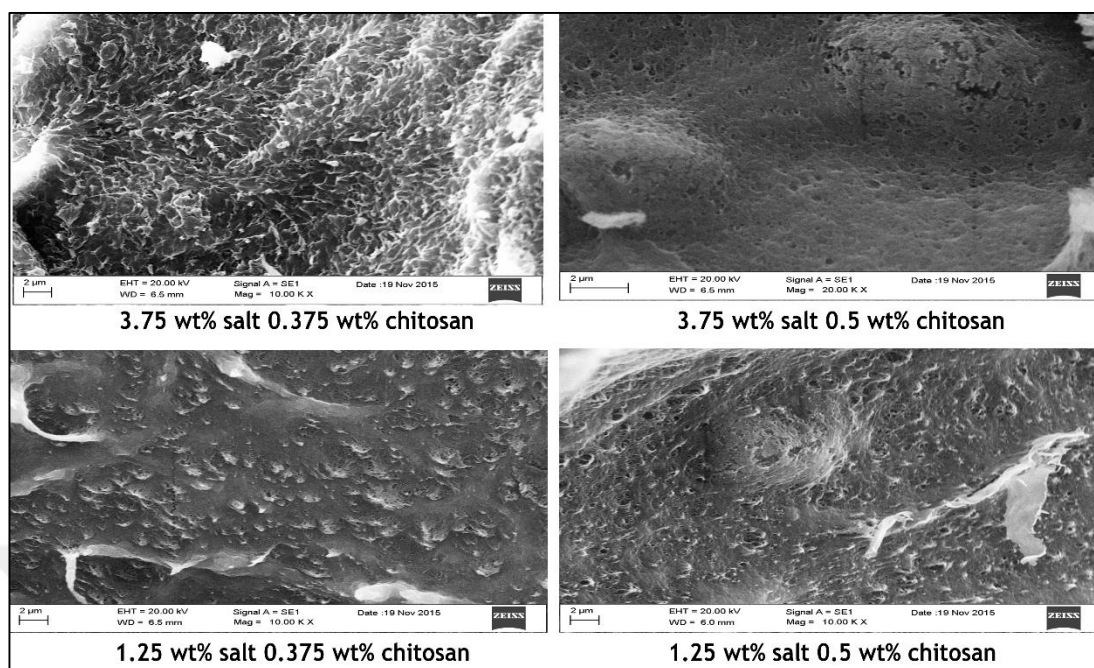


Figure 6.15. SEM images of chitosan NPs

($[\text{Na}_2\text{SO}_4 \cdot 10\text{H}_2\text{O}]_{\text{final}} = 3.75$ and 1.25 wt% ; $[\text{chitosan}]_{\text{final}} = 0.375$ and 0.5 wt%)

While the concentration of $\text{Na}_2\text{SO}_4 \cdot 10\text{H}_2\text{O}$ was increased to 7.5 wt% in the second method of formation of chitosan nanoparticles, also final concentrations of chitosan were increased to 0.375-0.5 %. Figure 6.15 shows that chitosan nanoparticles are not formed at high salt concentration. It can be easily said that in the presence of high amount of salt even if the chitosan concentration was increased, smooth surfaces were observed, and spherical chitosan nanoparticles were not obtained.

6.6.2.2. Size Measurement of Chitosan Nanoparticles

Size measurements were only performed for particles obtained using 2.5 wt% $\text{Na}_2\text{SO}_4 \cdot 10\text{H}_2\text{O}$ salt. 0.25 wt%, 0.75 wt% chitosan solutions were used and two different chitosan nanoparticles were synthesized using this method. In order to determine the size of these chitosan nanoparticles, Dynamic Light Scattering (DLS) was used. According to these data, % intensity and % number graphs were plotted as shown Figure 6.16. and 6.17.

Figure 6.16. shows that the size of the chitosan nanoparticles which contain 0.125 wt% chitosan and 1.25 wt% salt is approximately 44 nm with homogeneous size distribution.

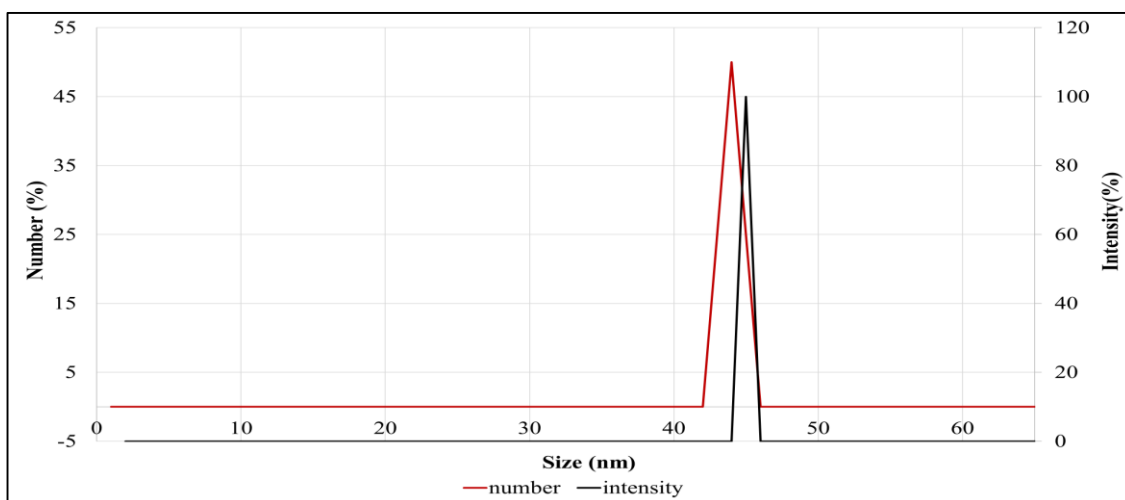


Figure 6.16. Size measurement of chitosan NPs

($[\text{Na}_2\text{SO}_4 \cdot 10\text{H}_2\text{O}]_{\text{final}} = 1.25 \text{ wt\%}$; $[\text{chitosan}]_{\text{final}} = 0.125 \text{ wt\%}$)

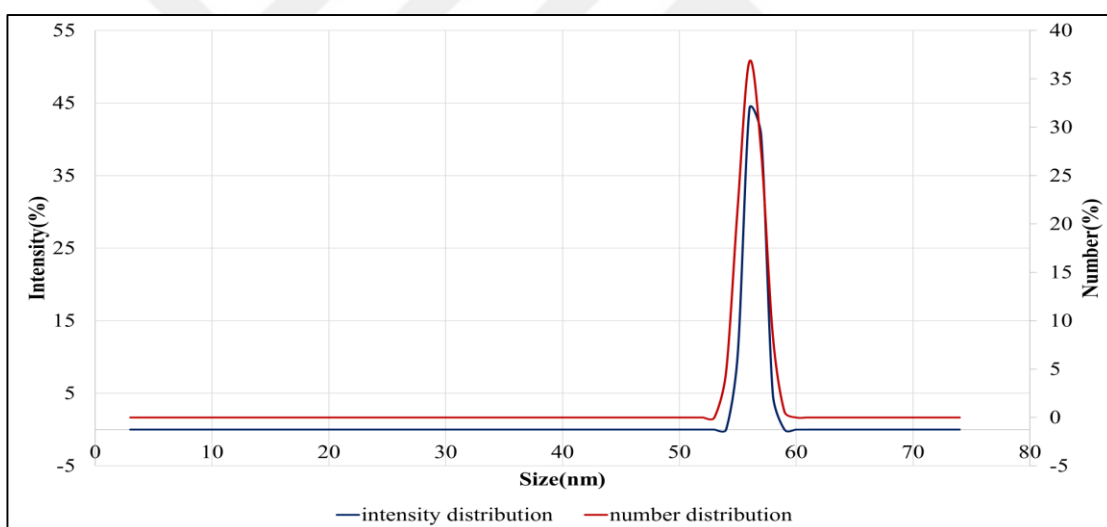


Figure 6.17. Size measurement of chitosan NPs

($[\text{Na}_2\text{SO}_4 \cdot 10\text{H}_2\text{O}]_{\text{final}} = 1.25 \text{ wt\%}$; $[\text{chitosan}]_{\text{final}} = 0.375 \text{ wt\%}$)

In addition, the size of the chitosan nanoparticles which were synthesized with 0.375 wt% chitosan and 1.25 wt% salt was approximately 56 nm as shown in Figure 6.17. As a result, it can be easily said that if concentration of chitosan is increased during the synthesis, the size of the chitosan nanoparticles increase. The overlap of intensity&number average data suggests a fairly homogeneous size distribution of particles.

6.6.2.3. Encapsulation of TMZ in chitosan nanoparticles

In order to synthesize chitosan NPs with TMZ, two different ways were employed for the addition of TMZ as mentioned Section in 6.3.

Table 6.1 % Encapsulated TMZ in chitosan nanoparticles after and during the formation

TMZ adding during the formation	TMZ adding after the formation	Final Concentration of chitosan (wt%)	Final Concentration of salt (wt%)	% Encapsulated TMZ
✓		0.11	2.2	13.5 ±5
	✓	0.11	2.2	8.3 ±2.5

Some drugs and chemicals were encapsulated in the chitosan nanoparticles such as anti-cancer drug Docetaxel [168], 5 fluorouracil [169], Indometacin [170] and Doxorubicin [171] and drug encapsulation efficiency were found approximately 70% [168], 30% [169], 65% [170] and 70% [171] respectively. In our work, firstly, chitosan NPs were synthesized (contains 0.11 wt% chitosan and 2.2 wt% salt) using the first way which is that TMZ was added during the formation. Table 6.1 shows that approximately 14 % encapsulation was obtained in the chitosan particles. However, when second way (TMZ was added after the formation) was used, approximately 8 % encapsulation was obtained in the chitosan nanoparticles. Therefore, first method was selected in order to obtain maximum encapsulation of TMZ in chitosan nanoparticles.

6.6.3. Magnetite-Chitosan Beads and Characterizations for Targeting Study

6.6.3.1. Morphology of the Magnetite-Chitosan Beads

Magnetite-Chitosan beads were synthesized by using two different methods as mentioned in Section 6.2. First method was used in order to obtain magnetite-chitosan beads which contain 2.2 % salt and 0.11 % chitosan with bare magnetite and SEM images show that magnetite-

chitosan beads do not have smooth surface and also they do not form spherically as shown in Figure 6.18.

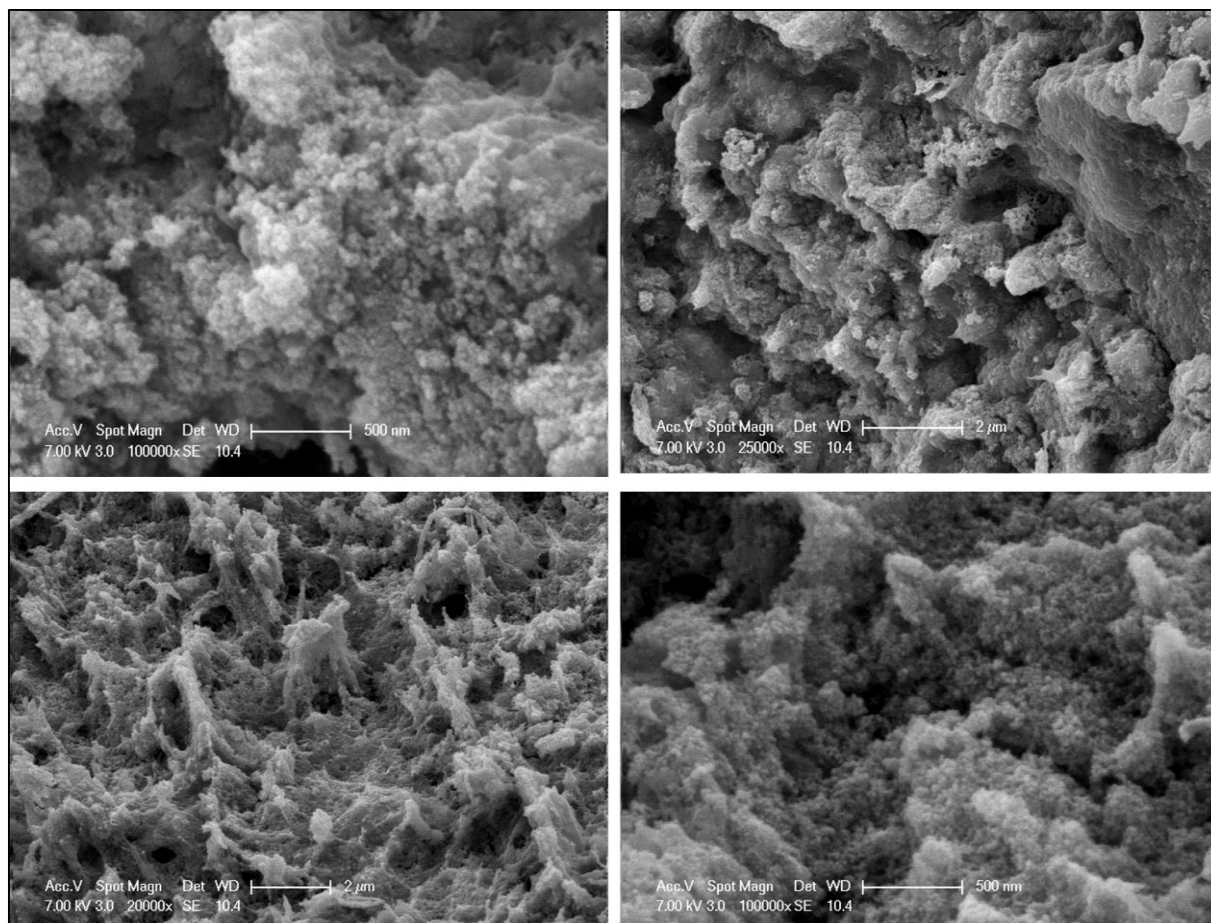


Figure 6.18. SEM images of bare magnetite-chitosan beads

($[\text{Na}_2\text{SO}_4 \cdot 10\text{H}_2\text{O}]_{\text{final}} = 2.2 \text{ wt\%}$; $[\text{chitosan}]_{\text{final}} = 0.11 \text{ wt\%}$; chitosan+bare magnetite solution)

Based on results from chitosan beads alone, concentration of salt was decreased and second method was used to obtain magnetite-chitosan beads which contain 1.1 % salt with bare magnetite and 0.22 % chitosan. Figure 6.19 shows that this method also did not result in the formation of distinct spherical nanoparticles.

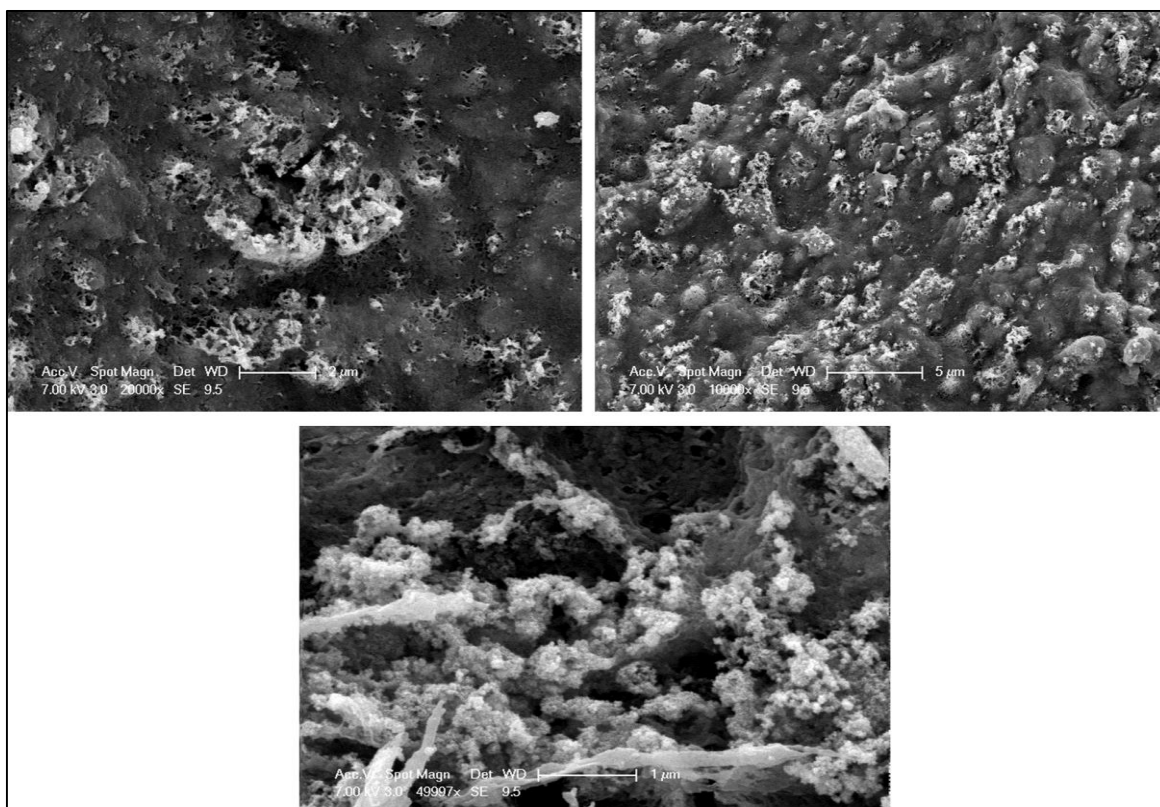


Figure 6.19. SEM images of bare magnetite-chitosan beads
 ([Na₂SO₄·10H₂O]_{final} = 1.1 wt% ; [chitosan]_{final} = 0.22 wt% ; salt + bare magnetite solution)

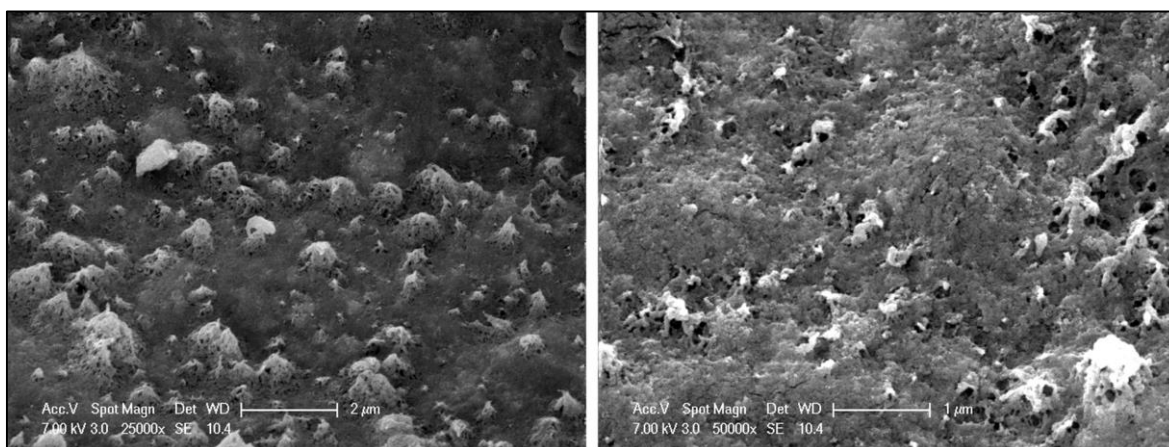


Figure 6.20. SEM images of β-CD magnetite-chitosan beads
 ([Na₂SO₄·10H₂O]_{final} = 1.1 wt% ; [chitosan]_{final} = 0.22 wt% ; chitosan + β-CD coated magnetite solution)

It should be noted that the same recipe in the absence of magnetite resulted in the formation of nanoparticles with better morphologies. To improve the morphology of the particles magnetite-chitosan beads were synthesized with β -CD coated magnetite by using two aforementioned methods. Figure 6.20 and 6.21 shows that there is not a significant difference between bare magnetite and β -CD coated magnetite in the presence of chitosan.

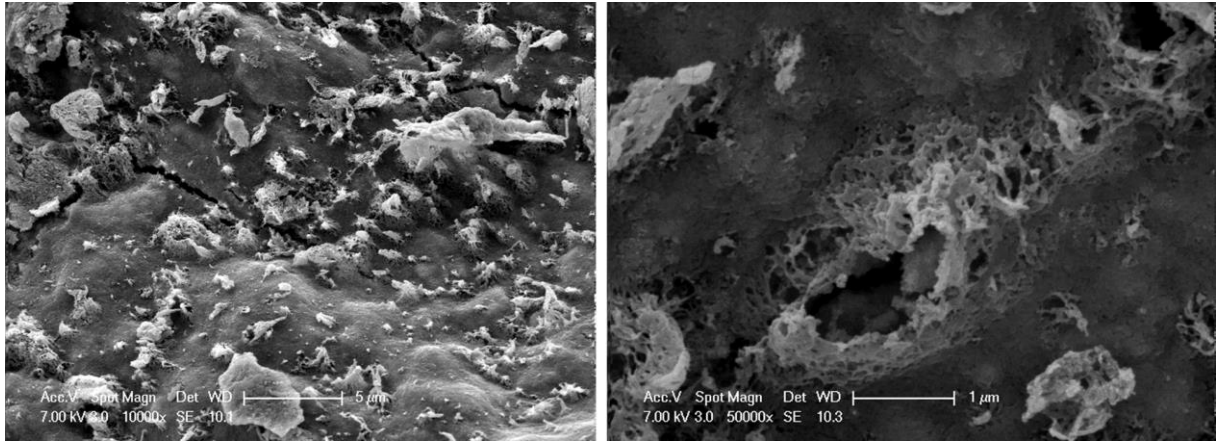


Figure 6.21. SEM images of β -CD magnetite-chitosan beads

($[\text{Na}_2\text{SO}_4 \cdot 10\text{H}_2\text{O}]_{\text{final}} = 1.1 \text{ wt\%}$; $[\text{chitosan}]_{\text{final}} = 0.22 \text{ wt\%}$; salt + β -CD coated magnetite solution)

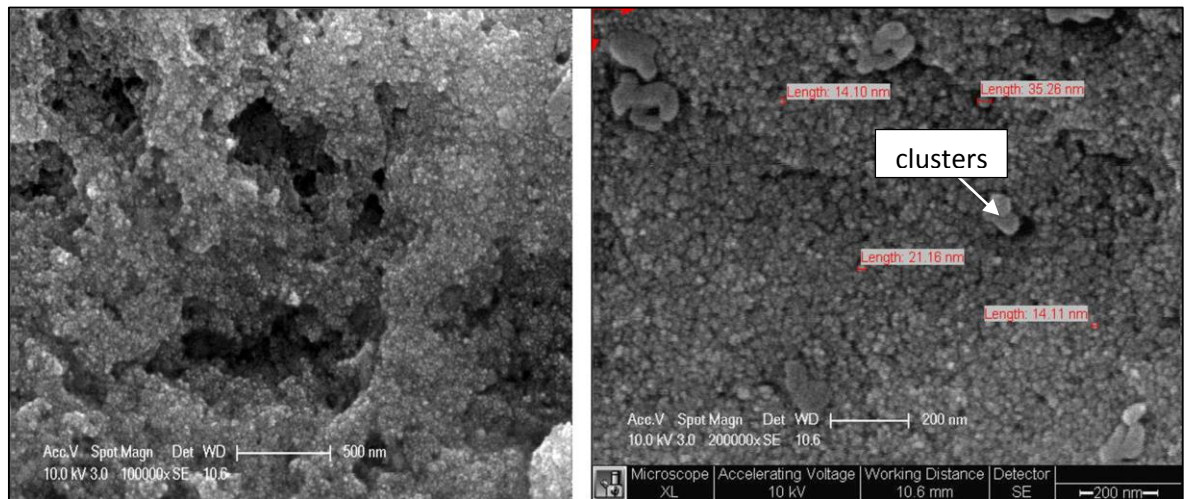


Figure 6.22. SEM images of β -CD magnetite-chitosan beads

($[\text{Na}_2\text{SO}_4 \cdot 10\text{H}_2\text{O}]_{\text{final}} = 1.1 \text{ wt\%}$; $[\text{chitosan}]_{\text{final}} = 0.09 \text{ wt\%}$; salt + β -CD coated magnetite solution)

Based on the results from magnetite-chitosan beads with β -CD coated magnetite in Figure 6.21 and 6.22, distinct spherical nanoparticles were not observed, so second method was used and stirring time was increased to one hour. After one hour, magnetite chitosan beads were obtained which contain 1.1 wt% salt with β -CD coated magnetite and 0.09 and 0.43 wt% chitosan as shown in Figures 6.22 and 6.23 respectively.

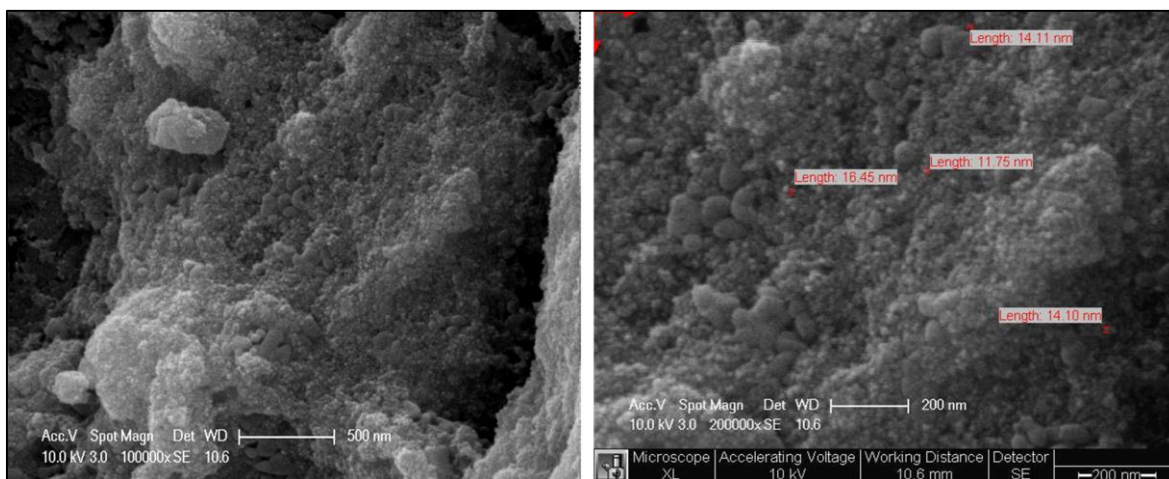


Figure 6.23. SEM images of β -CD magnetite-chitosan beads

($[\text{Na}_2\text{SO}_4 \cdot 10\text{H}_2\text{O}]_{\text{final}} = 1.1 \text{ wt\%}$; $[\text{chitosan}]_{\text{final}} = 0.43 \text{ wt\%}$; salt + β -CD coated magnetite solution)

Although the samples were gold coated before imaging, due to the nature of chitosan, application of high dose during measurements resulted in the destruction of the sample. To obtain images, low dose was used, resulting in compromise in the resolution of the obtained images. These figures show that spherical magnetite-chitosan beads which contain 0.09 and 0.043 wt% chitosan were obtained successfully and size of these magnetite beads are approximately 20 nm and 15 nm.

The size of the magnetite beads were already measured using DLS as mentioned Section 6.6.3.2. Size results were similar between DLS and SEM. However, it is known that DLS measures hydrodynamic radius of the nanoparticles. Therefore, higher size were obtained using DLS might be the associated water molecules around the chitosan nanoparticles. Also, some clusters that were observed in Figure 6.22 can cause the higher size shown in intensity averaged DLS measurements.

6.6.3.2. Size Measurements of magnetite-chitosan beads

Size measurements were only performed for particles obtained using 2.5 wt% $\text{Na}_2\text{SO}_4 \cdot 10\text{H}_2\text{O}$ salt, 0.25 wt%, 0.75 wt% chitosan solutions and β -CD coated magnetite nanoparticles were used and two different magnetite-chitosan beads were synthesized using second method mentioned in Section 6.1. Dynamic Light Scattering (DLS) was used to determine the size of the magnetite-chitosan beads. According to these data, % intensity and % number graphs are plotted as shown in Figures 6.24. and 6.25.

In literature, size of the bare magnetite-chitosan core shell was found to be 11 nm [172] and oleic acid coated magnetite-chitosan NPs was about 10.5 nm for hyperthermia [173]. Also, Denkba et al. [174] and Jiang et al. [175] reported that 100-250 μm magnetite-chitosan beads were prepared by cross-linking the linear chitosan chains in water-in-oil microemulsion. However, in our work, Number average means that majority of the particles have an average diameter of 31 nm. In the intensity average plot, another peak around 45 nm suggests few larger particles in the medium, possible aggregates. It can be said that the size of the magnetite-chitosan beads which finally contain 0.11 wt% chitosan and 1.1 wt% salt is approximately 31 nm.

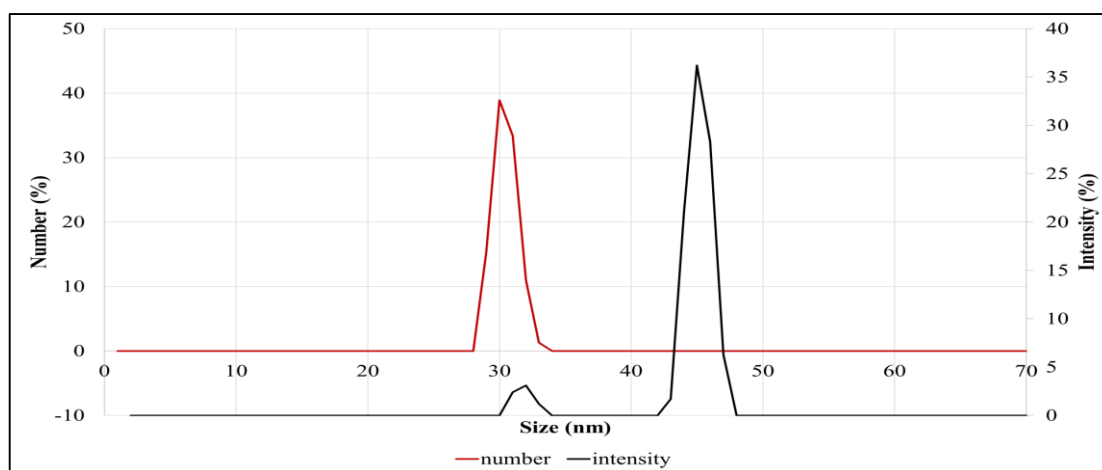


Figure 6.24. Size measurement of magnetite-chitosan beads with DLS

($[\text{Na}_2\text{SO}_4 \cdot 10\text{H}_2\text{O}]_{\text{final}} = 1.1 \text{ wt\%}$; $[\text{chitosan}]_{\text{final}} = 0.11 \text{ wt\%}$; salt + β -CD coated magnetite solution)

In addition, the size of the magnetite-chitosan beads which were synthesized using 0.33 wt% chitosan and 1.1 wt% salt with β -CD coated magnetite was approximately 46 nm as shown in Figure 6.25. As a result, it can be easily said that if concentration of chitosan is increased during the synthesis, the size of the chitosan nanoparticles is increased. The overlap of intensity&number average data suggests a fairly homogeneous size distribution of particles.

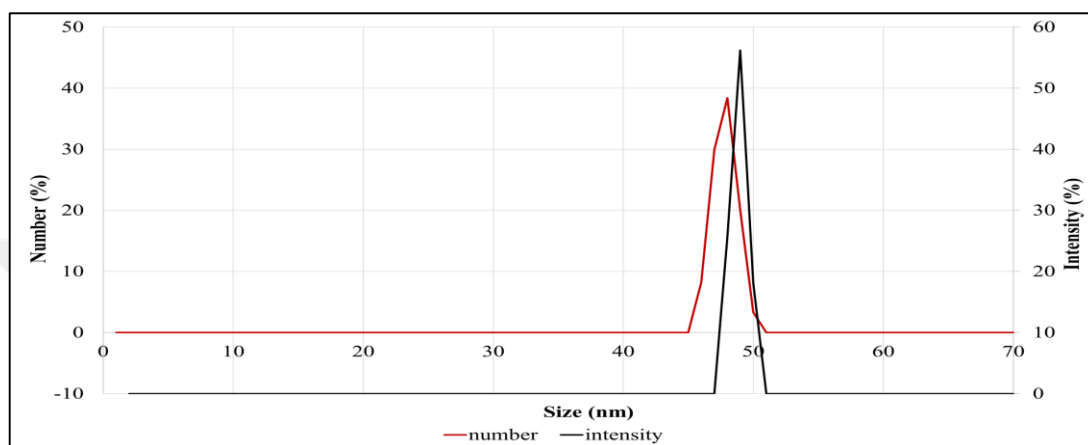


Figure 6.25. Size measurement of magnetite-chitosan beads with DLS ([$\text{Na}_2\text{SO}_4 \cdot 10\text{H}_2\text{O}$]_{final} = 1.1 wt% ; [chitosan]_{final} = 0.33 wt% ; salt + β -CD coated magnetite solution).

6.6.3.3. Encapsulation of TMZ in bare magnetite-chitosan beads

There are two different methods in order to synthesize magnetite-chitosan beads as mentioned in Section 6.2. For the encapsulation of TMZ in magnetite-chitosan beads with bare magnetite experiments, second method was used. However, also two ways were used for addition of TMZ in order to compare % encapsulated TMZ.

Some experiments showed that some drugs such as anti cancer drug Doxorubicin [176] and antibiotic Isoniazid [177] were encapsulated in magnetite-chitosan particles and encapsulated % were reported as an average 73% and 7%, respectively. There is a significant difference in the encapsulated percent between different drugs.

Table 6.2. % Encapsulated TMZ in magnetite-chitosan beads after and during the formation

TMZ adding during the synthesis	TMZ adding after the synthesis	Type of magnetite coating	Final [Chitosan] (wt%)	Final [Na ₂ SO ₄ . 10H ₂ O] (wt%)	% Encapsulated TMZ
✓		Bare	0.11	2.2	26
	✓	Bare	0.11	2.2	19

In our work, firstly, magnetite-chitosan beads were synthesized (0.11 wt% chitosan and 2.2 wt% salt as final concentrations) using the first way where TMZ was added during the formation of beads. Table 6.2. shows that approximately 26 % encapsulation was obtained in the magnetite-chitosan beads. However, when second way (TMZ was added after the formation) was used, approximately 19 % encapsulation was obtained in the magnetite-chitosan beads as shown Table 6.2.

Similar results were obtained when chitosan particles were used. For this reason, first way which is TMZ addition during the synthesis was selected in order to continue encapsulation experiments with magnetite-chitosan beads. In addition, first method is the one step method which is advantageous for experimental work.

6.6.3.4. Encapsulation of TMZ in β -CD magnetite-chitosan beads

Apart from the morphology of the particles, their encapsulation efficiencies should also be taken into consideration. Initially, magnetite-chitosan beads were formed using bare magnetite. Magnetite-chitosan beads were synthesized with 0.5 wt% different types of CD coated magnetic nanoparticles using the first way mentioned in Section 6.3. Two different concentrations of salt and three different concentrations of chitosan were used and encapsulated amounts of TMZ were measured by HPLC and the results are tabulated in Table 6.3.

Table 6.3. % Encapsulated TMZ in magnetite-chitosan beads comparing salt concentrations

Final [Chitosan] (wt%)	Final [salt] (wt%)	with β -CD coated magnetite (mg)	with H- β -CD coated magnetite (mg)	with H- γ -CD coated magnetite (mg)
0.22	1.1	35 \pm 2.8	37	29
0.22	2.2	16.5 \pm 11	20	26
0.33	1.1	35.5 \pm 7.8	39	36
0.33	2.2	35	32	19
0.43	1.1	35.5 \pm 3.5	38	45
0.43	2.2	37.5 \pm 3.5	41	45

According to Table 6.3, for fixed amount chitosan when the concentration of the salt was increased, encapsulated amounts of TMZ were similar or worse. For example, for 0.22 % chitosan and 1.1 % salt as final concentrations, encapsulated amount of TMZ was approximately 35 % with β -CD coated magnetite. However, for 0.22 % chitosan and 2.2 % salt as final concentrations, encapsulated amount of TMZ was approximately 17% with β -CD coated magnetite. In addition, for 0.33 % chitosan and 1.1 % salt and 2.2 % salt as final concentrations, encapsulated amount of TMZ was very similar and was approximately 35% with β -CD coated magnetite. As a result, final salt concentrations was selected as 1.1 % for the synthesis of magnetite-chitosan magnetic beads for optimization.

Finally, encapsulated amount of TMZ was calculated for only 1.1 % final salt concentration and four different concentrations of chitosan as shown Table 6.4.

Table 6.4. % Encapsulated TMZ in magnetite-chitosan beads with only 1.1 wt % final salt concentration

Final [Chitosan] (wt%)	Final [salt] (wt%)	with β -CD coated magnetite (mg)	with H- β -CD coated magnetite (mg)	with H- γ -CD coated magnetite (mg)
0.09	1.1	-	36	31
0.22	1.1	35 \pm 2.8	37	29
0.33	1.1	35.5 \pm 7.8	39	36
0.43	1.1	35.5 \pm 3.5	38	45

This table shows that increasing chitosan concentration is effective for encapsulated amount of TMZ for only H- γ -CD. However, encapsulated amounts of TMZ are very similar for β -CD and H- β -CD when concentration of chitosan is increased. As a result, increasing concentration of chitosan does not improve the encapsulation of TMZ in magnetite-chitosan beads. Boucicaut and Winstead studied about TMZ loaded chitosan nanoparticles for brain tumors and maximum loading of TMZ was found to be about 40%. Additionally, Tian et al., (2011) [178] reported that approximately 44% TMZ was entrapped in polysorbate-80 coated polybutyrlcyanoacrylate nanoparticles. It can be seen that the encapsulation % of the TMZ in prepared nanoparticles was not very high. This result might be due to the amphiphilic nature of TMZ, which is relatively highly lipophilic and somewhat soluble in water. According to these results, obtained percent encapsulations were comparable with our work.

6.6.4. Targeting Study of TMZ in magnetite-chitosan beads

Targeting study experiments were carried out using two different test sections in the set-up. Firstly, 1.49 mm thin test section was used and then, 2.19 mm thicker test section was used for optimization in order to collect maximum amount of TMZ in the desired area.

6.6.4.1. Targeting Study of TMZ in magnetite-chitosan beads with thin test section

Once the magnetic nanoparticles were removed from the targeted area in the thin test section, the amount of captured magnetite concentration, collected amount of chitosan and collected amount of TMZ were calculated and all values are tabulated in Table 6.5.

In this experiment, 3 magnets were used and these magnets generate 0.3 T magnetic field, so, small quantities (≈ 0.1 mg) of TMZ were collected in the test section, independent of the concentration of chitosan and salt as shown in Table 6.5.

In addition, large value of the ratio of the collected TMZ and collected chitosan can be an indication of a successful drug carrier. However, Table 6.5. shows that these values are not good enough for the collection of TMZ in the desired area.

Table 6.5. Targeting study with thin section (applying 0.3 T magnetic field)

Final [Chitosan] (wt%)	Final [Na₂SO₄.10H₂O] (wt%)	Collected amount of chitosan (mg)	Captured concentration of magnetite (mg)	Collected amount of TMZ (mg)	<u>TMZ</u> <u>Chitosan</u>
0.22	2.2	0.35	0.28	0.09	0.26
0.43	2.2	0.23	0.09	0.08	0.35
0.09	1.1	0.25	0.49	0.12	0.48
0.22	1.1	0.23	0.18	0.11	0.48
0.33	1.1	0.48	0.25	0.10	0.21

In an attempt to collect more magnetic particles in the test section, number of magnets were increased to 5 generating 0.5 T magnetic field. Some of the experiments were repeated and the results are tabulated in Table 6.6. In these experiments, concentration of magnetite is found to increase in the test section suggestion better capture of particles. For example, magnetite-chitosan beads which contain 1.1 wt % final salt and 0.09 wt % final chitosan concentrations with β -CD coated magnetite, magnetite concentration was duplicated according to the Table 6.5. and 6.6.

Table 6.6 Targeting study with thin section (applying 0.5 T magnetic field)

[Chitosan] (wt%)	[Na₂SO₄.10H₂O] (wt%)	Collected amount of chitosan (mg)	Captured concentration of magnetite (mg)	Collected amount of TMZ (mg)	<u>TMZ</u> <u>Chitosan</u>
0.09	1.1	0.44	0.86	0.13	0.30
0.22	1.1	0.51	0.39	0.07	0.14
0.33	1.1	0.88	0.56	0.06	0.07

However, the collected amount of TMZ was very similar. In addition, Table 6.6. shows that, collected amount of TMZ was approximately 0.1 mg similar to previous experiments. Somehow_although more magnetite was captured in the test section, targeting of higher amounts of TMZ was achieved.

6.6.4.2. Targeting Study of TMZ in magnetite-chitosan beads with thick test section

After targeting experiments of TMZ in magnetite-chitosan beads with thin test section, targeting experiments of TMZ also were carried out with thick test section as 1.49 mm in order to collect more TMZ in the desired area. After these experiments, magnetite-chitosan-TMZ nanofluid was collected as shown in Figure 6.26.



Figure 6.26. Captured magnetite-chitosan-TMZ nanofluid in the test section (0.5 %wt CD) after 1 hr

So, captured magnetite concentration, collected amount of chitosan and collected amount of TMZ in the test section were calculated and are tabulated in Table 6.7. Increasing the width of the test section clearly increases the efficiency of TMZ targeting.

In addition, Table 6.7. shows that magnetite-chitosan beads which contain 0.43 wt % final chitosan and 2.2 wt % final salt concentrations, approximately 0.32 mg was collected in the desired area and ratio of the collected TMZ and chitosan was 0.47. However, magnetite-chitosan beads which contain 0.09 wt % final chitosan and 2.2 wt % final salt concentrations, approximately 0.27 mg was collected in the desired area and ratio of the collected TMZ and chitosan was 1.05. This similar difference shows that if the final concentrations of chitosan was 0.09 wt % or 0.43 wt %, collected amounts of TMZ were very similar. In addition, if the ratio of collected TMZ and chitosan value is large that indicates maximum amount of TMZ can be collected by using minimum amount of chitosan.

Table 6.7. Targeting study with thick section

Final [Chitosan] (wt%)	Final [Na ₂ SO ₄ . 10H ₂ O] (wt%)	Collected amount of chitosan (mg)	Captured concentration of magnetite (mg)	Collected amount of TMZ (mg)	TMZ / Chitosan
0.09	1.1	0.32±0.007	0.63±0.013	0.27±0.03	0.82±0.09
0.09	2.2	0.26±0.02	0.51±0.04	0.27±0.01	1.05±0.05
0.22	1.1	0.72±0.03	0.56±0.02	0.33±0.02	0.44±0.01
0.22	2.2	0.33±0.02	0.26±0.02	0.25±0.02	0.75±0.08
0.33	1.1	0.84±0.06	0.44±0.03	0.31±0.03	0.37±0.07
0.33	2.2	0.73±0.09	0.38±0.05	0.29±0.006	0.53±0.2
0.43	1.1	0.52±0.14	0.21±0.05	0.27±0.03	0.53±0.15
0.43	2.2	0.68±0.17	0.27±0.07	0.32±0.05	0.47±0.05

For this reason, the small amount of chitosan was selected. According to the optimization, 0.09 wt % final chitosan concentration was selected with different two final concentrations of salt as 1.1 wt % and 2.2 wt%, because the ratio of collected TMZ and chitosan was 0.82 and 1.05 respectively. Halupka-Bryl et al., (2015) [179] created magnetic drug carriers using iron oxide NPs-PEG-b-poly(4-vinylbenzylphosphonate)/Doxorubicin system as a potential drug carrier for magnetically mediated targeted anticancer therapy to be used in biomedical applications. Also, Idarubicin-loaded, folic acid conjugated magnetic nanoparticles which have desired shape and size were reported by Gunduz et al.(2014) [180] and targeting ability under magnetic field were determined in vitro. Moreover, high gradient magnetic separation is useful technique in order to collect magnetite nanoparticles in desired area [181-183]. However, in our study, this technique did not simulate real blood flow therefore was not employed.

7. CONCLUSION AND FUTURE WORK

Cancer is the rapid growth and uncontrollable division of cells which then assemble into a tissue called tumor. These cells in tumor site cause formation of new blood vessels after a process called angiogenesis and by using these newly formed blood vessels, cancer cells can spread to other regions in the body (metastasis). Although there are many treatments for cancer, these treatments have severe side effects such as vomiting, hair loss, fatigue and anemia. In order to decrease these side effects, the drugs used for the treatment of cancer should be applied locally to the exact location of the tumors. Therefore, the objective of this study was to target an anti-cancer drug to the tumor site using magnetite nanoparticles by applying an external magnetic field.

Temozolomide is an anti-cancer drug that can be administered orally and has been approved for the treatment of malignant glioma. Malignant gliomas are the most common type of brain tumours. As TMZ is hydrophobic it has very low solubility and stability in aqueous medium. In order to increase bioavailability and solubility of the TMZ, various types of cyclic oligosaccharides i.e. cyclodextrins are used which has the potential to form inclusion complexes with the drug thus, enhance both the stability and solubility. For the solubility analysis of temozolomide both in the presence and absence of cyclodextrins UV-Vis Spectroscopy and High Pressure Liquid Chromatography were used. The results showed that the solubility of temozolomide was enhanced due to the formation of an inclusion complex with all studied cyclodextrins. In addition, heat profiles and weight loss were explored using DSC, TGA and also imaging with SEM demonstrated that inclusion complexes are formed between TMZ and CDs.

As the cyclodextrin – temozolomide complex should be targeted to an exact location in the body, magnetite nanoparticles were chosen due to their excellent magnetic properties as well as their biocompatibility. For this purpose magnetite nanoparticles were synthesized through facile co-precipitation method both in the presence and absence of cyclodextrins. The hydrodynamic size measurements were carried out with dynamic light scattering (DLS). The average hydrodynamic size of the nanoparticles synthesized in the absence of cyclodextrins were found to be 47 nm. On the other hand, the presence of cyclodextrins on the surface of

magnetite nanoparticles increased the hydrodynamic diameter to an average size of 57-61 nm. Furthermore, the existence of cyclodextrins on the surface of magnetite nanoparticles were validated by Thermogravimetric analysis (TGA). The presence of all types of cyclodextrins caused varying weight losses (2-17 wt %) indicating successful attachment onto the magnetite surface, additionally β -CD coated magnetite nanoparticles has maximum coating density. These results were also in line with the colloidal stability as magnetite – cyclodextrin complex could be dispersed in aqueous medium regardless of the type of cyclodextrin used. However, it was shown that 2-hydroxy propyl β -Cyclodextrin coated magnetite nanoparticles had the longest colloidal stability.

For targeting studies, firstly chitosan NPs and then, magnetite-chitosan beads were obtained using ionic gelation method. DLS was used for size measurement and SEM was used to image the morphologies. Size of the only chitosan NPs which contain final concentrations as 1.25 wt% salt and 0.125 wt% chitosan was approximately 44 nm where 1.25 wt% salt and 0.375 wt% chitosan was approximately 56 nm. In parallel, the size of the magnetite-chitosan beads which contain 1.1wt% salt and 0.11 wt% chitosan was 31 nm where 1.1wt% salt and 0.33 wt% chitosan particles were 46 nm. It can be easily said that if concentration of chitosan was increased during the synthesis, the size of the chitosan nanoparticles is increased. The morphologies of the obtained beads are imaged using SEM. TMZ was incorporated in these chitosan-magnetite particles to obtain a drug delivery system. Finally, magnetite-CD-TMZ and magnetite-chitosan-TMZ beads were used to target TMZ to the desired area applying an external magnetic field. Anti-cancer drug TMZ was encapsulated in only chitosan nanoparticles (\approx 10%) and magnetite-chitosan beads with bare magnetite (\approx 23%) and different types of CDs coated magnetite (\approx 30%). And finally, magnetite-chitosan beads (contain β -CD coated magnetite) were targeted to the desired section applying an external magnetic field. The amounts of encapsulated & targeted TMZ were determined by HPLC.

In summary, anti-cancer drug TMZ was encapsulated in chitosan beads with magnetite to obtain a magnetite drug carrier. Encapsulated in magnetite-chitosan beads, TMZ was successfully targeted to the desired area by the application of an external field. This work shows that a toxic anti-cancer drug TMZ can be localized by the help of a magnetic carrier, which lend itself to several application in biomedical field.

Nevertheless, there are several areas within the work that require further investigation. Magnetite NPs are used for biomedical applications so, cytotoxicity of β -CD coated magnetite- chitosan and β -CD coated magnetite- chitosan-TMZ will be investigate for various cell lines such as Huvec and Fibroblasts (L929) using MTA assay. Furthermore, magnetic properties of particles with cyclodextrins which were synthesized by co-precipitation method and magnetite-chitosan beads will be investigated by Vibrating Sample Magnetometer (VSM). In addition, drug release from the collected magnetite-chitosan-TMZ particles in the test section will be investigated to fully explore these systems as drug delivery vehicles. Once, these in vitro tests are satisfied, further research will be carried out to test the performance of these particles *in vivo*.

REFERENCES

1. R.R. German, A.K. Fink, M. Heron, S.L. Stewart, C.J. Johnson, J.L. Finch, and D. Yin, The Accuracy of Cancer Mortality Statistics Based on Death Certificates in the United States. *Cancer Epidemiology*, 2:126-131, 2011.
2. J.F.R. Kerr, C.M. Winterford, and B.V. Harmon, Apoptosis. Its Significance in Cancer and Cancer Therapy. *Cancer*, 8:2013-2026, 1994.
3. G. Schmid, *Nanoparticles: From Theory to Application*: Wiley, 2004.
4. F.Y. Cheng, C.H. Su, P.C. Wu, and C.S. Yeh, Multifunctional Polymeric Nanoparticles for Combined Chemotherapeutic and Near-Infrared Photothermal Cancer Therapy in Vitro and in Vivo. *Chemical Communications*, 18:3167-3169, 2010.
5. L. Barraud, P. Merle, E. Soma, L. Lefrançois, S. Guerret, M. Chevallier, C. Dubernet, P. Couvreur, C. Trépo, and L. Vitvitski, Increase of Doxorubicin Sensitivity by Doxorubicin-Loading into Nanoparticles for Hepatocellular Carcinoma Cells in Vitro and in Vivo. *Journal of Hepatology*, 5:736-743, 2005.
6. H.J. Byeon, L.Q. Thao, S. Lee, S.Y. Min, E.S. Lee, B.S. Shin, H.-G. Choi, and Y.S. Youn, Doxorubicin-Loaded Nanoparticles Consisted of Cationic- and Mannose-Modified-Albumins for Dual-Targeting in Brain Tumors. *Journal of Controlled Release*, 23:301-313, 2016.
7. C.D. Medley, J.E. Smith, Z. Tang, Y. Wu, S. Bamrungsap, and W. Tan, Gold Nanoparticle-Based Colorimetric Assay for the Direct Detection of Cancerous Cells. *Analytical Chemistry*, 4:1067-1072, 2008.

8. P.M.A. Farias, B.S. Santos, and A. Fontes. Semiconductor Fluorescent Quantum Dots: Efficient Biolabels in Cancer Diagnostics. In. S.R. Foote and W.J. Lee, Editors, *Micro and Nano Technologies in Bioanalysis: Methods and Protocols*. pages 407-419. Humana Press, Totowa, NJ, 2009.
9. A.M. Smith, S. Dave, S. Nie, L. True, and X. Gao, Multicolor Quantum Dots for Molecular Diagnostics of Cancer. *Expert Review of Molecular Diagnostics*, 2:231-244, 2006.
10. D. Brambilla, J. Nicolas, B. Le Droumaguet, K. Andrieux, V. Marsaud, P.-O. Couraud, and P. Couvreur, Design of Fluorescently Tagged Poly(Alkyl Cyanoacrylate) Nanoparticles for Human Brain Endothelial Cell Imaging. *Chemical Communications*, 15:2602-2604, 2010.
11. G.A. Craig, P.J. Allen, and M.D. Mason. Synthesis, Characterization, and Functionalization of Gold Nanoparticles for Cancer Imaging. In. R.S. Grobmyer and M.B. Moudgil, Editors, *Cancer Nanotechnology: Methods and Protocols*. pages 177-193. Humana Press, Totowa, NJ, 2010.
12. D. Kim, Y.Y. Jeong, and S. Jon, A Drug-Loaded Aptamer–Gold Nanoparticle Bioconjugate for Combined CT Imaging and Therapy of Prostate Cancer. *ACS Nano*, 7:3689-3696, 2010.
13. M. Liang, X. Liu, D. Cheng, G. Liu, S. Dou, Y. Wang, M. Rusckowski, and D.J. Hnatowich, Multimodality Nuclear and Fluorescence Tumor Imaging in Mice Using a Streptavidin Nanoparticle. *Bioconjugate Chemistry*, 7:1385-1388, 2010.
14. R. Nagarajan. Nanoparticles: Building Blocks for Nanotechnology. In, *Nanoparticles: Synthesis, Stabilization, Passivation, and Functionalization*. pages 2-14. American Chemical Society, 2008.

15. G.T. Burstein, The iron oxides: Structure, Properties, Reactions, Occurrence and Uses: R. M. Cornell and U. Schwertmann. 573 pp. VCH, Weinheim and New York, 1996. ISBN: 3-527-28576-8. *Corrosion Science*, 8:1499-1500, 1997.
16. R.M. Cornell and U. Schwertmann, *The Iron Oxides: Structure, Properties, Reactions, Occurrences and Uses*: Wiley, 2006.
17. A. Andrade-Eiroa, M. Canle, V. Leroy-Cancellieri, and V. Cerdà, Solid phase Extraction of Organic Compounds: a Critical Review. part i. *TrAC Trends in Analytical Chemistry*.
18. A.-H. Lu, E.L. Salabas, and F. Schüth, Magnetic Nanoparticles: Synthesis, Protection, Functionalization, and Application. *Angewandte Chemie International Edition*, 8:1222-1244, 2007.
19. R. Kumar, B.S. Inbaraj, and B.H. Chen, Surface Modification of Superparamagnetic Iron Nanoparticles with Calcium Salt of Poly(γ -Glutamic Acid) as Coating Material. *Materials Research Bulletin*, 11:1603-1607, 2010.
20. D. Ortega, J.S. Garitaonandia, C. Barrera-Solano, M. Ramírez-del-Solar, E. Blanco, and M. Domínguez, γ -Fe₂O₃/SiO₂ Nanocomposites for Magneto-Optical Applications: Nanostructural and Magnetic Properties. *Journal of Non-Crystalline Solids*, 26–27:2801-2810, 2006.
21. P.A. Dresco, V.S. Zaitsev, R.J. Gambino, and B. Chu, Preparation and Properties of Magnetite and Polymer Magnetite Nanoparticles. *Langmuir*, 6:1945-1951, 1999.
22. S. Si, A. Kotal, T.K. Mandal, S. Giri, H. Nakamura, and T. Kohara, Size-Controlled Synthesis of Magnetite Nanoparticles in the Presence of Polyelectrolytes. *Chemistry of Materials*, 18:3489-3496, 2004.

23. M. Chastellain, A. Petri, and H. Hofmann, Particle Size Investigations of a Multistep Synthesis of PVA Coated Superparamagnetic Nanoparticles. *Journal of Colloid and Interface Science*, 2:353-360, 2004.
24. D. Ramimoghadam, S. Bagheri, and S.B.A. Hamid, Progress in Electrochemical Synthesis of Magnetic Iron Oxide Nanoparticles. *Journal of Magnetism and Magnetic Materials*, 11:207-229, 2014.
25. R.D. Ambashta and M. Sillanpää, Water Purification Using Magnetic Assistance: A review. *Journal of Hazardous Materials*, 1–3:38-49, 2010.
26. B. Tang, G. Wang, L. Zhuo, J. Ge, and L. Cui, Facile Route to α -FeOOH and α -Fe₂O₃ Nanorods and Magnetic Property of α -Fe₂O₃ Nanorods. *Inorganic Chemistry*, 13:5196-5200, 2006.
27. C. Wu, P. Yin, X. Zhu, C. OuYang, and Y. Xie, Synthesis of Hematite (α -Fe₂O₃) Nanorods: Diameter-Size and Shape Effects on Their Applications in Magnetism, Lithium Ion Battery, and Gas Sensors. *The Journal of Physical Chemistry B*, 36:17806-17812, 2006.
28. A.S. Teja and P.-Y. Koh, Synthesis, Properties, and Applications of Magnetic Iron Oxide Nanoparticles. *Progress in Crystal Growth and Characterization of Materials*, 1–2:22-45, 2009.
29. Y.L. Pang, S. Lim, H.C. Ong, and W.T. Chong, Research Progress on Iron Oxide-Based Magnetic Materials: Synthesis Techniques and Photocatalytic Applications. *Ceramics International*, 1, Part A:9-34, 2016.
30. M.S. Marius, P.A.B. James, A.S. Bahaj, and D.J. Smallman, Development of a Highly Magnetic Iron Sulphide for Metal Uptake and Magnetic Separation. *Journal of Magnetism and Magnetic Materials*, 1:567-571, 2005.

31. D. Ho, X. Sun, and S. Sun, Monodisperse Magnetic Nanoparticles for Theranostic Applications. *Accounts of Chemical Research*, 10:875-882, 2011.
32. A.E. Panasenکو, I.A. Tkachenko, L.A. Zemnukhova, I.V. Shchetinin, and N.A. Didenko, Phase Composition, Magnetic Properties and Thermal Behavior of a Novel Fe₂O₃-SiO₂ Composite Material. *Journal of Magnetism and Magnetic Materials*:66-71, 2016.
33. M. Sonmez, M. Georgescu, L. Alexandrescu, D. Gurau, A. Fikai, D. Fikai, and E. Andronescu, Synthesis and Applications of Fe₃O₄/SiO₂ Core-Shell Materials. *Current Pharmaceutical Design*, 37:5324-5335, 2015.
34. R.B. Frankel and R.P. Blakemore, Magnetite and Magnetotaxis in Microorganisms. *Bioelectromagnetics*, 3:223-237, 1989.
35. S. Alibeigi and M.R. Vaezi, Phase Transformation of Iron Oxide Nanoparticles by Varying the Molar Ratio of Fe²⁺:Fe³⁺. *Chemical Engineering and Technology*, 11:1591-1596, 2008.
36. D. Arndt, V. Zielasek, W. Dreher, and M. Bäumer, Ethylene Diamine-Assisted Synthesis of Iron Oxide Nanoparticles in High-Boiling Polyols. *Journal of Colloid and Interface Science*, 56:188-198, 2014.
37. D. Wang, P. Yang, and Y. Zhu, Growth of Fe₃O₄ Nanoparticles with Tunable Sizes and Morphologies Using Organic Amine. *Materials Research Bulletin*, 13:514-520, 2014.
38. C.Y. Haw, F. Mohamed, C.H. Chia, S. Radiman, S. Zakaria, N.M. Huang, and H.N. Lim, Hydrothermal Synthesis of Magnetite Nanoparticles as MRI Contrast Agents. *Ceramics International*, 4:1417-1422, 2010.

39. A.K. Gupta and M. Gupta, Synthesis and Surface Engineering of Iron Oxide Nanoparticles for Biomedical Applications. *Biomaterials*, 18:3995-4021, 2005.
40. S.M. El-Sheikh, F.A. Harraz, and K.S. Abdel-Halim, Catalytic Performance of Nanostructured Iron Oxides Synthesized by Thermal Decomposition Technique. *Journal of Alloys and Compounds*, 1–2:716-723, 2009.
41. F. Ozel and H. Kockar, Growth and Characterizations of Magnetic Nanoparticles Under Hydrothermal Conditions: Reaction Time and Temperature. *Journal of Magnetism and Magnetic Materials*, 12:213-216, 2015.
42. G. Zhang, Y. Liao, and I. Baker, Surface Engineering of Core/Shell Iron/Iron Oxide Nanoparticles from Microemulsions for Hyperthermia. *Materials Science and Engineering: C*, 1:92-97, 2010.
43. X.-M. Li, G. Xu, Y. Liu, and T. He, Magnetic Fe₃O₄ Nanoparticles: Synthesis and Application in Water Treatment. *Nanoscience and Nanotechnology-Asia*, 1:14-24, 2011.
44. Z. Jia, J. Liu, Q. Wang, S. Li, Q. Qi, and R. Zhu, Synthesis of 3D Hierarchical Porous Iron Oxides for Adsorption of Congo Red from Dye Wastewater. *Journal of Alloys and Compounds*:587-595, 2015.
45. A. Ahniyaz, G.A. Seisenbaeva, L. Häggström, S. Kamali, V.G. Kessler, P. Nordblad, C. Johansson, and L. Bergström, Preparation of Iron Oxide Nanocrystals by Surfactant-Free or Oleic Acid-Assisted Thermal Decomposition of a Fe(III) Alkoxide. *Journal of Magnetism and Magnetic Materials*, 6:781-787, 2008.
46. D. Amara, J. Grinblat, and S. Margel, Solventless Thermal Decomposition of Ferrocene as a New Approach for One-Step Synthesis of Magnetite Nanocubes and Nanospheres. *Journal of Materials Chemistry*, 5:2188-2195, 2012.

47. J. Liu, L. Wang, J. Wang, and L. Zhang, Simple Solvothermal Synthesis of Hydrophobic Magnetic Monodispersed Fe₃O₄ Nanoparticles. *Materials Research Bulletin*, 2:416-421, 2013.
48. J. Jing, Y. Zhang, J. Liang, Q. Zhang, E. Bryant, C. Avendano, V.L. Colvin, Y. Wang, W. Li, and W.W. Yu, One-Step Reverse Precipitation Synthesis of Water-Dispersible Superparamagnetic Magnetite Nanoparticles. *Journal of Nanoparticle Research*, 4:1-8, 2012.
49. D.S. Mathew and R.-S. Juang, An Overview of the Structure and Magnetism of Spinel Ferrite Nanoparticles and Their Synthesis in Microemulsions. *Chemical Engineering Journal*, 1–3:51-65, 2007.
50. M. Zhu, Y. Wang, D. Meng, X. Qin, and G. Diao, Hydrothermal Synthesis of Hematite Nanoparticles and Their Electrochemical Properties. *The Journal of Physical Chemistry C*, 30:16276-16285, 2012.
51. G. Muscas, N. Yaacoub, G. Concas, F. Sayed, R. Sayed Hassan, J.M. Greneche, C. Cannas, A. Musinu, V. Foglietti, S. Casciardi, C. Sangregorio, and D. Peddis, Evolution of the Magnetic Structure with Chemical Composition in Spinel Iron Oxide Nanoparticles. *Nanoscale*, 32:13576-13585, 2015.
52. M.J. Roberts, M.D. Bentley, and J.M. Harris, Chemistry for Peptide and Protein PEGylation. *Advanced Drug Delivery Reviews*, 4:459-476, 2002.
53. D.E. Owens, 3rd and N.A. Peppas, Opsonization, Biodistribution, and Pharmacokinetics of Polymeric Nanoparticles. *International Journal of Pharmaceutics*, 1:93-102, 2006.
54. G. Orive, R.M. Hernández, A.R.g. Gascón, A. Domínguez-Gil, and J.L. Pedraz, Drug Delivery in Biotechnology: Present and Future. *Current Opinion in Biotechnology*, 6:659-664, 2003.

55. J.-P. Fortin, F. Gazeau, and C. Wilhelm, Intracellular Heating of Living Cells through Néel Relaxation of Magnetic Nanoparticles. *European Biophysics Journal*, 2:223-228, 2007.
56. P. Pouponneau, J.-C. Leroux, and S. Martel, Magnetic Nanoparticles Encapsulated into Biodegradable Microparticles Steered with an Upgraded Magnetic Resonance Imaging System for Tumor Chemoembolization. *Biomaterials*, 31:6327-6332, 2009.
57. S. Shabestari Khiabani, M. Farshbaf, A. Akbarzadeh, and S. Davaran, Magnetic Nanoparticles: Preparation Methods, Applications in Cancer Diagnosis and Cancer Therapy. *Artif Cells Nanomed Biotechnology*, 12:1-12, 2016.
58. K. Nagpal, S.K. Singh, and D.N. Mishra, Chitosan Nanoparticles: a Promising System in Novel Drug Delivery. *Chemical and Pharmaceutical Bulletin (Tokyo)*, 11:1423-1430, 2010.
59. Y. Yun, Y.W. Cho, and K. Park, Nanoparticles for Oral Delivery: Targeted Nanoparticles with Peptidic Ligands for Oral Protein Delivery. *Advanced Drug Delivery Reviews*, 6:822-832, 2013.
60. K.T. Nguyen and Y. Zhao, Engineered Hybrid Nanoparticles for On-Demand Diagnostics and Therapeutics. *Accounts of Chemical Research*, 12:3016-3025, 2015.
61. J. Panyam and V. Labhasetwar, Biodegradable Nanoparticles for Drug and Gene Delivery to Cells and Tissue. *Advance Drug Delivery Reviews*, 3:329-347, 2003.
62. R.H. Müller, D. Rühl, S. Runge, K. Schulze-Forster, and W. Mehnert, Cytotoxicity of Solid Lipid Nanoparticles as a Function of the Lipid Matrix and the Surfactant. *Pharmaceutical Research*, 4:458-462.

63. R. Cavalli, M.R. Gasco, P. Chetoni, S. Burgalassi, and M.F. Saettone, Solid lipid Nanoparticles (SLN) as Ocular Delivery System for Tobramycin. *International Journal of Pharmaceutics*, 1–2:241-245, 2002.
64. S.C. Yang, L.F. Lu, Y. Cai, J.B. Zhu, B.W. Liang, and C.Z. Yang, Body Distribution in Mice of Intravenously Injected Camptothecin Solid Lipid Nanoparticles and Targeting Effect on Brain. *Journal of Controlled Release*, 3:299-307, 1999.
65. J.F. Hainfeld, D.N. Slatkin, T.M. Focella, and H.M. Smilowitz, Gold Nanoparticles: a New X-ray Contrast Agent. *The British Journal of Radiology*, 939:248-253, 2006.
66. V.P. Torchilin, Targeted Polymeric Micelles for Delivery of Poorly Soluble Drugs. *Cellular and Molecular Life Sciences CMLS*, 19:2549-2559.
67. J.L. Arias, M. López-Viota, J. López-Viota, and Á.V. Delgado, Development of Iron/Ethylcellulose (Core/Shell) Nanoparticles Loaded with Diclofenac Sodium for Arthritis Treatment. *International Journal of Pharmaceutics*, 1–2:270-276, 2009.
68. C. Sun, J.S.H. Lee, and M. Zhang, Magnetic nanoparticles in MR imaging and drug delivery. *Advance Drug Delivery Reviews*, 11:1252-1265, 2008.
69. T.G. Singh, S. Dhiman, M. Jindal, I.S. Sandhu, and M. Chitkara. Chapter 13 - Nanobiomaterials: Applications in Biomedicine and Biotechnology A2 - Grumezescu, Alexandru Mihai. In, *Fabrication and Self-Assembly of Nanobiomaterials*. pages 401-429. William Andrew Publishing, 2016.
70. R. Fernández-Pacheco, C. Marquina, J. Gabriel Valdivia, M. Gutiérrez, M. Soledad Romero, R. Cornudella, A. Laborda, A. Vilorio, T. Higuera, A. García, J.A.G. de Jalón, and M. Ricardo Ibarra, Magnetic Nanoparticles for Local Drug Delivery Using Magnetic Implants. *Journal of Magnetism and Magnetic Materials*, 1:318-322, 2007.

71. M. Arruebo, R. Fernández-Pacheco, M.R. Ibarra, and J. Santamaría, Magnetic Nanoparticles for Drug Delivery. *Nano Today*, 3:22-32, 2007.
72. S. Baboota and S.P. Agarwal, Meloxicam Complexation with Beta-Cyclodextrin: Influence on the Anti-Inflammatory and Ulcerogenic Activity. *Pharmazie*, 1:73-74, 2003.
73. H.J. Buschmann and E. Schollmeyer, Applications of Cyclodextrins in Cosmetic Products: A review. *Journal of Cosmetic Science*, 3:185-191, 2002.
74. D.G. Fatouros, K. Hatzidimitriou, and S.G. Antimisiaris, Liposomes Encapsulating Prednisolone and Prednisolone–Cyclodextrin Complexes: Comparison of Membrane Integrity and Drug Release. *European Journal of Pharmaceutical Sciences*, 3:287-296, 2001.
75. B. Chankvetadze, N. Burjanadze, G. Pintore, D. Strickmann, D. Bergenthal, and G. Blaschke, Chiral Recognition of Verapamil by Cyclodextrins Studied with Capillary Electrophoresis, NMR Spectroscopy, and Electrospray Ionization Mass Spectrometry. *Chirality*, 8:635-644, 1999.
76. D. Wang, R. Miller, J. Zheng, and C. Hu, Comparative Population Pharmacokinetic-Pharmacodynamic Analysis for Piroxicam- β -Cyclodextrin and Piroxicam. *The Journal of Clinical Pharmacology*, 11:1257-1266, 2000.
77. Y. Horiuchi, F. Hirayama, and K. Uekama, Slow-Release Characteristics of Diltiazem from Ethylated Beta-Cyclodextrin Complexes. *Journal of Pharmaceutical Science*, 2:128-132, 1990.
78. B. Cappello, C. Carmignani, M. Iervolino, M. Immacolata La Rotonda, and M. Fabrizio Saettone, Solubilization of Tropicamide by Hydroxypropyl-Beta-Cyclodextrin and Water-Soluble Polymers: in Vitro/in Vivo Studies. *International Journal of Pharmaceutics*, 1-2:75-81, 2001.

79. F. Acartürk, Ö. Kişlal, and N. Çelebi, The Effect of Some Natural Polymers on the Solubility and Dissolution Characteristics of Nifedipine. *International Journal of Pharmaceutics*, 1:1-6, 1992.
80. M.E. Dalmora, S.L. Dalmora, and A.G. Oliveira, Inclusion Complex of Piroxicam with β -Cyclodextrin and Incorporation in Cationic Microemulsion. In vitro Drug Release and in Vivo Topical Anti-Inflammatory Effect. *International Journal of Pharmaceutics*, 1:45-55, 2001.
81. A. Doliwa, S. Santoyo, and P. Ygartua, Transdermal Iontophoresis and Skin Retention of Piroxicam from Gels Containing Piroxicam: Hydroxypropyl-Beta-Cyclodextrin Complexes. *Drug Development and Industrial Pharmacy*, 8:751-758, 2001.
82. D. Duchene, G. Ponchel, and D. Wouessidjewe, Cyclodextrins in Targeting. Application to Nanoparticles. *Advance Drug Delivery Reviews*, 1:29-40, 1999.
83. G. Tiwari, R. Tiwari, and A.K. Rai, Cyclodextrins in Delivery Systems: Applications. *Journal of Pharmacy and Bioallied Sciences*, 2:72-79, 2010.
84. M.E. Brewster and T. Loftsson, The Use of Chemically Modified Cyclodextrins in the Development of Formulations for Chemical Delivery Systems. *Pharmazie*, 2:94-101, 2002.
85. S. Tavornvipas, F. Hirayama, H. Arima, K. Uekama, T. Ishiguro, M. Oka, K. Hamayasu, and H. Hashimoto, 6-O- α -(4-O- α -d-glucuronyl)-d-glucosyl- β -Cyclodextrin: Solubilizing Ability and Some Cellular Effects. *International Journal of Pharmaceutics*, 1-2:199-209, 2002.
86. D.C. Bibby, N.M. Davies, and I.G. Tucker, Mechanisms by which Cyclodextrins Modify Drug Release from Polymeric Drug Delivery Systems. *International Journal of Pharmaceutics*, 1-2:1-11, 2000.

87. M. Becirevic-Lacan and J. Filipovic-Grcic, Effect of Hydroxypropyl-Beta-Cyclodextrin on Hydrocortisone Dissolution from Films Intended for Ocular Drug Delivery. *Pharmazie*, 7:518-520, 2000.
88. R. Riva, H. Ragelle, A. Rieux, N. Duhem, C. Jérôme, and V. Prémat. Chitosan and Chitosan Derivatives in Drug Delivery and Tissue Engineering. In. R. Jayakumar, M. Prabakaran, and A.R.A. Muzzarelli, Editors, *Chitosan for Biomaterials II*. pages 19-44. Springer Berlin Heidelberg, Berlin, Heidelberg, 2011.
89. R.H. Müller, Colloidal Carriers for Controlled Drug Delivery and Targeting: Modification, Characterization and in Vivo Distribution. *Wiss. Verlag-Ges.*, 1991.
90. S. Cohen and H. Bernstein, *Microparticulate Systems for the Delivery of Proteins and Vaccines*: Taylor and Francis, 1996.
91. J. Kreuter, *Colloidal Drug Delivery Systems*: Taylor and Francis, 1994.
92. F. Brasseur, P. Couvreur, B. Kante, L. Deckers-Passau, M. Roland, C. Deckers, and P. Speiser, Actinomycin D Absorbed on Polymethylcyanoacrylate Nanoparticles: Increased Efficiency Against an Experimental Tumor. *European Journal of Cancer*, 11:1441-1445, 1980.
93. S.C. Gad, *Pharmaceutical Manufacturing Handbook: Production and Processes*: Wiley, 2008.
94. M.J. Alonso and A. Sánchez, The Potential of Chitosan in Ocular Drug Delivery. *Journal of Pharmacy and Pharmacology*, 11:1451-1463, 2003.
95. A.M. De Campos, A. Sanchez, and M.J. Alonso, Chitosan Nanoparticles: a New Vehicle for the Improvement of the Delivery of Drugs to the Ocular Surface. Application to Cyclosporin A. *International Journal of Pharmaceutics*, 1-2:159-168, 2001.

96. M.M. de Villiers, P. Aramwit, and G.S. Kwon, *Nanotechnology in Drug Delivery*: Springer New York, 2008.
97. A. Trapani, N. Denora, G. Iacobellis, J. Sitterberg, U. Bakowsky, and T. Kissel, Methotrexate-Loaded Chitosan- and Glycolchitosan-Based Nanoparticles: A Promising Strategy for the Administration of the Anticancer Drug to Brain Tumors. *AAPS PharmSciTech*, 4:1302-1311, 2011.
98. B.R. Ferrell, C. Pasero, and M. McCaffery, *Pain Assessment and Pharmacologic Management*: Elsevier Health Sciences, 2010.
99. E.H. Lo, J. Lok, M.M. Ning, and M. Whalen, *Vascular Mechanisms in CNS Trauma*: Springer New York, 2013.
100. P.K. Dutta, *Chitin and Chitosan for Regenerative Medicine*: Springer India, 2015.
101. I.M. van der Lubben, J.C. Verhoef, G. Borchard, and H.E. Junginger, Chitosan and its Derivatives in Mucosal Drug and Vaccine Delivery. *European Journal of Pharmaceutical Science*, 3:201-207, 2001.
102. M.P. Deacon, S. McGurk, C.J. Roberts, P.M. Williams, S.J. Tendler, M.C. Davies, S.S. Davis, and S.E. Harding, Atomic Force Microscopy of Gastric Mucin and Chitosan Mucoadhesive Systems. *Biochemistry Journal*, 21:557-563, 2000.
103. J. Wang, Y. Tauchi, Y. Deguchi, K. Morimoto, Y. Tabata, and Y. Ikada, Positively Charged Gelatin Microspheres as Gastric Mucoadhesive Drug Delivery System for Eradication of *H. pylori*. *Drug Delivery*, 4:237-243, 2000.
104. W. Wang and M. Singh, *Biological Drug Products: Development and Strategies*: Wiley, 2013.

105. R. Stupp, M. Gander, S. Leyvraz, and E. Newlands, Current and Future Developments in the Use of Temozolomide for the Treatment of Brain Tumours. *The Lancet Oncology*, 9:552-560, 2001.
106. E.A.E. Garelnabi, D. Pletsas, L. Li, K. Kiakos, N. Karodia, J.A. Hartley, R.M. Phillips, and R.T. Wheelhouse, Strategy for Imidazotetrazine Prodrugs with Anticancer Activity Independent of MGMT and MMR. *ACS Medicinal Chemistry Letters*, 12:965-968, 2012.
107. H.S. Friedman, T. Kerby, and H. Calvert, Temozolomide and Treatment of Malignant Glioma. *Clinical Cancer Research*, 7:2585-2597, 2000.
108. A.C. Sartorelli and D.G. Johns, *Antineoplastic and Immunosuppressive Agents*: Springer Berlin Heidelberg, 2013.
109. M. Belanich, T. Randall, M.A. Pastor, J.T. Kibitel, L.G. Alas, M.E. Dolan, S.C. Schold, Jr., M. Gander, F.J. Lejeune, B.F. Li, A.B. White, P. Wasserman, M.L. Citron, and D.B. Yarosh, Intracellular Localization and Intercellular Heterogeneity of the Human DNA Repair Protein O(6)-Methylguanine-DNA Methyltransferase. *Cancer Chemotherapy Pharmacol*, 6:547-555, 1996.
110. M.F. Stevens, J.A. Hickman, S.P. Langdon, D. Chubb, L. Vickers, R. Stone, G. Baig, C. Goddard, N.W. Gibson, J.A. Slack, and et al., Antitumor Activity and Pharmacokinetics in Mice of 8-Carbamoyl-3-Methyl-Imidazo[5,1-d]-1,2,3,5-Tetrazin-4(3H)-One (CCRG 81045; M and B 39831), a Novel Drug with Potential as an Alternative to Dacarbazine. *Cancer Research*, 22:5846-5852, 1987.
111. N.J. Babu, P. Sanphui, and A. Nangia, Crystal Engineering of Stable Temozolomide Cocrystals. *Chemistry Asian Journal*, 10:2274-2285, 2012.
112. R. Challa, A. Ahuja, J. Ali, and R.K. Khar, Cyclodextrins in Drug Delivery: An Updated Review. *AAPS PharmSciTech*, 2:E329-E357, 2005.

113. S.D. Eastburn and B.Y. Tao, Applications of Modified Cyclodextrins. *Biotechnology Advances*, 2:325-339, 1994.
114. S.V. Kurkov and T. Loftsson, Cyclodextrins. *International Journal of Pharmaceutics*, 1:167-180, 2013.
115. M. Vecsernyes, F. Fenyvesi, I. Bacskay, M.A. Deli, L. Szente, and E. Fenyvesi, Cyclodextrins, Blood-Brain Barrier, and Treatment of Neurological Diseases. *Archives of Medical Research*, 8:711-729, 2014.
116. R. Challa, A. Ahuja, J. Ali, and R.K. Khar, Cyclodextrins in Drug Delivery: An Updated Review. *AAPS PharmSciTech*, 2:E329-E357.
117. B. Hakkarainen, K. Fujita, S. Immel, L. Kenne, and C. Sandstrom, ¹H NMR Studies on the Hydrogen-Bonding Network in Mono-Altro-Beta-Cyclodextrin and Its Complex with Adamantane-1-carboxylic acid. *Carbohydrate Research*, 8:1539-1545, 2005.
118. E.M.M. Del Valle, Cyclodextrins and Their Uses: a Review. *Process Biochemistry*, 9:1033-1046, 2004.
119. T. Loftsson and D. Duchêne, Cyclodextrins and Their Pharmaceutical Applications. *International Journal of Pharmaceutics*, 1–2:1-11, 2007.
120. H.A. Archontaki, M.V. Vertzoni, and M.H. Athanassiou-Malaki, Study on the Inclusion Complexes of Bromazepam with β - and β -Hydroxypropyl-Cyclodextrins. *Journal of Pharmaceutical and Biomedical Analysis*, 3–4:761-769, 2002.
121. H. Arima, K. Yunomae, K. Miyake, T. Irie, F. Hirayama, and K. Uekama, Comparative Studies of the Enhancing Effects of Cyclodextrins on the Solubility and Oral Bioavailability of Tacrolimus in Rats. *Journal of Pharmaceutical Science*, 6:690-701, 2001.

122. H. Arima, T. Miyaji, T. Irie, F. Hirayama, and K. Uekama, Enhancing Effect of Hydroxypropyl-Beta-Cyclodextrin on Cutaneous Penetration and Activation of Ethyl 4-biphenyl Acetate in Hairless Mouse Skin. *European Journal of Pharmaceutical Science*, 1:53-59, 1998.
123. S.S. Dhule, P. Penfornis, T. Frazier, R. Walker, J. Feldman, G. Tan, J. He, A. Alb, V. John, and R. Pochampally, Curcumin-Loaded Gamma-Cyclodextrin Liposomal Nanoparticles as Delivery Vehicles for Osteosarcoma. *Nanomedicine*, 4:440-451, 2012.
124. G. Piel, M. Piette, V. Barillaro, D. Castagne, B. Evrard, and L. Delattre, Betamethasone-in-Cyclodextrin-in-Liposome: the Effect of Cyclodextrins on Encapsulation Efficiency and Release Kinetics. *International Journal of Pharmaceutics*, 1-2:75-82, 2006.
125. A. Ascenso, M. Cruz, C. Euleterio, F.A. Carvalho, N.C. Santos, H.C. Marques, and S. Simoes, Novel Tretinoin Formulations: a Drug-in-Cyclodextrin-in-Liposome Approach. *Journal of Liposome Research*, 3:211-219, 2013.
126. R. Gharib, H. Greige-Gerges, S. Fourmentin, C. Charcosset, and L. Auezova, Liposomes Incorporating Cyclodextrin-Drug Inclusion Complexes: Current State of Knowledge. *Carbohydrate Polymers*, 45:175-186, 2015.
127. J.R. Moyano, M.J. Arias-Blanco, J.M. Ginés, and F. Giordano, Solid-State Characterization and Dissolution Characteristics of Gliclazide- β -Cyclodextrin Inclusion Complexes. *International Journal of Pharmaceutics*, 2:211-217, 1997.
128. H. Chen, J. Gao, F. Wang, and W. Liang, Preparation, Characterization and Pharmacokinetics of Liposomes-Encapsulated Cyclodextrins Inclusion Complexes for Hydrophobic Drugs. *Drug Delivery*, 4:201-208, 2007.

129. N. Škalko, M. Brandl, M. Bećirević-Laćan, J. Filipović-Grčić, and I. Jalšenjak, Liposomes with Nifedipine and Nifedipine-Cyclodextrin Complex: Calorimetric and Plasma Stability Comparison. *European Journal of Pharmaceutical Sciences*, 6:359-366, 1996.
130. Q. Zhu, T. Guo, D. Xia, X. Li, C. Zhu, H. Li, D. Ouyang, J. Zhang, and Y. Gan, Pluronic F127-Modified Liposome-Containing Tacrolimus–Cyclodextrin Inclusion Complexes: Improved Solubility, Cellular Uptake and Intestinal Penetration. *Journal of Pharmacy and Pharmacology*, 8:1107-1117, 2013.
131. F. Maestrelli, M.L. González-Rodríguez, A.M. Rabasco, and P. Mura, Preparation and Characterisation of Liposomes Encapsulating Ketoprofen–Cyclodextrin Complexes for Transdermal Drug Delivery. *International Journal of Pharmaceutics*, 1:55-67, 2005.
132. F. Maestrelli, M.L. González-Rodríguez, A.M. Rabasco, and P. Mura, Effect of Preparation Technique on the Properties of Liposomes Encapsulating Ketoprofen–Cyclodextrin Complexes Aimed for Transdermal Delivery. *International Journal of Pharmaceutics*, 1–2:53-60, 2006.
133. I. Younes and M. Rinaudo, Chitin and Chitosan Preparation from Marine Sources. Structure, Properties and Applications. *Marine Drugs*, 3:1133-1174, 2015.
134. J.H. Park, Y.W. Cho, H. Chung, I.C. Kwon, and S.Y. Jeong, Synthesis and Characterization of Sugar-Bearing Chitosan Derivatives: Aqueous Solubility and Biodegradability. *Biomacromolecules*, 4:1087-1091, 2003.
135. M.E.I. Badawy and E.I. Rabea, A Biopolymer Chitosan and Its Derivatives as Promising Antimicrobial Agents against Plant Pathogens and Their Applications in Crop Protection. *International Journal of Carbohydrate Chemistry*, 2011.

136. K. Bowman and K.W. Leong, Chitosan Nanoparticles for Oral Drug and Gene Delivery. *International Journal of Nanomedicine*, 2:117-128, 2006.
137. C. Liu, Y. Tan, C. Liu, X. Chen, and L. Yu, Preparations, Characterizations and Applications of Chitosan-Based Nanoparticles. *Journal of Ocean University of China*, 3:237-243.
138. T. López-León, E.L.S. Carvalho, B. Seijo, J.L. Ortega-Vinuesa, and D. Bastos-González, Physicochemical Characterization of Chitosan Nanoparticles: Electrokinetic and Stability Behavior. *Journal of Colloid and Interface Science*, 2:344-351, 2005.
139. W. Fan, W. Yan, Z. Xu, and H. Ni, Formation Mechanism of Monodisperse, Low Molecular Weight Chitosan Nanoparticles by Ionic Gelation Technique. *Colloids and Surfaces B: Biointerfaces*, 46:21-27, 2012.
140. M. Bodnar, J.F. Hartmann, and J. Borbely, Preparation and Characterization of Chitosan-Based Nanoparticles. *Biomacromolecules*, 5:2521-2527, 2005.
141. S. Mitra, U. Gaur, P.C. Ghosh, and A.N. Maitra, Tumour Targeted Delivery of Encapsulated Dextran–Doxorubicin Conjugate Using Chitosan Nanoparticles as Carrier. *Journal of Controlled Release*, 1–3:317-323, 2001.
142. A. Grenha, Chitosan Nanoparticles: a Survey of Preparation Methods. *Journal of Drug Targeting*, 4:291-300, 2012.
143. Z.X. Tang, J.Q. Qian, and L.E. Shi, Preparation of Chitosan Nanoparticles as Carrier for Immobilized Enzyme. *Applied Biochemistry Biotechnology*, 1:77-96, 2007.
144. H. Tokumitsu, H. Ichikawa, and Y. Fukumori, Chitosan-Gadopentetic Acid Complex Nanoparticles for Gadolinium Neutron-Capture Therapy of Cancer: Preparation by

Novel Emulsion-Droplet Coalescence Technique and Characterization. *Pharmaceutical Research*, 12:1830-1835, 1999.

145. A. Meng, S. Chen, H. Zhou, Y. Long, Y. Zhang, and Q. Li, Pyrolysis and Simulation of Typical Components in Wastes with Macro-TGA. *Fuel*, 7:1-8, 2015.
146. G. Höhne, W. Hemminger, and H.J. Flammersheim, *Differential Scanning Calorimetry: An Introduction for Practitioners*: Springer-Verlag, 1996.
147. O. T. *Fundamentals of UV-Visible Spectroscopy*, Agilent Technologies. 2000.
148. T. Owen, *Fundamentals of UV-visible Spectroscopy: A Primer*: Hewlett Packard, 1996.
149. S. Ahuja and M. Dong, *Handbook of Pharmaceutical Analysis by HPLC*: Elsevier Science, 2005.
150. L. Reimer, *Scanning Electron Microscopy: Physics of Image Formation and Microanalysis*: Springer, 1998.
151. Q. Zhang, M.S. Thompson, A.Y. Carmichael-Baranauskas, B.L. Caba, M.A. Zalich, Y.-N. Lin, O.T. Mefford, R.M. Davis, and J.S. Riffle, Aqueous Dispersions of Magnetite Nanoparticles Complexed with Copolyether Dispersants: Experiments and Theory. *Langmuir*, 13:6927-6936, 2007.
152. Y. Zu, W. Wu, X. Zhao, Y. Li, C. Zhong, and Y. Zhang, The High Water Solubility of Inclusion Complex of Taxifolin- γ -CD Prepared and Characterized by the Emulsion Solvent Evaporation and the Freeze Drying Combination Method. *International Journal of Pharmaceutics*, 1-2:148-158, 2014.
153. R. Yang, J.-B. Chen, C.-F. Xiao, Z.-C. Liu, Z.-Y. Gao, S.-J. Yan, J.-H. Zhang, H.-B. Zhang, and J. Lin, Inclusion Complex of GA13316 with β -cyclodextrin: Preparation,

Characterization, Molecular Modeling, and In Vitro Evaluation. *Carbohydrate Polymers*, 12:655-662, 2014.

154. J. Zhang, K. Jiang, K. An, S.H. Ren, X.G. Xie, Y. Jin, and J. Lin, Novel Water-Soluble Fisetin/Cyclodextrins Inclusion Complexes: Preparation, Characterization, Molecular Docking and Bioavailability. *Carbohydrate Research*, 1:20-28, 2015.
155. Y. Bai, J. Wang, M. Bashari, X. Hu, T. Feng, X. Xu, Z. Jin, and Y. Tian, A Thermogravimetric Analysis (TGA) Method Developed for Estimating The Stoichiometric Ratio of Solid-State α -Cyclodextrin-Based Inclusion Complexes. *Thermochimica Acta*, 2:62-69, 2012.
156. M.F. Canbolat, A. Celebioglu, And T. Uyar, Drug Delivery System Based on Cyclodextrin-Naproxen Inclusion Complex Incorporated in Electrospun Polycaprolactone Nanofibers. *Colloids and Surfaces Biointerfaces*, 2:15-21, 2014.
157. D.R. De Araujo, S.S. Tsuneda, C.M. Cereda, G.F.C.F. Del, P.S. Prete, S.A. Fernandes, F. Yokaichiya, M.K. Franco, I. Mazzaro, L.F. Fraceto, F.A.B.A. De, and E. De Paula, Development and Pharmacological Evaluation of Ropivacaine-2-Hydroxypropyl-Beta-Cyclodextrin Inclusion Complex. *European Journal of Pharmaceutical Science*, 1:60-71, 2008.
158. P. Tang, S. Li, L. Wang, H. Yang, J. Yan, and H. Li, Inclusion Complexes of Chlorzoxazone with Beta- and Hydroxypropyl-Beta-Cyclodextrin: Characterization, Dissolution, and Cytotoxicity. *Carbohydrate Polymers*, 2:297-305, 2015.
159. V.D. Bulani, P.S. Kothavade, H.S. Kundaikar, N.B. Gawali, A.A. Chowdhury, M.S. Degani, and A.R. Juvekar, Inclusion Complex of Ellagic Acid with B-Cyclodextrin: Characterization and in Vitro Anti-Inflammatory Evaluation. *Journal of Molecular Structure*, 2:308-315, 2016.

160. L.M.A. Pinto, L.F. Fraceto, M.H.A. Santana, T.A. Pertinhez, S.O. Junior, And E. De Paula, Physico-Chemical Characterization of Benzocaine-B-Cyclodextrin Inclusion Complexes. *Journal of Pharmaceutical and Biomedical Analysis*, 5:956-963, 2005.
161. D. Zhang, J. Zhang, K. Jiang, K. Li, Y. Cong, S. Pu, Y. Jin, and J. Lin, Preparation, Characterisation and Antitumour Activity of B and HPB Cyclodextrin Inclusion Complexes of Oxaliplatin. *Spectrochimica Acta Part A: Molecular and Biomolecular Spectroscopy*, 1:501-508, 2016.
162. A. Figueiras, R.A. Carvalho, L. Ribeiro, J.J. Torres-Labandeira, and F.J.B. Veiga, Solid-State Characterization and Dissolution Profiles of the Inclusion Complexes of Omeprazole with Native and Chemically Modified B-Cyclodextrin. *European Journal of Pharmaceutics and Biopharmaceutics*, 2:531-539, 2007.
163. Y. Dong, W.K. Ng, S. Shen, S. Kim, and R.B.H. Tan, Scalable Ionic Gelation Synthesis of Chitosan Nanoparticles for Drug Delivery in Static Mixers. *Carbohydrate Polymers*, 2:940-945, 2013.
164. A. Fàbregas, M. Miñarro, E. García-Montoya, P. PérezLozano, C. Carrillo, R. Sarrate, N. Sánchez, J.R. Ticó, And J.M. Suñé-Negre, Impact of Physical Parameters on Particle Size and Reaction Yield When Using the Ionic Gelation Method to Obtain Cationic Polymeric Chitosan Tripolyphosphate Nanoparticles. *International Journal Of Pharmaceutics*, 1–2:199-204, 2013.
165. K.A.M. O'Callaghan and J.P. Kerry, Preparation of Low and Medium Molecular Weight Chitosan Nanoparticles and Their Antimicrobial Evaluation Against A Panel of Microorganisms, Including Cheese-Derived Cultures. *Food Control*, 2:256-261, 2016.
166. W. Fan, W. Yan, Z. Xu, and H. Ni, Formation Mechanism of Monodisperse, Low Molecular Weight Chitosan Nanoparticles by Ionic Gelation Technique. *Colloids and Surfaces and Biointerfaces*, 2:21-27, 2012.

167. A.L. De Pinho Neves, C.C. Milioli, L. Müller, H.G. Riella, N.C. Kuhnen, and H.K. Stulzer, Factorial Design as Tool in Chitosan Nanoparticles Development by Ionic Gelation Technique. *Colloids and Surfaces A: Physicochemical and Engineering Aspects*, 2:34-39, 2014.
168. W. Wang, S. Chen, L. Zhang, X. Wu, J. Wang, J.-F. Chen, And Y. Le, Poly(Lactic Acid)/Chitosan Hybrid Nanoparticles for Controlled Release of Anticancer Drug. *Materials Science and Engineering C*, 2:514-520, 2015.
169. K.I. David, L.R. Jaidev, S. Sethuraman, and U.M. Krishnan, Dual Drug Loaded Chitosan Nanoparticles—Sugar-Coated Arsenal Against Pancreatic Cancer. *Colloids Surfaces and Biointerfaces*, 2:689-698, 2015.
170. M. Abul Kalam, A.A. Khan, S. Khan, A. Almalik, and A. Alshamsan, Optimizing Indomethacin-Loaded Chitosan Nanoparticle Size, Encapsulation, and Release Using Box–Behnken Experimental Design. *International Journal Of Biological Macromolecules*, 2:329-340, 2016.
171. P.I.P. Soares, A.I. Sousa, J.C. Silva, I.M.M. Ferreira, C.M.M. Novo, and J.P. Borges, Chitosan Based Nanoparticles as Drug Delivery Systems for Doxorubicin: Optimization and Modelling. *Carbohydrate Polymers*, 2:304-312, 2016.
172. R.M. Patil, P.B. Shete, N.D. Thorat, S.V. Otari, K.C. Barick, A. Prasad, R.S. Ningthoujam, B.M. Tiwale, and S.H. Pawar, Superparamagnetic Iron Oxide/Chitosan Core/Shells for Hyperthermia Application: Improved Colloidal Stability and Biocompatibility. *Journal of Magnetism and Magnetic Materials*, 2:22-30, 2014.
173. J. Qu, G. Liu, Y. Wang, and R. Hong, Preparation of Fe₃O₄–Chitosan Nanoparticles Used for Hyperthermia. *Advanced Powder Technology*, 4:461-467, 2010.

174. Y. Dong, W.K. Ng, S. Shen, S. Kim, and R.B.H. Tan, Scalable Ionic Gelation Synthesis of Chitosan Nanoparticles for Drug Delivery in Static Mixers. *Carbohydrate Polymers*, 2:940-945, 2013.
175. A. Fàbregas, M. Miñarro, E. García-Montoya, P. Pérez-Lozano, C. Carrillo, R. Sarrate, N. Sánchez, J.R. Ticó, And J.M. Suñé-Negre, Impact of Physical Parameters on Particle Size and Reaction Yield When Using the Ionic Gelation Method to Obtain Cationic Polymeric Chitosan–Triphosphosphate Nanoparticles. *International Journal of Pharmaceutics*, 1–2:199-204, 2013.
176. L. Zhu, J. Ma, N. Jia, Y. Zhao, and H. Shen, Chitosan-Coated Magnetic Nanoparticles as Carriers of 5-Fluorouracil: Preparation, Characterization and Cytotoxicity Studies. *Colloids and Surfaces B: Biointerfaces*, 1:1-6, 2009.
177. H. Qin, C.M. Wang, Q.Q. Dong, L. Zhang, X. Zhang, Z.Y. Ma, and Q.R. Han, Preparation and Characterization of Magnetic Fe₃O₄–Chitosan Nanoparticles Loaded with Isoniazid. *Journal of Magnetism and Magnetic Materials*, 2:120-126, 2015.
178. X.-H. Tian, X.-N. Lin, F. Wei, W. Feng, Z.-C. Huang, P. Wang, L. Ren, and Y. Diao, Enhanced Brain Targeting of Temozolomide in Polysorbate-80 Coated Polybutylcyanoacrylate Nanoparticles. *International Journal of Nanomedicine*, 1:445-452, 2011.
179. M. Hałupka-Bryl, M. Bednarowicz, B. Dobosz, R. Krzyminiewski, T. Zalewski, B. Wereszczyńska, G. Nowaczyk, M. Jarek, and Y. Nagasaki, Doxorubicin Loaded PEG-B-Poly(4-Vinylbenzylphosphonate) Coated Magnetic Iron Oxide Nanoparticles for Targeted Drug Delivery. *Journal of Magnetism and Magnetic Materials*, 2:320-327, 2015.
180. U. Gunduz, T. Keskin, G. Tansik, P. Mutlu, S. Yalcin, G. Unsoy, A. Yakar, R. Khodadust, And G. Gunduz, Idarubicin-Loaded Folic Acid Conjugated Magnetic

Nanoparticles as a Targetable Drug Delivery System for Breast Cancer. *Biomedicine and Pharmacotherapy*, 6:729-736, 2014.

181. K. Menzel, J. Lindner, And H. Nirschl, Removal of Magnetite Particles and Lubricant Contamination from Viscous Oil by High-Gradient Magnetic Separation Technique. *Separation and Purification Technology*, 2:122-128, 2012.
182. S. Hayashi, F. Mishima, Y. Akiyama, and S. Nishijima, Development of Superconducting High Gradient Magnetic Separation System for Highly Viscous Fluid for Practical Use. *Physica C: Superconductivity*, 21–22:1511-1515, 2011.
183. S. Zeng, W. Zeng, L. Ren, D. An, and H. Li, Development of A High Gradient Permanent Magnetic Separator (HGPMS). *Minerals Engineering*, 1:21-26, 2015.

APPENDIX A: EXAMPLES OF TMZ SCANS FOR INCLUSION COMPLEX AND TARGETING STUDIES

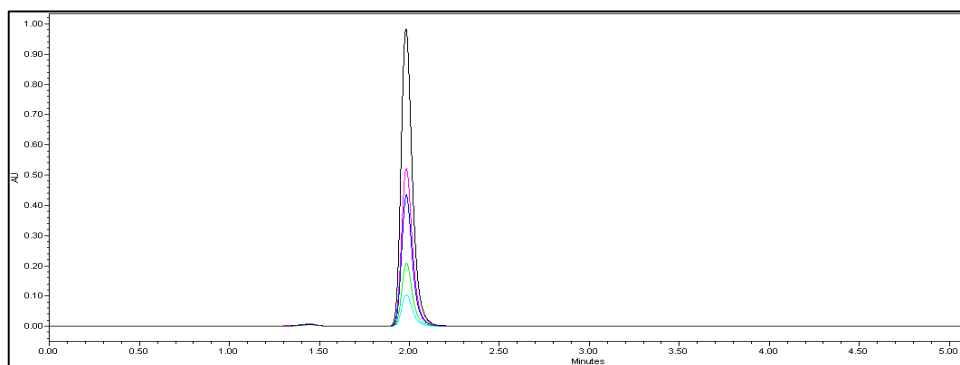


Figure A.1. Standard peaks of TMZ in 0.1 M HCl

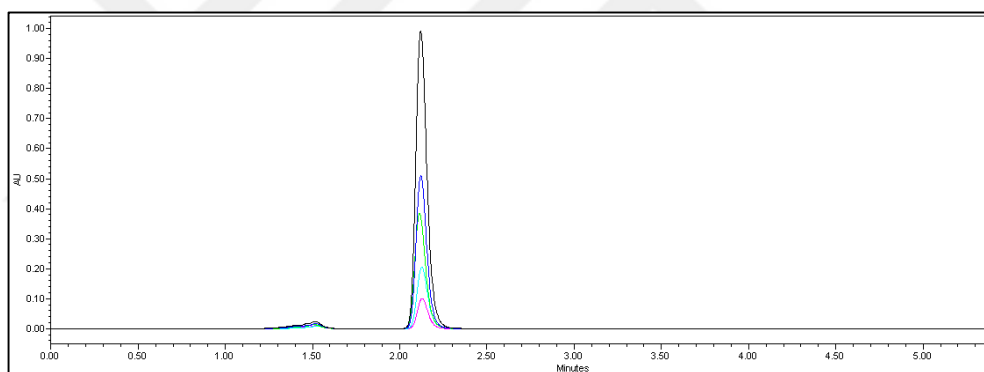


Figure A.2. Standard peaks of TMZ in 1 M HCl

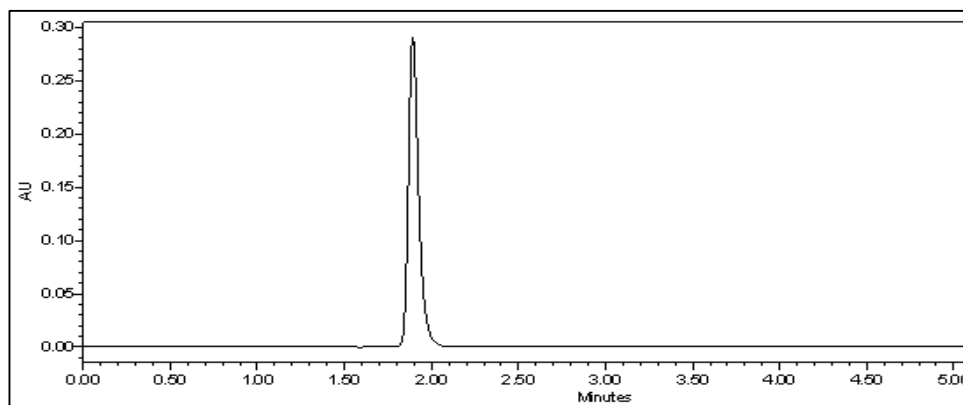


Figure A.3. TMZ scan (β -CD-TMZ complexation after 1 hour)

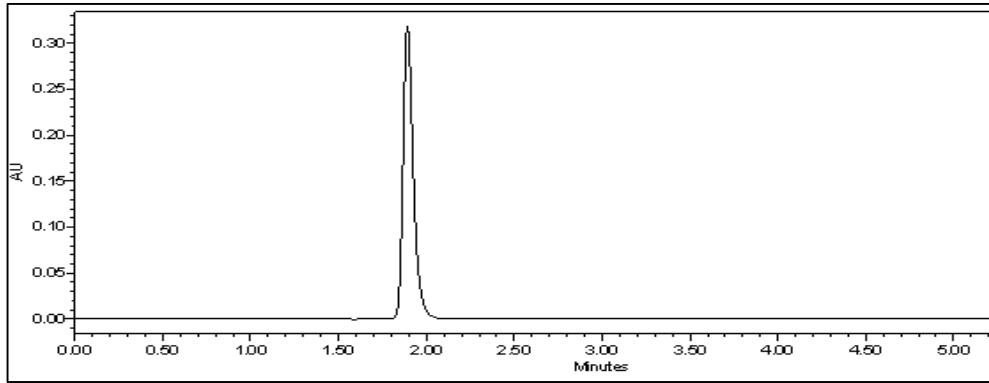


Figure A.4. TMZ scan (H- β -CD-TMZ complexation after 1 hour)

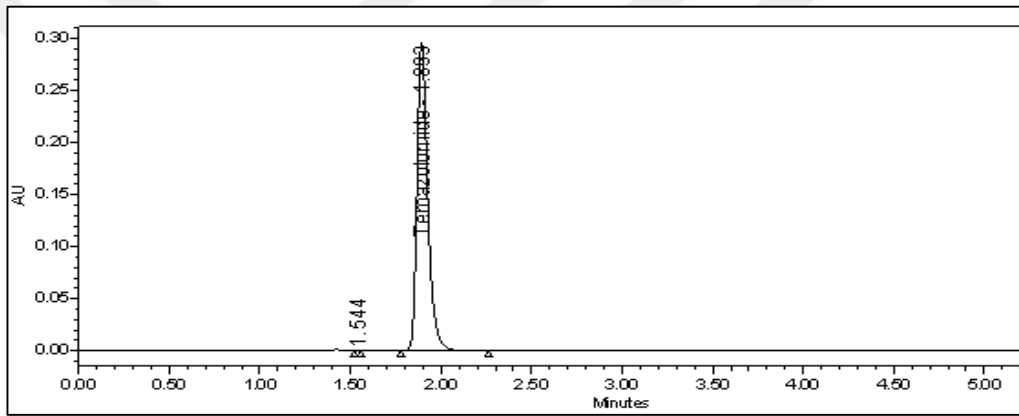


Figure A.5. TMZ scan (H- γ -CD-TMZ complexation after 1 hour)

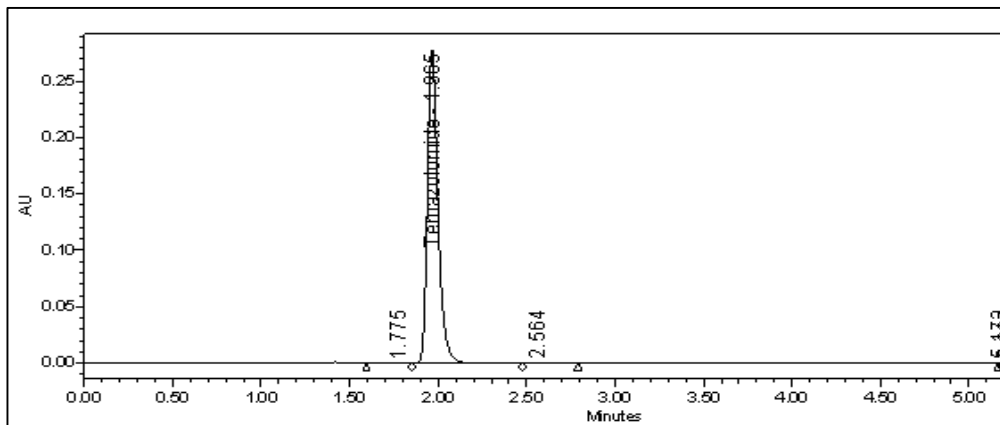


Figure A.6. TMZ scan (β -CD-TMZ complexation after 24 hours)

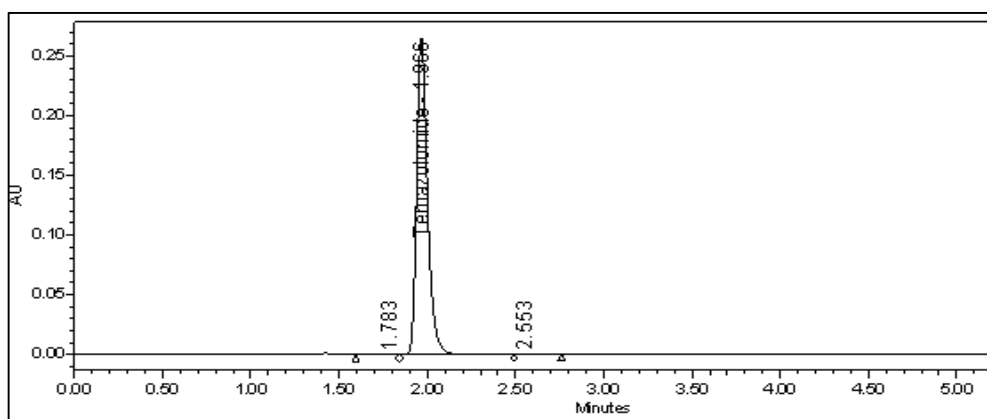


Figure A.7. TMZ scan (H- β -CD-TMZ complexation after 24 hours)

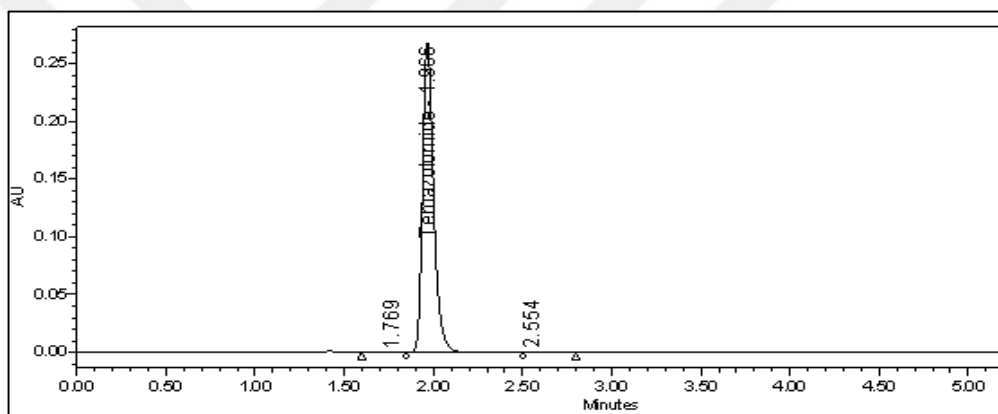


Figure A.8. TMZ scan (H- γ -CD-TMZ complexation after 24 hours)

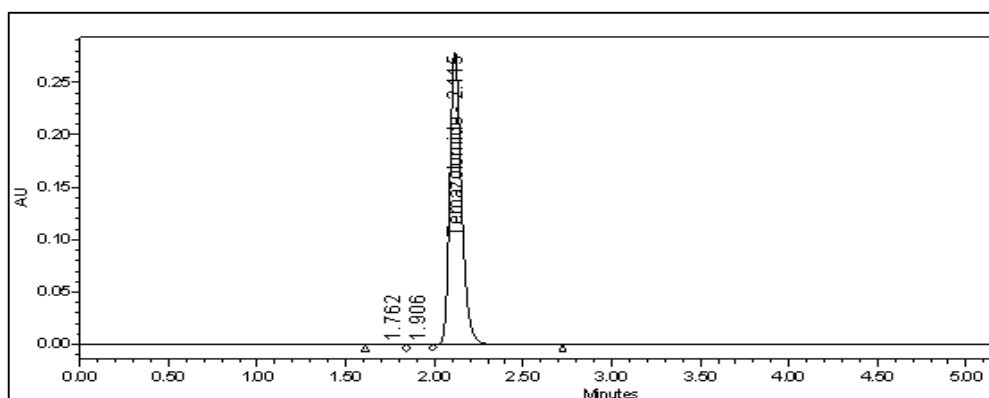


Figure A.9. TMZ scan (β -CD-TMZ complexation after 48 hours)

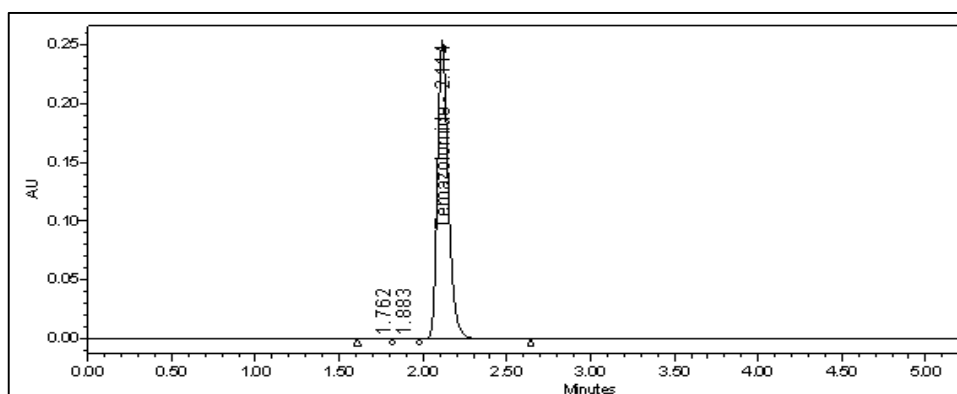


Figure A.10. TMZ scan (H- β -CD-TMZ complexation after 48 hours)

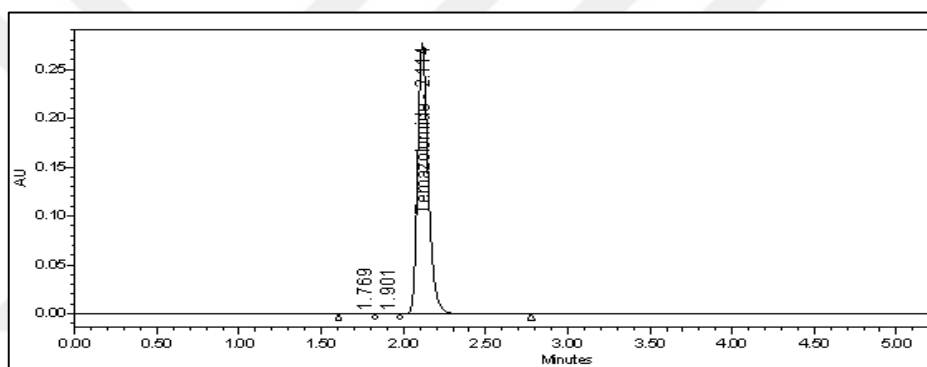


Figure A.11. TMZ scan (H- γ -CD-TMZ complexation after 48 hours)

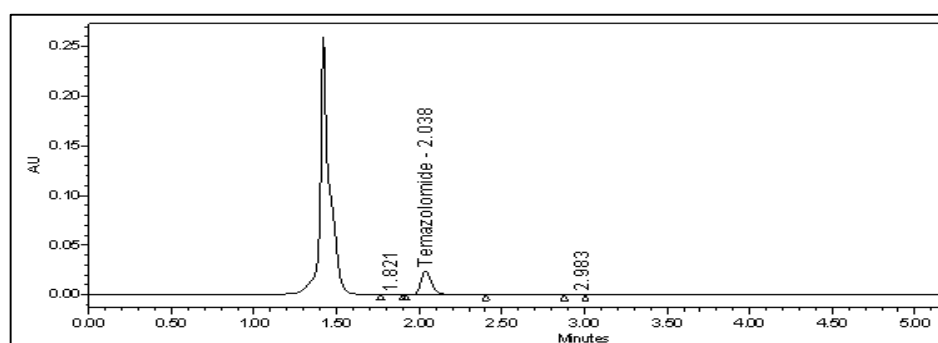


Figure A.12. TMZ scan (targeting study with thin test section)

([Na₂SO₄.10H₂O]_{final} = 2.2 wt% + β -CD coated magnetite solution ; [chitosan]_{final} = 0.22 wt% ; chitosan)

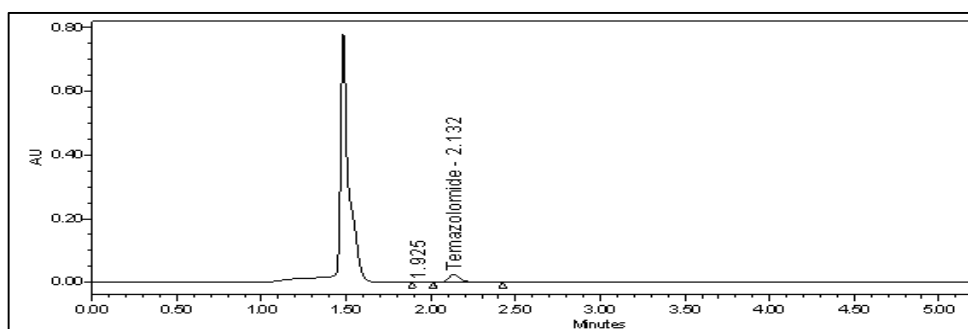


Figure A.13. TMZ scan (targeting study with thin test section)

($[\text{Na}_2\text{SO}_4 \cdot 10\text{H}_2\text{O}]_{\text{final}} = 2.2 \text{ wt\%} + \beta\text{-CD coated magnetite solution} ; [\text{chitosan}]_{\text{final}} = 0.43 \text{ wt\% ; chitosan}$)

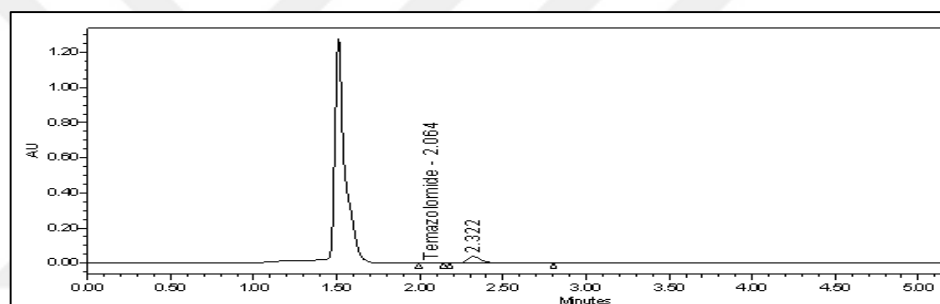


Figure A.14. TMZ scan (targeting study with thin test section)

($[\text{Na}_2\text{SO}_4 \cdot 10\text{H}_2\text{O}]_{\text{final}} = 1.1 \text{ wt\%} + \beta\text{-CD coated magnetite solution} ; [\text{chitosan}]_{\text{final}} = 0.09 \text{ wt\% ; chitosan}$)

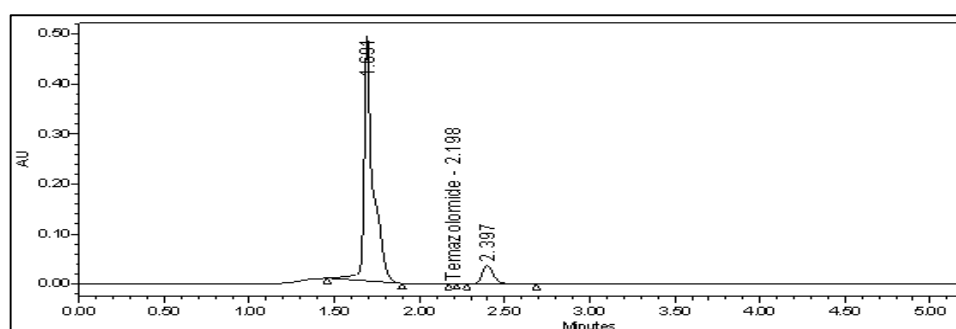


Figure A.15. TMZ scan (targeting study with thin test section)

($[\text{Na}_2\text{SO}_4 \cdot 10\text{H}_2\text{O}]_{\text{final}} = 1.1 \text{ wt\%} + \beta\text{-CD coated magnetite solution} ; [\text{chitosan}]_{\text{final}} = 0.43 \text{ wt\% ; chitosan}$)

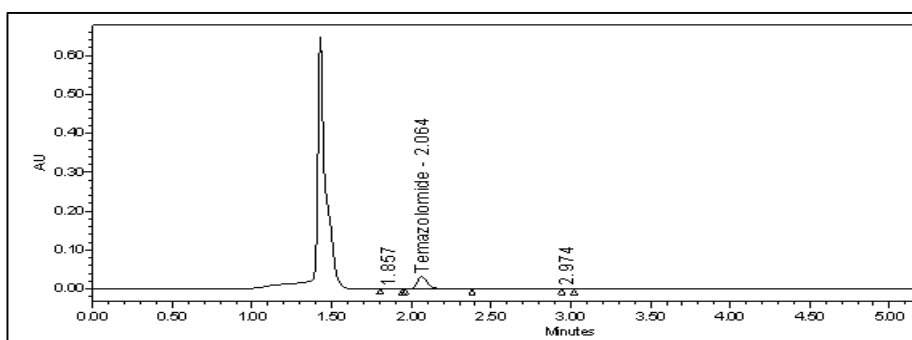


Figure A.16. TMZ scan (targeting study with thin test section)

($[\text{Na}_2\text{SO}_4 \cdot 10\text{H}_2\text{O}]_{\text{final}} = 1.1 \text{ wt\%} + \beta\text{-CD coated magnetite solution} ; [\text{chitosan}]_{\text{final}} = 0.33 \text{ wt\% ; chitosan}$)

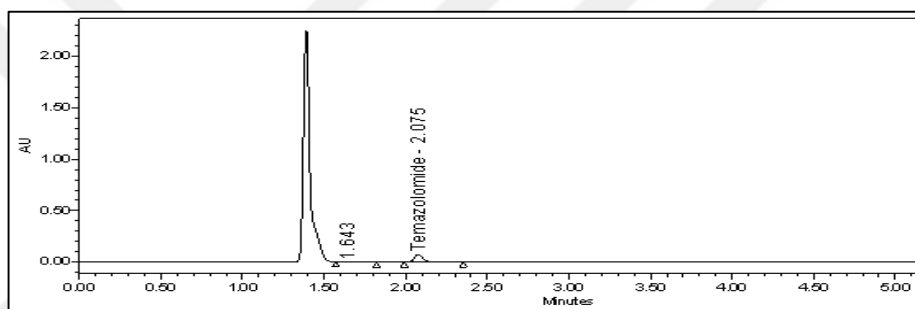


Figure A.17. TMZ scan (Targeting study with thick test section)

($[\text{Na}_2\text{SO}_4 \cdot 10\text{H}_2\text{O}]_{\text{final}} = 1.1 \text{ wt\%} + \beta\text{-CD coated magnetite solution} ; [\text{chitosan}]_{\text{final}} = 0.33 \text{ wt\% ; chitosan}$)

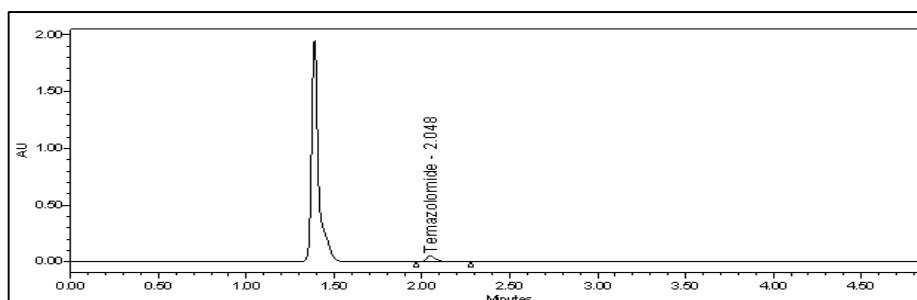


Figure A.18. TMZ scan (Targeting study with thick test section)

($[\text{Na}_2\text{SO}_4 \cdot 10\text{H}_2\text{O}]_{\text{final}} = 1.1 \text{ wt\%} + \beta\text{-CD coated magnetite solution} ; [\text{chitosan}]_{\text{final}} = 0.09 \text{ wt\% ; chitosan}$)

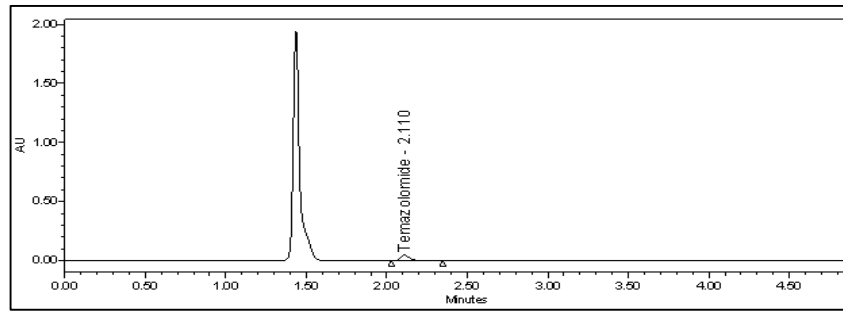


Figure A.19. TMZ scan (Targeting study with thick test section)

($[\text{Na}_2\text{SO}_4 \cdot 10\text{H}_2\text{O}]_{\text{final}} = 2.2 \text{ wt\%}$ + β -CD coated magnetite solution ; $[\text{chitosan}]_{\text{final}} = 0.09$
wt% ; chitosan)

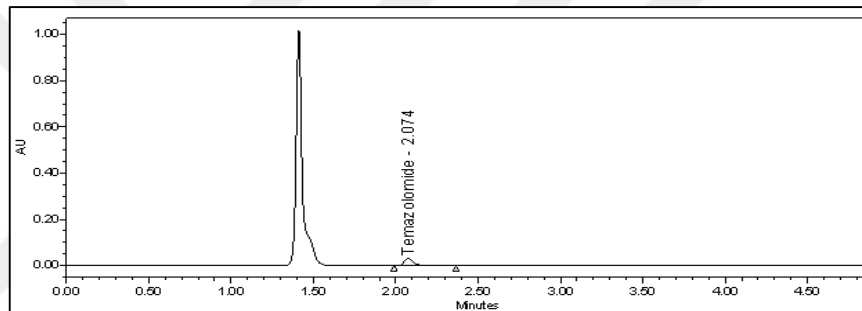


Figure A.20. TMZ scan (Targeting study with thick test section)

($[\text{Na}_2\text{SO}_4 \cdot 10\text{H}_2\text{O}]_{\text{final}} = 2.2 \text{ wt\%}$ + β -CD coated magnetite solution ; $[\text{chitosan}]_{\text{final}} = 0.22$
wt% ; chitosan)

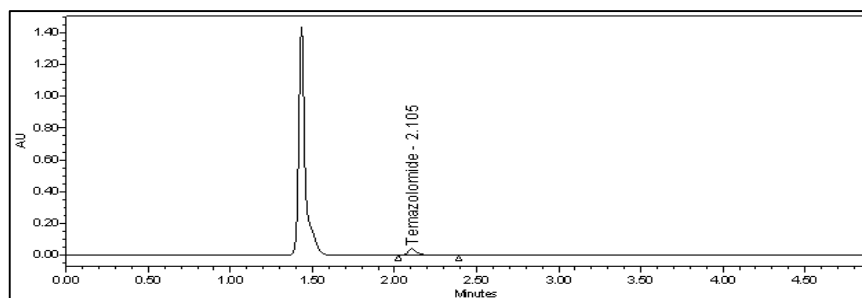


Figure A.21. TMZ scan (Targeting study with thick test section)

($[\text{Na}_2\text{SO}_4 \cdot 10\text{H}_2\text{O}]_{\text{final}} = 1.1 \text{ wt\%}$ + β -CD coated magnetite solution ; $[\text{chitosan}]_{\text{final}} = 0.33$
wt% ; chitosan)

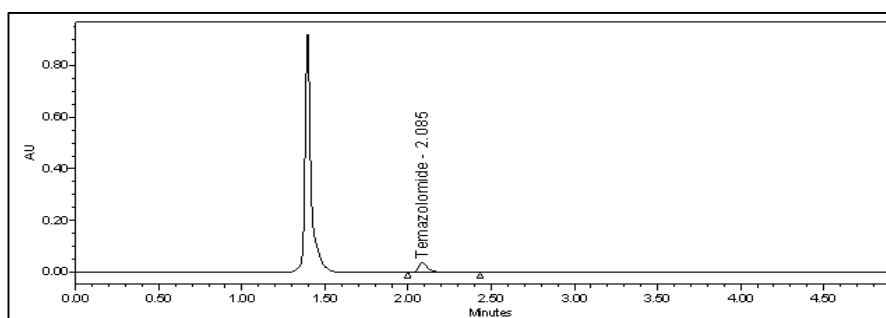


Figure A.22. TMZ scan (Targeting study with thick test section)

($[\text{Na}_2\text{SO}_4 \cdot 10\text{H}_2\text{O}]_{\text{final}} = 1.1 \text{ wt\%} + \beta\text{-CD coated magnetite solution} ; [\text{chitosan}]_{\text{final}} = 0.43 \text{ wt\%} ; \text{chitosan}$)

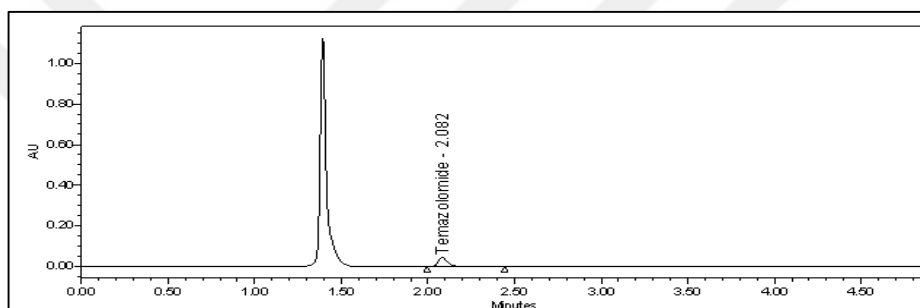


Figure A.23. TMZ scan (Targeting study with thick test section)

($[\text{Na}_2\text{SO}_4 \cdot 10\text{H}_2\text{O}]_{\text{final}} = 2.2 \text{ wt\%} + \beta\text{-CD coated magnetite solution} ; [\text{chitosan}]_{\text{final}} = 0.43 \text{ wt\%} ; \text{chitosan}$)

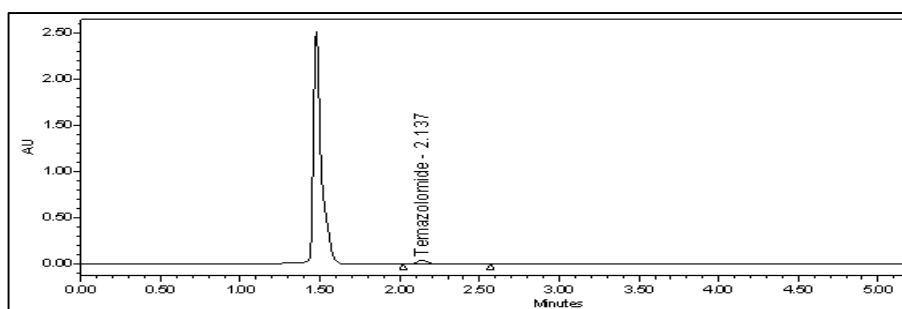


Figure A.24. TMZ scan (Targeting study with thick test section)

($[\text{Na}_2\text{SO}_4 \cdot 10\text{H}_2\text{O}]_{\text{final}} = 2.2 \text{ wt\%} + \beta\text{-CD coated magnetite solution} ; [\text{chitosan}]_{\text{final}} = 0.43 \text{ wt\%} ; \text{chitosan}$)

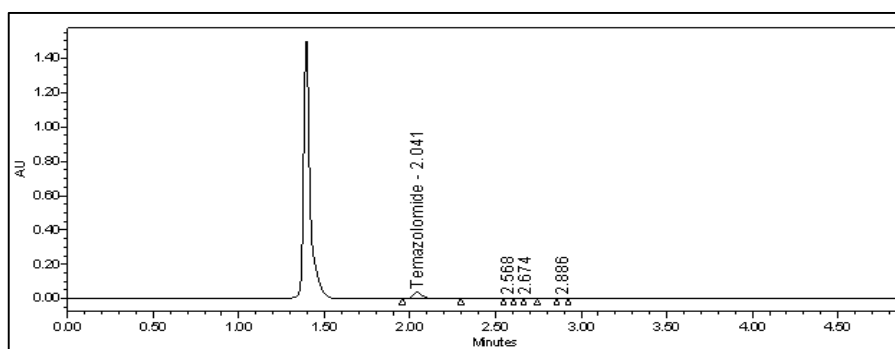


Figure A.25. TMZ scan (Targeting study with thick test section)

($[\text{Na}_2\text{SO}_4 \cdot 10\text{H}_2\text{O}]_{\text{final}} = 2.2 \text{ wt\%} + \beta\text{-CD coated magnetite solution} ; [\text{chitosan}]_{\text{final}} = 0.33 \text{ wt\%} ; \text{chitosan}$)

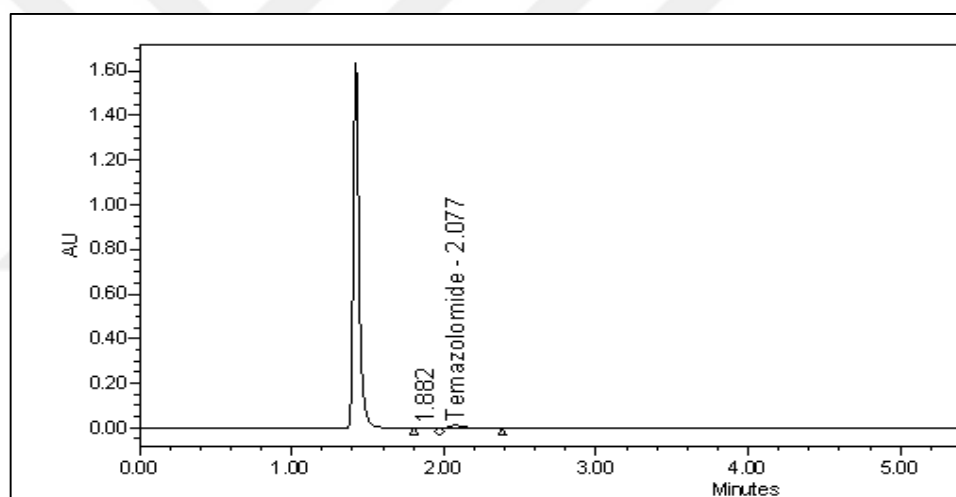


Figure A.26. TMZ scan for magnetite-CD targeting study